INFORMATION TO USERS

This was produced from a copy of a document sent to us for microfilming. While the most advanced technological means to photograph and reproduce this document have been used, the quality is heavily dependent upon the quality of the material submitted.

The following explanation of techniques is provided to help you understand markings or notations which may appear on this reproduction.

1. The sign or "target" for pages apparently lacking from the document photographed is "Missing Page(s)". If it was possible to obtain the missing page(s) or section, they are spliced into the film along with adjacent pages. This may have necessitated cutting through an image and duplicating adjacent pages to assure you of complete continuity.

2. When an image on the film is obliterated with a round black mark it is an indication that the film inspector noticed either blurred copy because of movement during exposure, or duplicate copy. Unless we meant to delete copyrighted materials that should not have been filmed, you will find a good image of the page in the adjacent frame.

3. When a map, drawing or chart, etc., is part of the material being photographed the photographer has followed a definite method in "sectioning" the material. It is customary to begin filming at the upper left hand corner of a large sheet and to continue from left to right in equal sections with small overlaps. If necessary, sectioning is continued again—beginning below the first row and continuing on until complete.

4. For any illustrations that cannot be reproduced satisfactorily by xerography, photographic prints can be purchased at additional cost and tipped into your xerographic copy. Requests can be made to our Dissertations Customer Services Department.

5. Some pages in any document may have indistinct print. In all cases we have filmed the best available copy.

University
Microfilms
International

300 N. ZEEB ROAD, ANN ARBOR, MI 48106
18 BEDFORD ROW, LONDON WC1R 4EJ, ENGLAND

WU, RANDALL

THEORETICAL AND EXPERIMENTAL STUDIES IN TRANSIENT MEMBRANE-FLUID FILM INTERACTIONS FOR SINGLE CELLS AND ASSEMBLAGES

City University of New York PH.D. 1981

PLEASE NOTE:

In all cases this material has been filmed in the best possible way from the available copy. Problems encountered with this document have been identified here with a check mark ✓.

1. Glossy photographs or pages _____
2. Colored illustrations, paper or print _____
3. Photographs with dark background ✓
4. Illustrations are poor copy _____
5. Pages with black marks, not original copy _____
6. Print shows through as there is text on both sides of page _____
7. Indistinct, broken or small print on several pages _____
8. Print exceeds margin requirements _____
9. Tightly bound copy with print lost in spine _____
10. Computer printout pages with indistinct print _____
11. Page(s) _____ lacking when material received, and not available from school or author.
12. Page(s) _____ seem to be missing in numbering only as text follows.
13. Two pages numbered _____. Text follows.
14. Curling and wrinkled pages _____
15. Other _____

THEORETICAL AND EXPERIMENTAL STUDIES IN TRANSIENT MEMBRANE-FLUID FILM INTERACTIONS FOR SINGLE CELLS AND ASSEMBLAGES

by

RANDALL WU

A dissertation submitted to the Graduate Faculty in Engineering in partial fulfillment of the requirements for the degree of Doctor of Philosophy, The City University of New York.

1981

This manuscript has been read and accepted for the Graduate Faculty in Engineering in satisfaction of the dissertation requirement for the degree of Doctor of Philosophy.

1/27/81
date

Sheldon Weinbaum
Chairman of Examining Committee

1/27/81
date

Paul R Kaumeyer
Executive Officer

Sheldon Weinbaum, Chairman

Robert Pfeffer

Carl Costantino

Herbert Weinstein

Supervisory Committee

The City University of New York

To my mother Lillian and my late father
Shang with love and devotion.

Abstract

THEORETICAL AND EXPERIMENTAL STUDIES IN TRANSIENT MEMBRANE-FLUID FILM INTERACTIONS FOR SINGLE CELLS AND ASSEMBLAGES

by

Randall Wu

Adviser: Professor Sheldon Weinbaum

In vitro experiments performed on excised artery segments have shown that the artery wall possesses non-linear filtration properties. The high deformability of the smooth muscle cells in the artery's media region might be a major factor contributing to this non-linear behavior. Since it is not possible to measure the local excess pore pressure in the interstitial space of the media region a laboratory model of the cellular component of the artery wall is used to obtain the draining behavior of a two phase system, with the particulate phase composed of membrane bound fluid filled cells, under a consolidating load. The experiments are performed for various values of initial porosity.

A comparison is made between Terzaghi's one-dimensional consolidation theory and the experimental results for excess

pore pressure. This comparison shows that at an initial matrix porosity of 0.25 the assemblage consolidates according to classical theory. As initial porosity is decreased a departure from classical theory is evident. At a physiologically significant initial porosity of 0.10 all similarities with the classical linear theory are absent. The time dependent draining of the interstitial fluid is seen to be on a longer time scale as initial porosity is decreased.

A quantitative theoretical model is developed to describe the draining of a fluid film between a membrane bound fluid filled cell and a planar surface in an effort to understand the local mechanisms involved in the consolidating specimen. Order of magnitude analysis performed on the non-linear equations shows two characteristic times are required to describe the draining behavior of the fluid film. The two time scales are called the characteristic time for fluid trapping and the characteristic time for draining the fluid film. During the early period following the loading of the cell the fluid film exhibits a behavior unique to the membrane squeeze film theory. A bidirectional flow is set up in the lubricating layer due to an off axis pressure peak. This dual flow condition is not seen in elastohydrodynamic squeeze film theory, where the maximum pressure is always located at the point of maximum deformation and the flow is directed radially outward everywhere. The bidirectional flow causes a gradual thickening of the

film in the central region and the formulation of a narrow gap region of high curvature near the edge of the near contact area where the flow is directed radially outward. On the longer time scale, after the fluid trapping has been achieved, the off axis pressure peak is replaced by a characteristic pressure plateau in the inner region of the near contact area. The membrane descends monotonically from this time on and the flow rate is positive at every location. The characteristic time for draining is typically several orders of magnitude larger than the trapping time. During this larger time period changes in the flow behavior are characterized by a nearly constant edge region and greatly diminished velocities in the lubricating film.

For the case of a rigid disc replacing the membrane bound cell the characteristic time for draining the fluid film is equal to the trapping time of the membrane problem. This comparison shows that the membrane boundary increases draining time by several orders of magnitude when the initial film thickness is two or more orders of magnitude smaller than the typical cell size. At an initial porosity of 0.10 the typical channel dimensions in the consolidation experiment have reached the point where the membrane squeeze film theory is valid.

A simple experiment has been constructed to confirm the existance of the bidirectional flow and the fluid trapping phenomena. Experimental photographs graphically illustrate the gradual thickening of the lubricating layer near

the origin and the formation and draining of the edge region as predicted by the membrane squeeze film theory.

ACKNOWLEDGEMENTS

I wish to express my thanks to my mentor Professor Sheldon Weinbaum whose guidance through the years has made this work possible. Professor Weinbaum has opened new vistas in scientific investigation to me and has expanded my theoretical background through many enlightening discussions. My co-mentor Professor Robert Pfeffer has been a continuing source of advice in the development of the many experiments I have designed and operated while in the Ph.D. program. Considering his position as chairman of the Chemical Engineering Department, I am especially grateful of the time he has spent with me on the experimental projects I have undertaken. The opportunity Professors Weinbaum and Pfeffer have given me in presenting my work at the 1980 A.S.M.E. Winter Annual Conference is one that I will always remember with appreciation.

The construction of my experiments could not have been accomplished without the expert technical support of the Chemical Engineering Department. In particular I wish to express my gratitude to Duby Firnberg, John Bodnaruk and Bill Hall for their hard work and suggestions for improving my preliminary designs. I am indebted to Mrs. Muriel Pader and Mrs. Norma Cohen for typing my manuscripts for the papers presented at the 1980 A.S.M.E. Winter Annual Conference. Mrs. Pader has also been a source of encouragement during the difficult periods of my research.

I greatly appreciate the efforts of my sister Stephanie Wu Gittell who worked into the late hours typing this manuscript.

Dr. Zeev Dagan, who started working with me as a research assistant, has been an invaluable friend during the last several years. He has always made himself available to hear my ideas and gave responsible feedback. The other members of the Mechanical Engineering Department have also added to my growth from the undergraduate years to the present and I know that I have gained through our association.

I wish to thank Professor Peter Ganatos for allowing me the opportunity to audit his course in numerical methods. He has always made himself available to my questions on the finer points of programing. Professor Donald Goldfarb of the Computer Science Department is the one responsible for making the Bell Laboratories code package known to me and Professor Melvin Lax of the Physics Department was instrumental in helping me get the tapes loaded at the Computer Center. Mr. Norman Schryer of Bell Laboratories, the author of the code package, was available to answer questions about the limitations and use of the code that did not appear in the documentation.

Without question the person most responsible for my completion of this thesis and all that it took to reach this point in my life is my wife Edna. Her support allowed

me to complete my undergraduate education under the most difficult of circumstances. At times when it would have been easier to quit, she gave me the inspiration to go on.

This research was sponsored by the National Science Foundation under Grant no. ENG 78-22101.

TABLE OF CONTENTS

LIST OF FIGURES

CHAPTER I

INTRODUCTION

I - INTRODUCTION

The slow motion of fluids in channels which change dimensions as a consequence of the fluid motion has been of interest to engineers and scientists for many years. For the civil engineer, this behavior is seen in the settling of the soil following the construction of a building. The soil undergoes the process of consolidation, where the fluid between soil particles is exuded from the mineral skeleton due to the building's load. The mechanical engineer encounters the channel draining problem in dealing with hydroplaning of rubber tires and the lubrication of gears and other rotating machine elements. In these problems there is deformation of the solid components due to the hydrodynamic pressure developed in the lubricating layer. This deformation obeys the linear elastic law for deformable solids.

More recently there has been growing interest in the interaction of biological cells with a fluid film separating them. This interest is manifested in the study of cellular assemblages as well as isolated pairs of cells. The artery wall under compression can be viewed as an assemblage of highly deformable cellular matrix undergoing the process of consolidation, with the endothelial cell layer acting as the load surface. The interstitial fluid percolates through the media region of the artery wall to the relatively resistance free adventitial layer. The driving force is the increase in mean blood pressure which can be

the result of a pathological condition.

Due to the difficulties in measuring the time dependent excess pore pressure across the thickness of the largest arteries under compression, a simplified laboratory model was constructed to simulate the consolidation of the cellular component of the wall. Water filled polyethylene sacs were used as models for the highly deformable smooth muscle cells of the media region of the artery wall. Time dependent excess pore pressures are obtained under various conditions of load and initial porosity. The laboratory model for the cellular component of the artery wall is discussed in chapter II. The results of the experiments, with comparison to classical consolidation theory, are presented in the latter sections of chapter II.

In chapter III a theory for predicting the draining behavior of a lubricating film adjacent to a membrane bound fluid filled cell is presented to give a better understanding of the local mechanisms involved in the multi-particle assemblage problem of chapter II. The isolated cell problem has merit in its own right. The phenomena predicted by the theory developed in chapter III has application to microscopic slide preparations of simple cells, the squeezing of a fluid film between an air bubble and a planar surface as the bubble rises toward the surface due to buoyancy, the insertion of a soft contact lens in the eye and the settling of a thin wall balloon tire on a fluid film. The mathematical model treats the problem of a lubricating film

squeezed between a membrane bound fluid filled cell and a rigid planar surface. The membrane squeeze film theory predicts a fluid trapping phenomena with a dual flow condition that has not been previously reported in the literature. An experimental verification of this unique behavior is presented in the end of chapter III. The extension of the theory to include translational motion of the cell has important application to the passage of a red cell through a capillary.

CHAPTER II

CONSOLIDATION OF A CELLULAR-FLUID MATRIX; A SIMPLIFIED MODEL OF AN ARTERY WALL

II - CONSOLIDATION OF A CELLULAR-FLUID MARTIX; A SIMPLIFIED MODEL OF AN ARTERY WALL

A - Introduction

There has been a growing interest in the behavior of an assemblage of particles with a fluid interstitial space undergoing the process of consolidation, where the assemblage is biological in nature. An artery wall can be viewed as such an assemblage, where the particles are smooth muscle cells of the media region of the artery wall. Whole blood in an ultracentrifuge also behaves as such an assemblage. The common factor in these two situations is that the particles under consideration are membrane bound fluid filled cells with an inability to support significant bending stresses. There has been no previous literature on the theory of consolidation of this type of assemblage.

Consolidation theory has its beginnings in soil mechanics, where prediction of ground settlement under the load of an architectural structure is the primary motivation. This settlement rate is dependent on the rate at which excess pore pressure is dissipated from the interstitial space. Terzaghi (1925) pioneered consolidation theory with his one-dimensional problem. Terzaghi treated the soil as a porous material with certain elastic properties and the voids as a water filled interstitium. Terzaghi's treatment, although restricted to a column of soil under a constant load and restrained from lateral expansion, has had remarkable success in predicting the settlement of many types of soils. Biot

(1941a) improved the state of condolidation theory with his general theory of three dimensional consolidation. In this latter paper equations valid for any arbitrary load, variable with time, were developed. Biot's theory is limited to small strains, where strain is linearly related to stress. An additional improvement made by Biot is that the soil may be only partially saturated with water. Application of this theory was made in specific cases of load and boundary conditions (Biot, 1941b; Biot and Clingan, 1941; Biot and Clingan, 1942).

In all the previously mentioned papers material isotropy was assumed with constant permeability. Biot (1955, 1956) extended his previous theory to include the general case of an anisotropic material and a porous viscoelastic anisotropic solid. As with his earlier work closed form solutions were obtained only in simple cases due to the complexity of the governing equations.

The consolidation of soil composed of finite layers with different permeabilities is the subject of several papers (Carillo, 1942; Rowe, 1959; Horn, 1963). The influence of regions of high permeability on the overall consolidation behavior of a composite soil was the primary motivation of these investigations.

Several authors sought to extend classical theory to include the influence of variation of permeability and compressibility during consolidation (Richart, 1957; Lo, 1960; Davis and Raymond, 1965). Gibson et al (1967) developed

a weakly non-linear theory of consolidation for thin layers of saturated clays. In the latter paper the coefficient of consolidation is assumed to be linearly related to the void ratio. The resulting expression for void ratio has the same form as the transient one-dimensional heat conduction equation with a variable diffusivity.

The consolidation of biological tissue has received considerable attention in the study of articular cartilage. Like soil, articular cartilage may be considered a two-phase system (Edwards, 1967; Torzilli and Mow, 1967a). The solid phase is composed of chondrocytes, collagen fibers and proteoglycan ground substance, while the fluid phase is the interstitial fluid which is 65 per cent to 85 per cent of the cartilage by weight (Mankin and Thrasher, 1975; Mansour and Mow, 1976). The latter experimental paper showed that cartilage permeability decreased with increasing compressive strain. The theoretical treatment of articular cartilage under consolidation and direct pressure gradient was developed in a series of papers (Torzilli and Mow, 1976a, b; Mow and Mansour, 1977). In these papers the cartilage is assumed to be composed of a deformable viscoelastic solid with an incompressible interstitial fluid. The latter paper developed a theory for a permeability coefficient that is a function of compressive strain.

Kenyon (1978) treated the problem of consolidation of compressible mixtures with a constant permeability. He is able to identify the specific role of solid and fluid com-

pressibility on the consolidation behavior. Kenyon's (1976) work in consolidation also included the theoretical treatment of thin walled elastic tubes with application to the artery wall. The artery wall in the latter paper was assumed to have constant elastic properties and permeability during compression.

A number of anomalies have arisen in filtration studies of the arterial wall substance (Vargas et al, 1979; Harrison and Massaro, 1976; Yarmartino et al, 1974; Wilens and McClusky, 1952, 1954) and perfusion studies of the artery wall denuded of its endothelium (Fry, 1972; Siflinger et al, 1975). In all these studies, which were performed in vitro, the excised artery segment is either cut open along its length and laid flat upon a supporting screen or examined in cylindrical geometry which is pressurized from within. The important results that have not been satisfactorily explained are;

1. The hydraulic permeability of the cylindrical geometry is about an order of magnitude larger than the planar geometry once the latter has achieved a steady state.
2. The hydraulic permeability of the artery wall in the planar geometry is strongly time dependent changing by a factor of 5 or more in the first several hours following the initial application of pressure.

3. The uptake of tagged albumin is visibly larger in the cylindrical geometry when pressurized than when there is zero transmural pressure (Caro 1978, private communication), while the uptake in planar geometry (Fry, 1972) is essentially independent of pressure.

A fourth related observation is that the artery wall is nearly incompressible (Carew et al, 1968) and has a free water volume which is a small percentage of the total wall volume. The interstitial space, which is composed primarily of collagen fibers and a gel substance (slightly cross linked hyaluronic acid molecules) is known in other tissues to offer a flow resistance which is a highly non-linear function of the interstitial pressure (Guyton et al, 1966).

It seems reasonable to hypothesize that this non-linear behavior is due in part to the high deformability of the cellular component of the wall, particularly the smooth muscle cells. This suggests that the artery wall possesses time dependent consolidation properties and a Darcy law with a permeability coefficient that is a non-linear function of local tissue pressure. All existing theory has been based on Biot's or Terzaghi's consolidation theory in which the Darcy law permeability for a porous elastic solid is either assumed constant or linearly related to compressive strain and a linear elastic law assumed for the deformation of the solid phase.

There has been no previous investigation treating the

consolidation of a particle-fluid assemblage where the particles are membrane bound fluid filled cells, to determine the time history of the excess pore pressure in the assemblage. Since it is not possible, at present, to measure the excess pore pressure at intervals across the thickness of an artery wall a greatly simplified laboratory model of the wall has been constructed to simulate the consolidation of the cellular component of the artery wall. The experimental results for excess pore will be compared with the solution of Terzaghi's one-dimensional theory for various loads and initial porosities.

B - Apparatus and experimental procedure

An instrumented piston-cylinder arrangement, figure II-1a, containing distilled water and approximately 2,000 neutrally buoyant water filled sacs is used to quantitatively model the consolidation of a two-phase medium with a highly deformable but incompressible particulate phase. The flaccidly filled sacs are a greatly simplified model of the smooth muscle cells in the media region of the artery wall. No attempt was made to model the other components of the interstitial space. Due to the small fraction of free water in the artery's interstitial space the model cells may be considered effective cells.

The membrane of the sacs are polyethylene sheets 1.5 mil. thick. The polyethylene sheets are made into small sacs with a three sided seam enveloping a maximum volume of 5 cc. The sacs are then flaccidly filled with distilled water and the last seam is made. The seams are heat sealed to provide a leak-proof closure. Excess plastic is trimmed from the seams to minimize the influence of the seamed area. The finished sacs are examined over a period of several days and those which contain air bubbles are discarded.

The piston and cylinder are constructed from lucite tubing with a 0.63 cm wall thickness. Two neoprene O-rings are set into grooves machined into the piston (figure II-1b) and provides leak-free contact with the precision machined inside surface of the experimental test cylinder. The maxi-

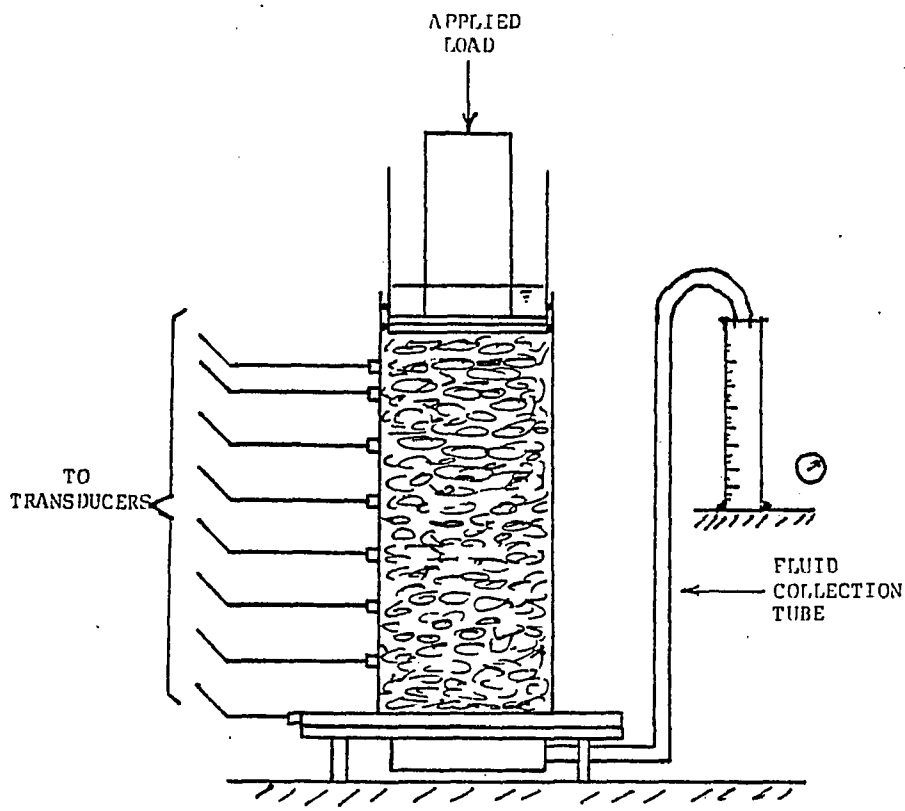

Figure II-1a Schematic representation of the experimental apparatus.

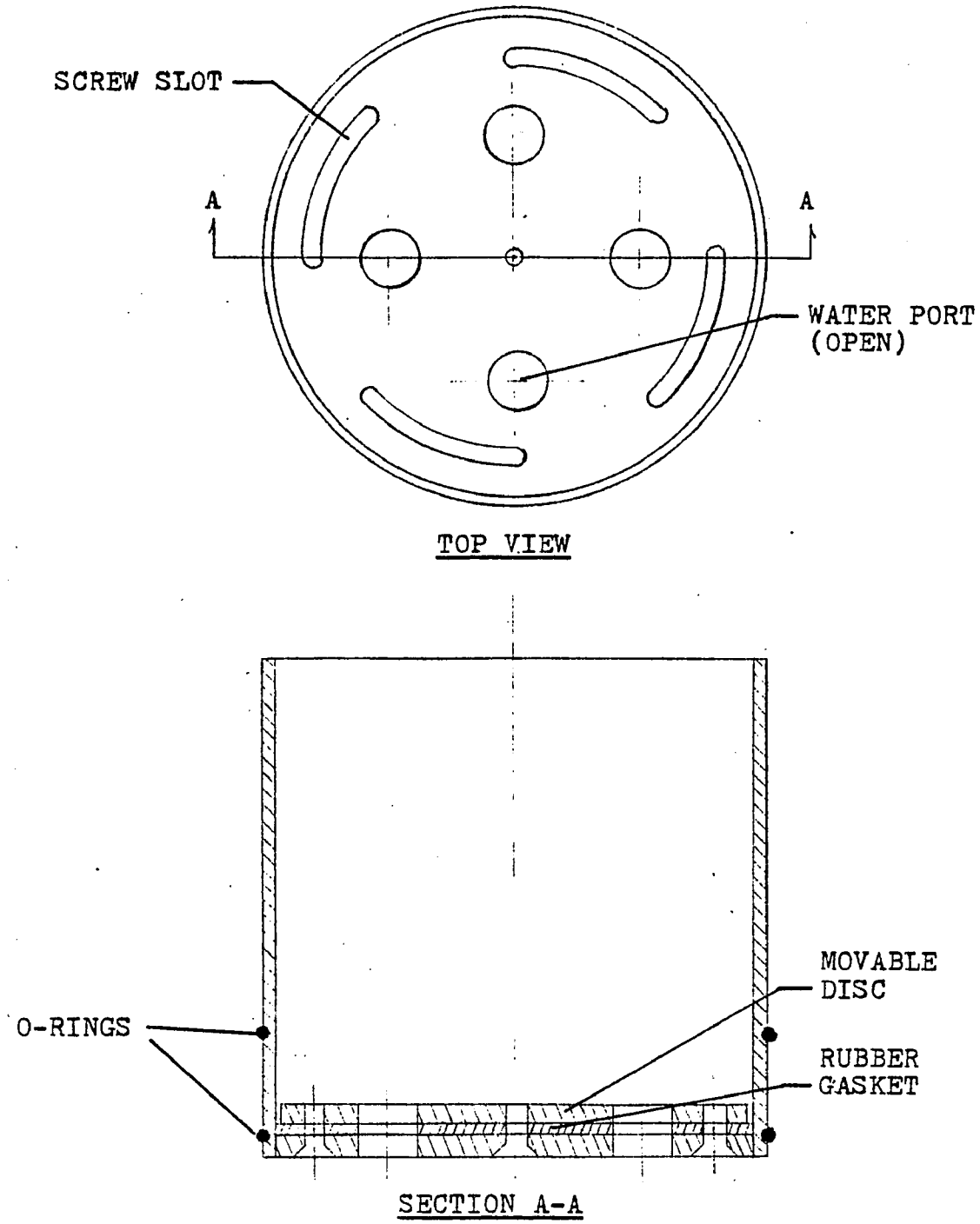

Figure II-1b Load bearing piston.

mum piston stroke from its predetermined zero position is 3.25 cm. The piston face is made of two lucite discs separated by a rubber gasket. The discs are drilled with four 1.3 cm holes to allow for free water movement as the piston is lowered to its zero position. The outer disc rotates on five screws to open or close these ports and five wing nuts provide leak-free contact with the rubber gasket.

The experimental test cylinder has six lucite rings 5 cm in height bonded to its inner surface with a 1 mm clearance between successive rings. Pressure taps are machined into the cylinder at each clearance location. This clearance volume precludes the possibility that a model cell will block a pressure port and give erroneous readings. This clearance also serves as a circumferential reservoir that equalizes excess pore pressure at its given height in the cylinder.

The consolidation specimen occupies 38.5 cm of the cylinder's height, having a nominal diameter of 16 cm. A fine wire mesh laid over a coarse wire mesh restrains the sacs at the bottom of the cylinder, while offering no pressure drop for the exuded liquid. Below the wire screens is a plenum chamber with a 3.8 cm inside diameter fluid collection tube attached. The open end of the fluid collection tube is located at the liquid level in the piston to ensure that there is no driving force due to hydrostatic pressure. The free water volume that is

squeezed out of the cylinder is collected in a graduated cylinder. A movie camera is focused on the graduated cylinder for accurate determination of the change in volume of the test specimen.

Rigid vinyl hoses connect the experimental cylinder's pressure ports to low pressure transducers. The time dependent excess pore pressure is measured using Validyne DP-15 differential pressure transducers and CD-15 sine wave carrier demodulators with a frequency response of 1000 Hz. The transducers are mounted on a sliding rack which is locked into the same plane as the liquid level to ensure that only the excess pore pressure is measured. The demodulators amplify and linearize the input signal from the transducers. The controls on the demodulators facilitate calibration of each unit (transducer, cable and demodulator). The output signal from each demodular is continuously recorded on an Offner strip chart recorder.

A load platform, connected to the release mechanism by a threaded rod, fits in a groove machined into the movable disc on top of the piston face. This ensures that the load is applied axisymmetrically to the piston face. The threaded rod carries the load of the dead weight until the cam-like release mechanism is actuated. The combined mass of the piston, load platform and threaded rod are enough to balance slide friction in the two O-rings. The experimental cylinder rested on legs that are adjustable to allow for the leveling of the apparatus.

Upon determining the zero position of the piston the total specimen volume is easily obtained. The desired cell volume used for a given experimental run is obtained using the volume displacement method. The cylinder is carefully packed to ensure that there are no trapped air bubbles in the interstitial space. This is accomplished by gradually raising the water level in the cylinder and adding the water filled sacs in increments, removing bubbles at each stage. Before the packing begins, the inside surface of the cylinder is sprayed with a dry silicon lubricant to reduce slide friction between the cylinder walls and the water filled sacs.

Once the experimental cylinder is properly packed the piston (with its O-rings well greased) is moved to its predetermined zero position, while the ports in the piston face are kept open to allow for free water movement. When this task is completed, distilled water is added to the top section of the piston until the meniscus in the collection tube drains into the graduated cylinder. When the draining ceases the transducer rack is moved until all transducers read zero excess pore pressure.

Once the water level is in the correct location the piston ports are closed and locked. The load platform is then lowered into the grooves in the piston face and locked using an adjustment nut attached to the threaded rod and release cam. Before the start of an experimental run the instrumentation is calibration checked.

After the dead weight load is placed on the locked-up platform, the strip chart recorder is turned on and the movie camera focused on the graduated cylinder is actuated. With all the instrumentation in operation the release mechanism is actuated and the dead weight load is applied to the specimen.

Initial porosities, n, used varied from 0.10 to 0.25. The dead weight loads used varied from 4.5 kg to 13.6 kg with the maximum load used at a given initial porosity dependent on the maximum piston travel available. The experiment was conducted in an air-conditioned room which was maintained at 25°c.

C - Theoretical background

The science of soil mechanics provides the necessary definitions used in this study of the consolidation of a cellular-fluid matrix. The two phase medium under consideration is composed of membrane bound fluid filled cells and distilled water as the interstitial fluid. The porosity of a particulate assemblage is commonly used in soil mechanics as a measure of the space occupied by the interstitial fluid.

Porosity is, thus defined as

$$n = \frac{V_v}{V_t} , \qquad (II-1)$$

where V_v is the initial void volume and V_t is the total initial volume of the assemblage. Another useful parameter is the void ratio, e, defined as

$$e = \frac{V_v}{V_c} , \qquad (II-2)$$

where V_c is the total volume of all cells in the assemblage. The obvious relations between e and n are then,

$$n = \frac{e}{1+e} , \quad e = \frac{n}{1-n} . \qquad (II-3a,b)$$

An average Darcy law permeability, k, was determined for each experimental run corresponding to each initial porosity and applied load. Using an average value for flow

rate Q over the duration of an experimental run, one can define the average permeability by

$$k = \frac{Q H}{A \Delta h} , \qquad (II-4)$$

where H is the height of the matrix, A is the cross-sectional area of the matrix and Δh is the difference in head across the matrix height.

With data collected from the film the change in void ratio, Δe, for an experimental run is obtained and used to determine an average value for the coefficient of compression a_v.

$$a_v = - \frac{\Delta e}{\Delta \sigma_v} . \qquad (II-5)$$

Where $\Delta \sigma_v$ is the change in total vertical stress on the assemblage. The coefficient of volume change, m_v, is readily determined using the result of equation (II-5) and the initial void ratio in the following equation,

$$m_v = \frac{a_v}{1+e} . \qquad (II-6)$$

The coefficient of consolidation, C_v, based on the results of equations (II-4) and (II-6) is an average value for the duration of a given consolidation test.

$$C_v = \frac{k}{\gamma m_v} \qquad (II-7)$$

Where γ is the density of the interstitial fluid.

A Reynold's number based on the superficial velocity v_s and typical channel thickness ϵ is determined from the following relations.

$$v_s = \frac{Q}{A} \qquad (II-8)$$

$$R_e = \frac{v_s \epsilon}{\nu} \qquad (II-9)$$

where ν is the kinematic viscosity of the interstitial fluid. The typical channel thickness ϵ is obtained by assuming uniform cubic cells with sides of length c and a distance ϵ between successive cells. One then requires the volume of all the cells in the assemblage to be equal to the fraction of space occupied by these cells times the total volume of the assemblage or simply,

$$l c^3 = l(\epsilon + c)^3 (1-n). \qquad (II-10)$$

Where l is the number of cells in the system and 1-n is the fraction of space occupied by cells. This reduces to

$$\epsilon = c\left[(1-n)^{-1/3} - 1\right]. \qquad (II-11)$$

Where c is equal to 1.5 cm for a typical cell size in this experiment. Values for the above mentioned parameters can be found on the experimental graphs for excess pore pressure.

The influence of cell deformability is readily apparent in the magnitude of the coefficient of compressibility and subsequently in the coefficients of volume change and consolidation. The coefficient of volume change in these experimental investigations is typically three to four orders of magnitude larger than for more loosely packed soils. The compliance of the membrane boundaries of each cell contribute to this great difference in the coefficient of compressibility. For soils extremely high pressures are required to alter the shape of individual soil particles, whereas small pressures are required to alter the shape of a membrane bound fluid filled cell.

The Reynold's number for the experiments is of order unity which is in the range of validity of the Darcy law, when used for soils. Due to the compliant nature of the fluid filled sacs one would expect that the upper limit of Reynold's number could be extended.

For a consolidation specimen in which the particulate phase cannot support significant bending moments, Biot's equation and Terzaghi's equation reduce to the form of the transient heat conduction equation with constant diffusivity. Comparison of experimental results, for excess pore pressure, will be made with Terzaghi's

theoretical prediction because of its remarkable success in predicting the settlement of many types of soils under a constant load.

For one-dimensional consolidation the non-dimensional equation governing excess pore pressure, with constant total vertical stress, is:

$$\frac{\partial^2 U}{\partial Z^2} = \frac{\partial U}{\partial T} , \qquad (II-12)$$

where the consolidation ratio U, non-dimensional time T and non-dimensional elevation Z are defined as follows:

$$U = 1 - \frac{u_e(z,t)}{u_o} \qquad (II-13a)$$

$$T = \frac{C_v t}{H^2} \qquad (II-13b)$$

$$Z = \frac{z}{H} . \qquad (II-13c)$$

In the above relations $u_e(z,t)$ is the instantaneous excess pore pressure at a given elevation in the stratum, H is the stratum height and C_v is the coefficient of consolidation defined in equation (II-7).

The solution to equation (II-12) is plotted in figures II-2 through II-6, for various values of T, subject to the following initial and boundary conditions:

$$U(Z,0) = 0 \qquad \text{(II-14a)}$$

$$U(0,T) = 1 \qquad \text{(II-14b)}$$

$$\frac{\partial U(1,T)}{\partial Z} = 0. \qquad \text{(II-14c)}$$

Initial condition (II-14a) requires the interstitial fluid throughout the assemblage to experience the load instantaneously. Boundary condition (II-14b) represents the free drainage condition at the bottom of the test cylinder and (II-14c) is the impermeable condition at the piston face. The solution to equation (II-12) is in the form of the infinite series

$$U(Z,T) = 1 - \sum_{n=0}^{\infty} \frac{2}{\lambda n} (\sin \lambda_n Z)\, e^{-\lambda_n^2 T} \qquad \text{(II-15)}$$

where

$$\lambda_n = \frac{\pi}{2}(2n+1)\,; \quad n = 0,1,2,3.... \qquad \text{(II-16)}$$

The experimental results are compared to the solution given by equation (II-15) in figures II-2 through II-6.

D - Results

The major objective of this experimental investigation was to see the effect that membrane bound cells have on the consolidation behavior of the bulk specimen. Initial porosities, n, much smaller than those encountered in soil mechanics were used due to the low free water volume found in artery walls. The initial void volume used varied from 10 per cent to 25 per cent of the total initial matrix volume. The assemblage occupies a total initial volume of 7,200 cc, therefore the initial volume of the interstitial fluid varies from 720 cc to 1800 cc. The kinematic viscosity, ν , of the interstitial fluid is 9.25×10^{-3} cm^2/s at a temperature of $25^{\circ}c$. The surface area of the load bearing piston is 218 cm^2.

Two experimental runs were required to complete each graph for excess pore pressure (figures II-2 through II-6). The consolidation cylinder has eight pressure ports, however I had only five differential transducers available to me. One transducer monitored the excess pore pressure 0.6 cm above the restraining mesh (port no. 1) for all experimental runs. This transducer's output was recorded on a digital voltmeter. Since the excess pore pressure at this point in the assemblage never exceeded five per cent of the initial excess pore pressure it was not plotted. Another transducer was used to monitor the excess pore pressure near the middle of the cylinder's height (port no. 5) for both runs. The remaining three transducers alternately

monitored the lower (port nos. 2, 3 and 4) and upper (port nos. 6, 7 and 8) portions of the cylinder. The two runs were considered identical when the two experimental pressure curves for port no. 5 were in agreement and when the volume of water squeezed out of the assemblage for each run differed by only a few per cent.

The time dependent change in matrix volume is presented in non-dimensional form in figures II-7 through II-11. The change in volume at any time following the application of the consolidating load is normalized with respect to the total volume change ΔV_T. The volume change data was recorded on film using a Bauer super 8 mm movie camera focused on the graduated cylinder.

Time is non-dimensionalized using an average value of the coefficient of consolidation C_v for a given experimental run. It should be noted that the instantaneous value of the coefficient of consolidation may vary by a factor of five during a given consolidation test, with the largest variation for the situation of high porosity and large applied load.

A discussion of the results for excess pore pressure and volume change is presented in the following section.

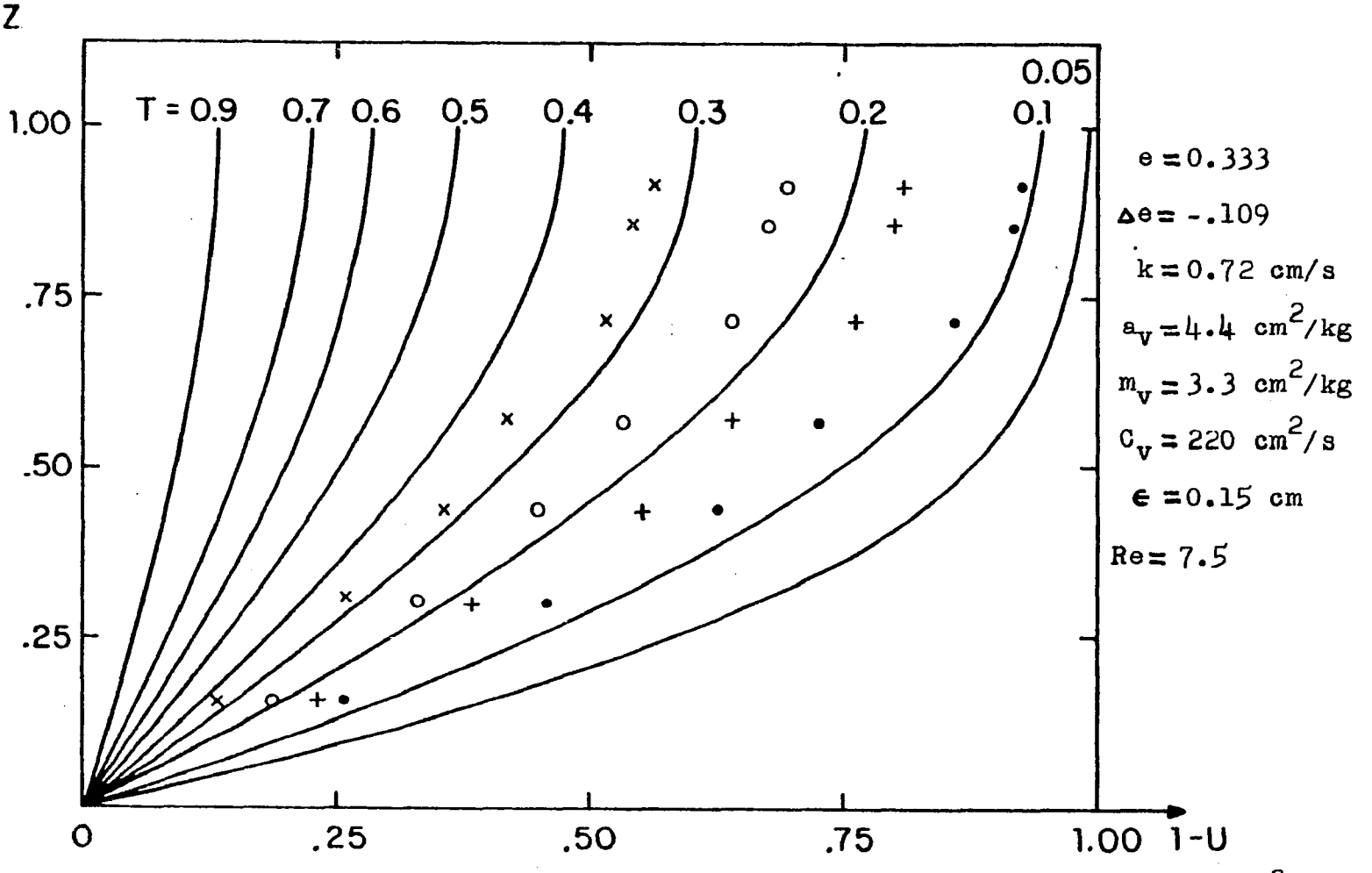

Figure II-2 Time dependent excess pore pressure, n = 0.25, u_o = 0.206 N/cm^2
T = (0.11 - ●, 0.18 - +, 0.26 - o, 0.31 - x).
Theoretical solution of Terzaghi ——.

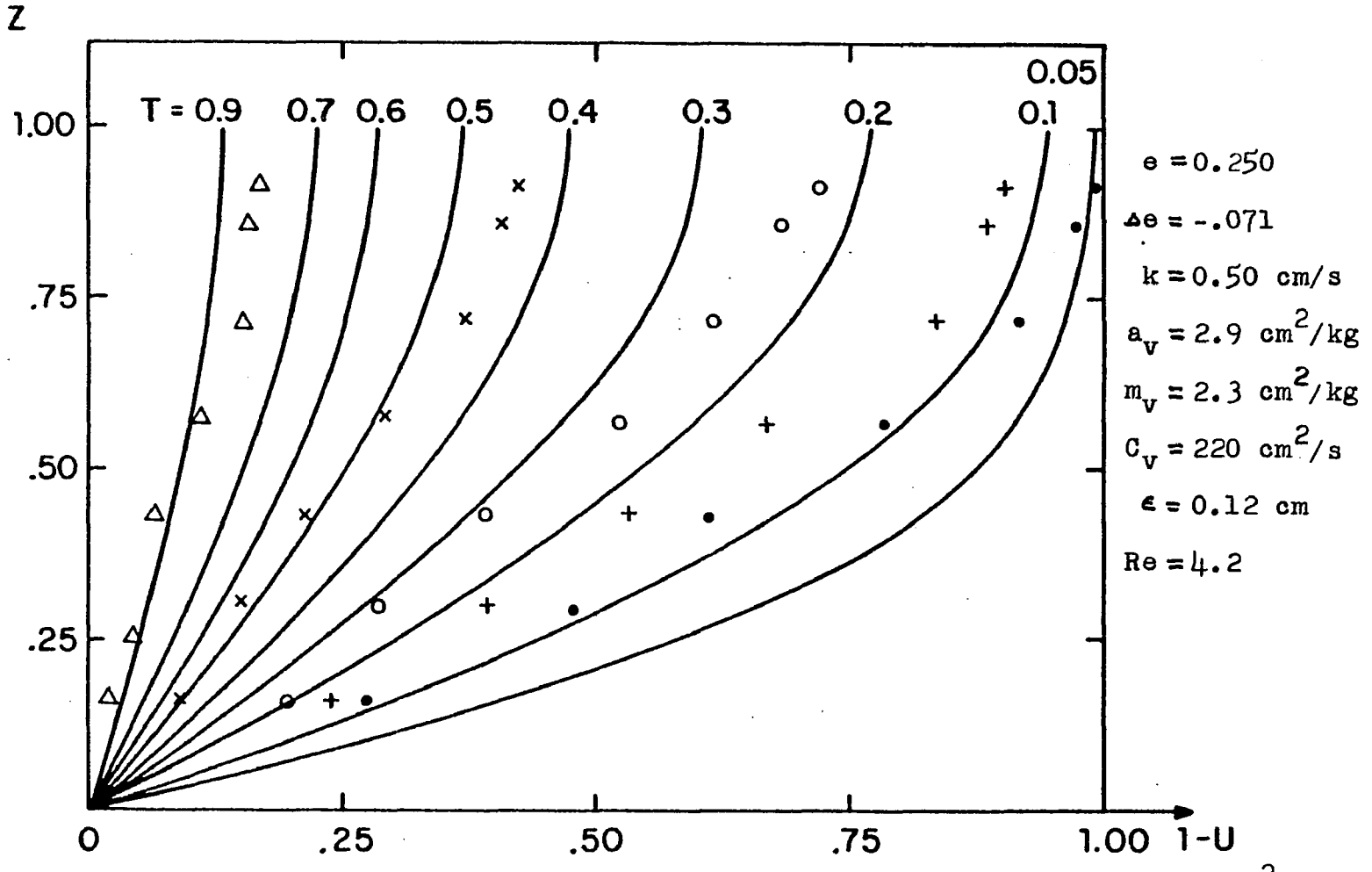

Figure II-3 Time dependent excess pore pressure, n = 0.20, u_o = 0.245 N/cm^2
T = (0.11 - ●, 0.32 - +, 0.48 - o, 0.64 - x, 0.79 - Δ).
Theoretical solution of Terzaghi ——.

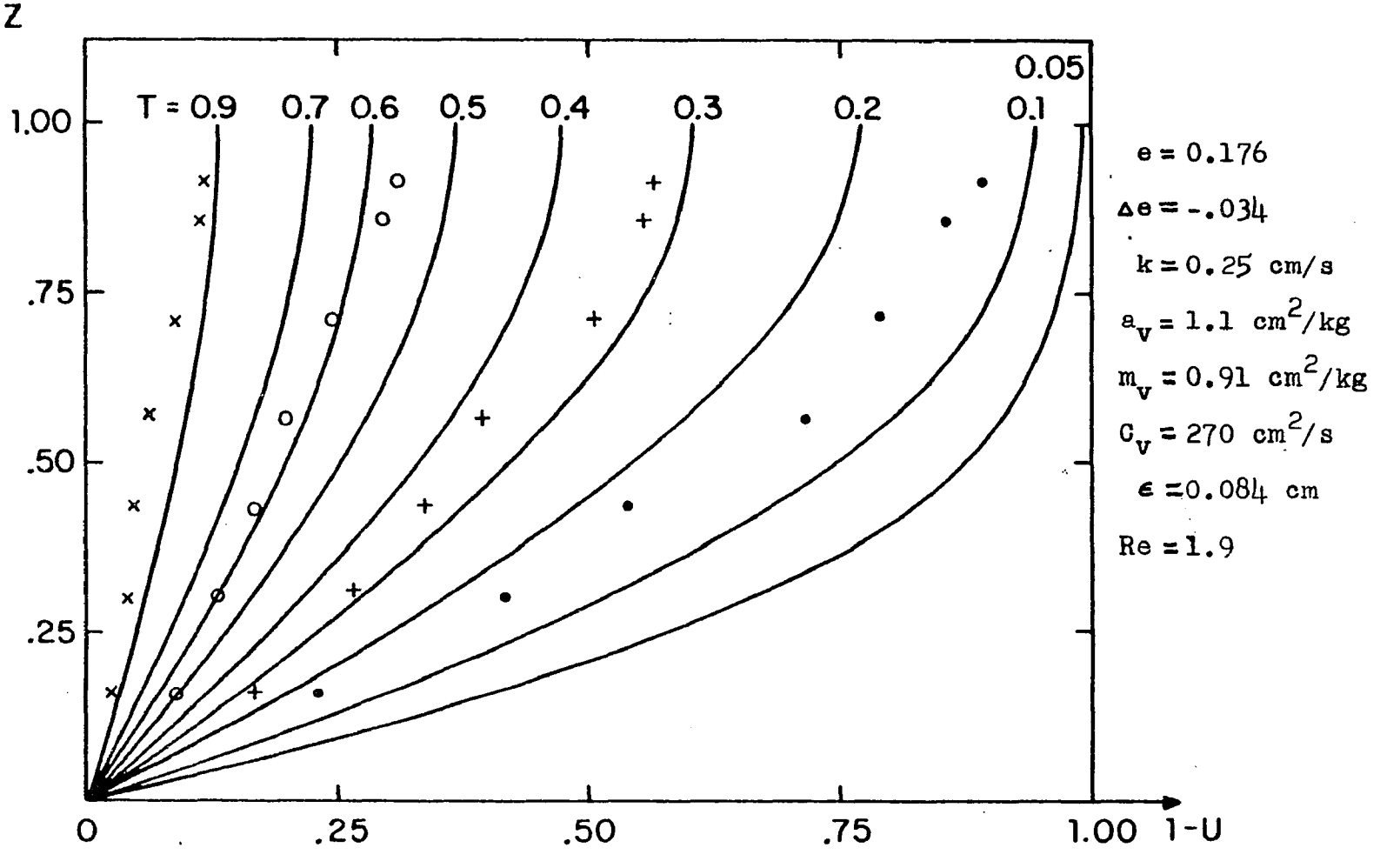

Figure II-4 Time dependent excess pore pressure, n = 0.15, u_o = .304 N/cm^2
T = (0.14 - ● , 0.39 - + , 0.59 - o , 0.79 - ×).
Theoretical solution of Terzaghi ——— .

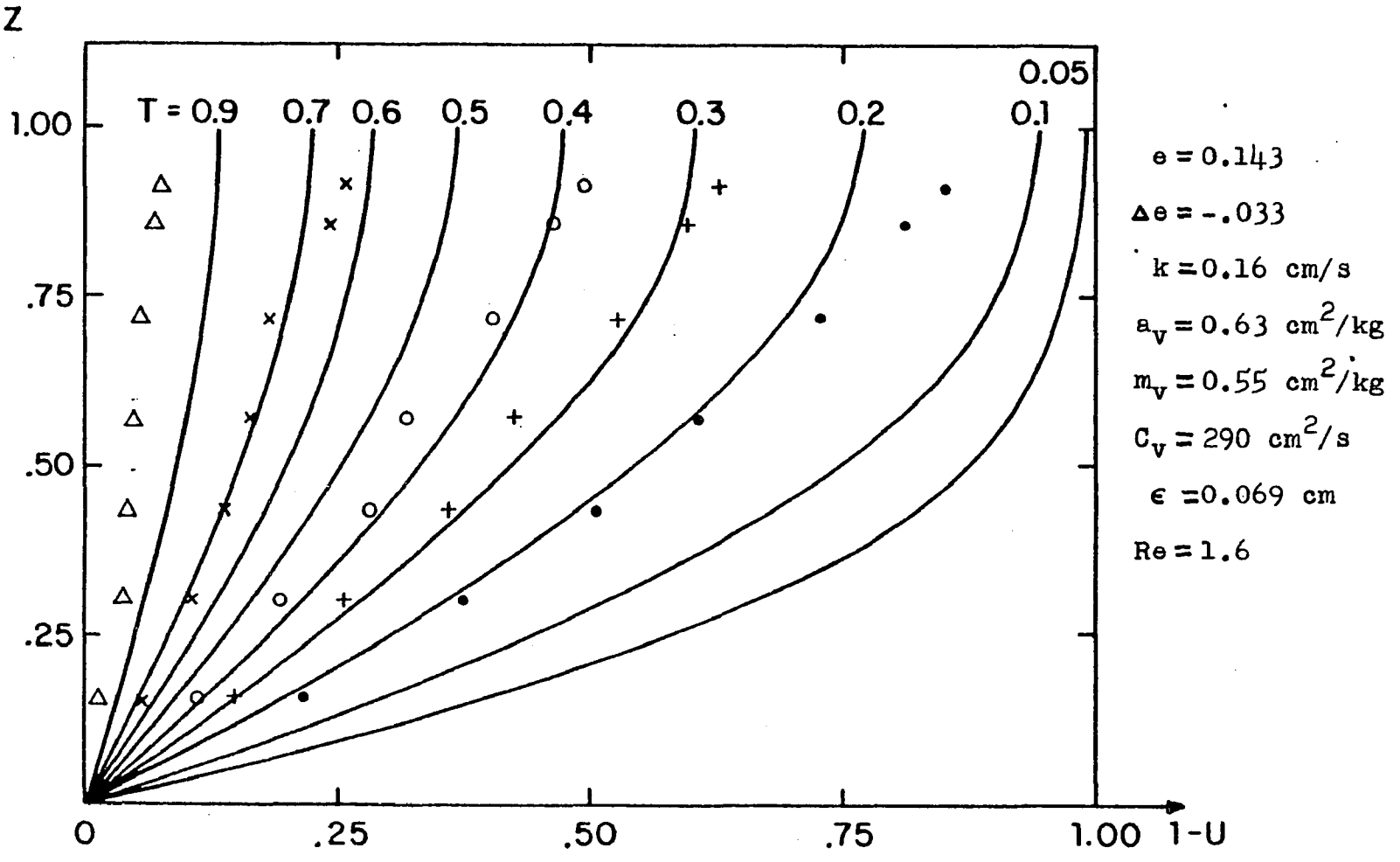

Figure II-5 Time dependent excess pore pressure, n = 0.125, u_o = 0.510 N/cm^2
T = (0.10 - ●, 0.31 - +, 0.41 - o, 0.62 - ×, 0.83 - Δ).
Theoretical solution of Terzaghi——.

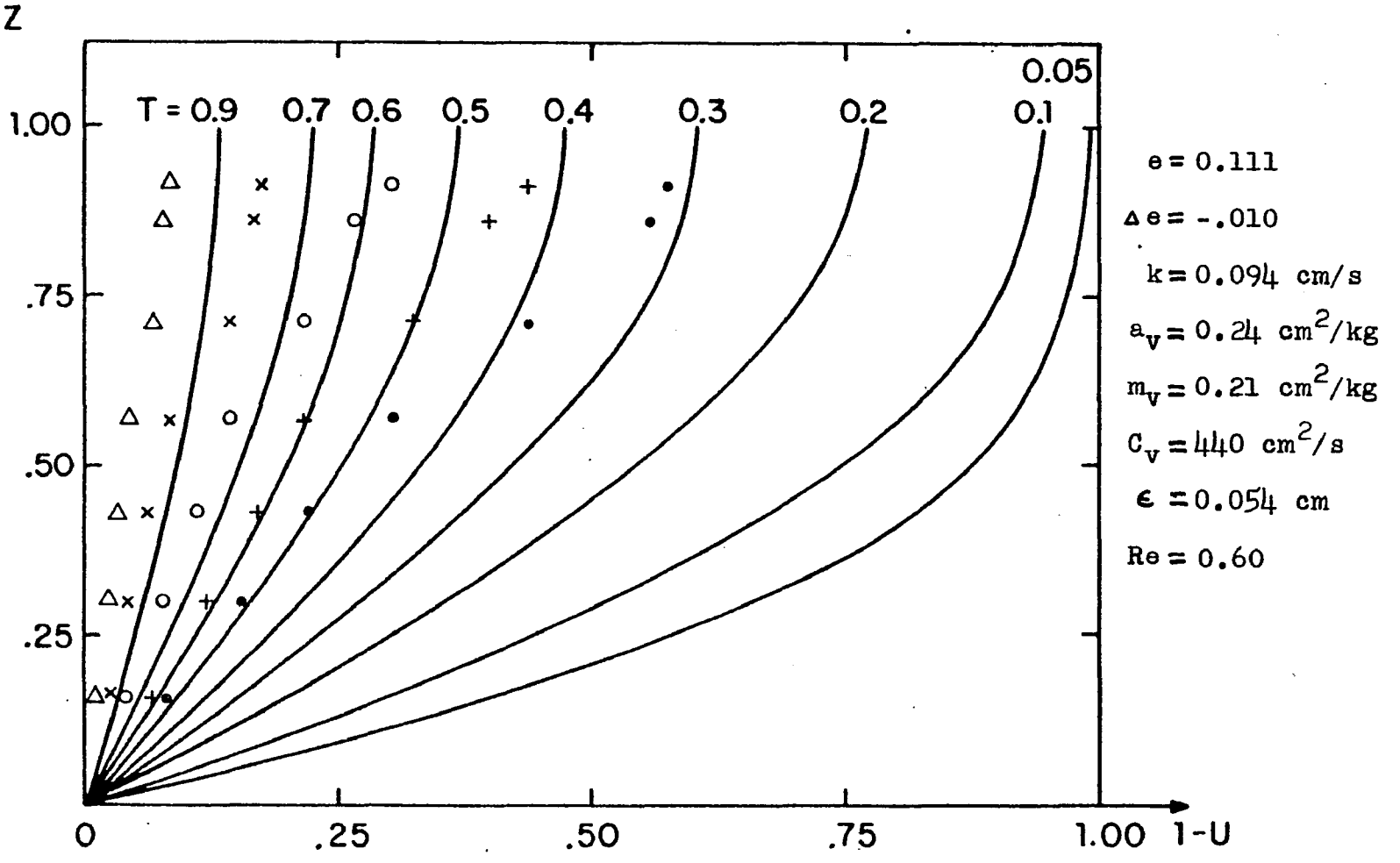

Figure II-6a Time dependent excess pore pressure, n = 0.10, u_o = 0.412 N/cm^2
T = (0.16 - ●, 0.32 - +, 0.48 - o, 0.64 - ×, 0.80 - Δ).
Theoretical solution of Terzaghi ——.

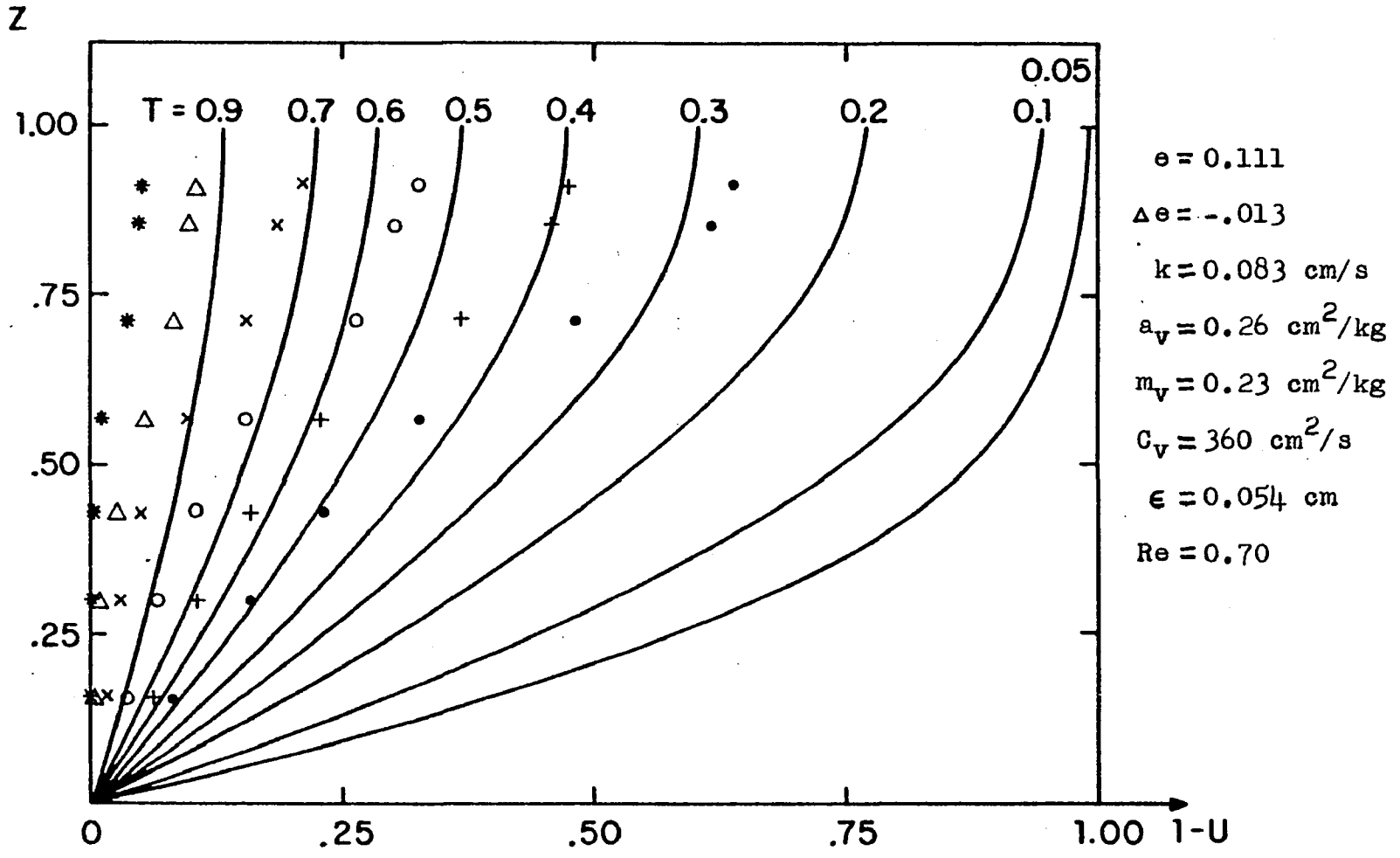

Figure II-6b Time dependent excess pore pressure, n = 0.10, u_o = 0.510 N/cm^2
T = (0.13 - ●, 0.26 - +, 0.39 - o, 0.52 - ×, 0.65 - Δ, 0.78 - ✱).
Theoretical solution of Terzaghi ——.

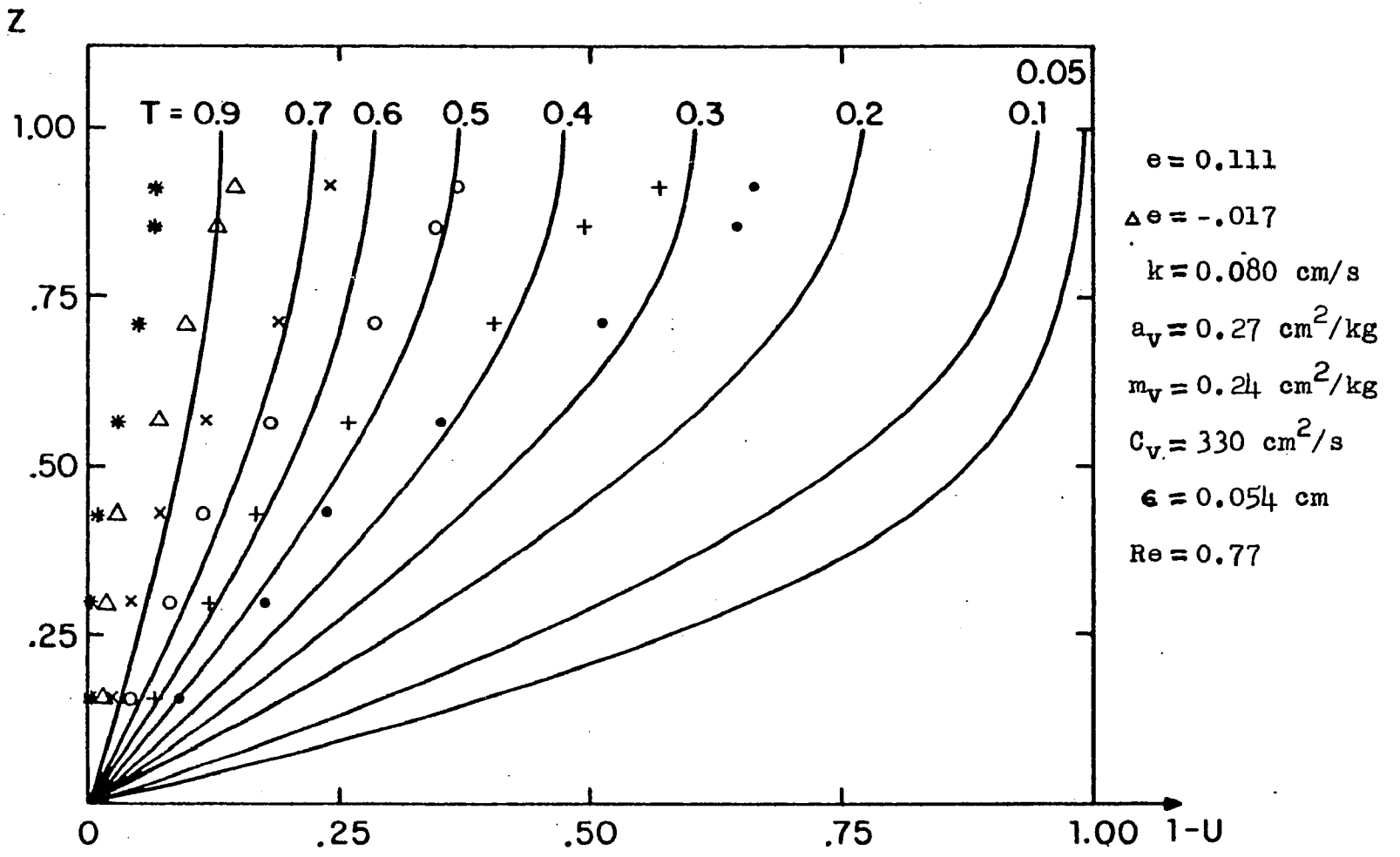

Figure II-6c Time dependent excess pore pressure, n = 0.10, u_o = 0.613 N/cm^2
T = (0.12 - ●, 0.24 - +, 0.36 - o, 0.48 - ×, 0.60 - Δ, 0.72 - ✱).
Theoretical solution of Terzaghi——.

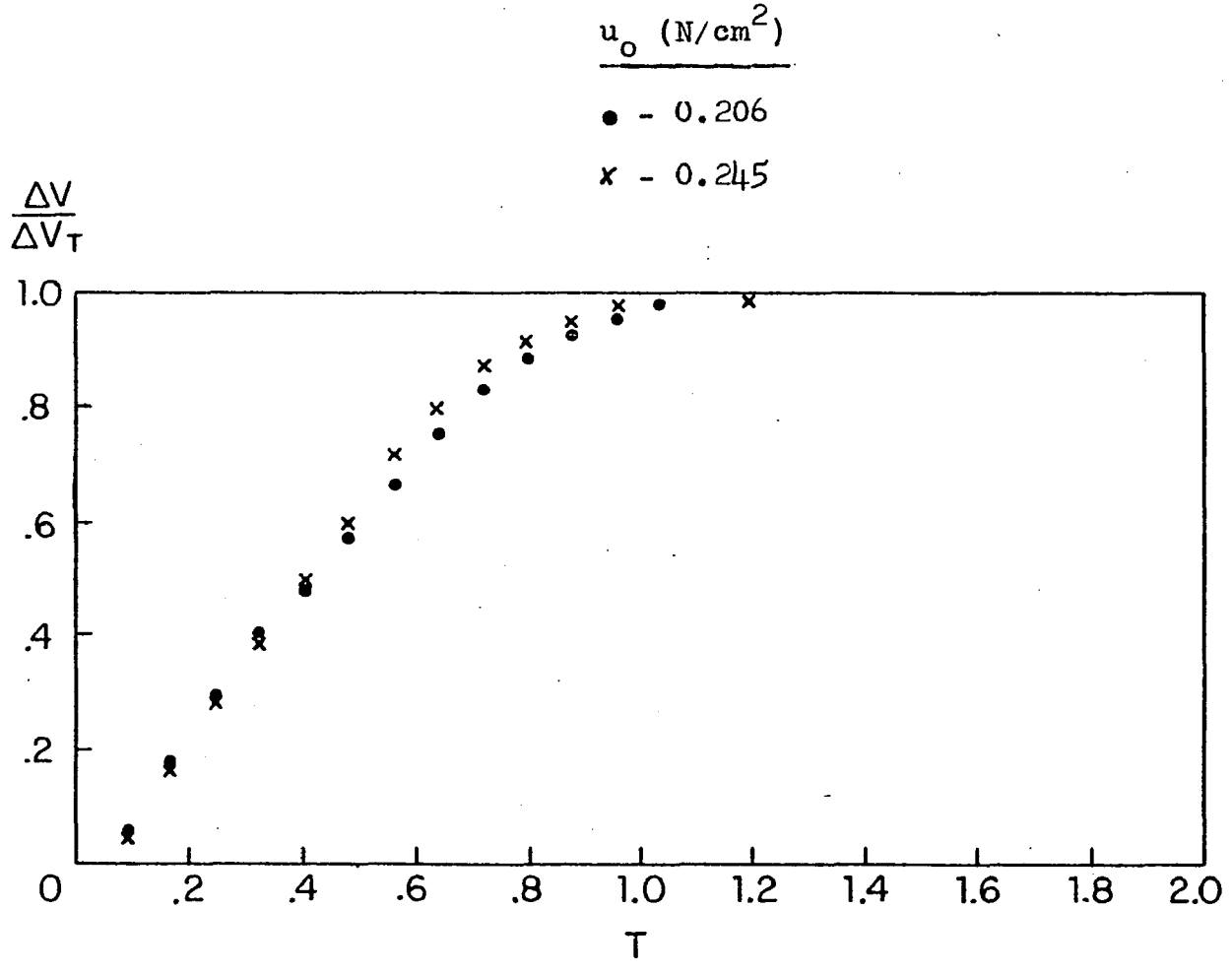

Figure II-7 Time dependent change in void volume, n = 0.25.

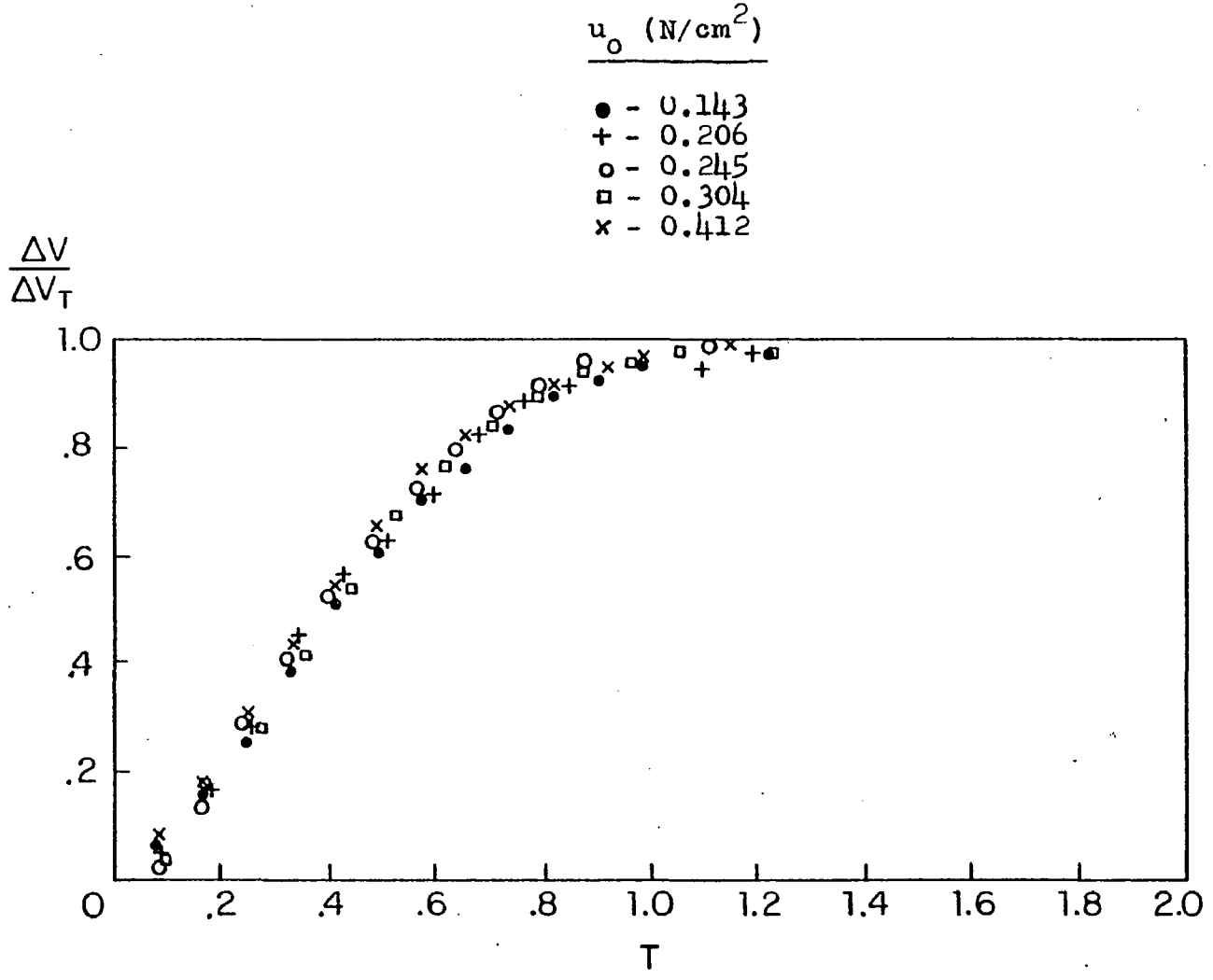

Figure II-8 Time dependent change in void volume, n = 0.20.

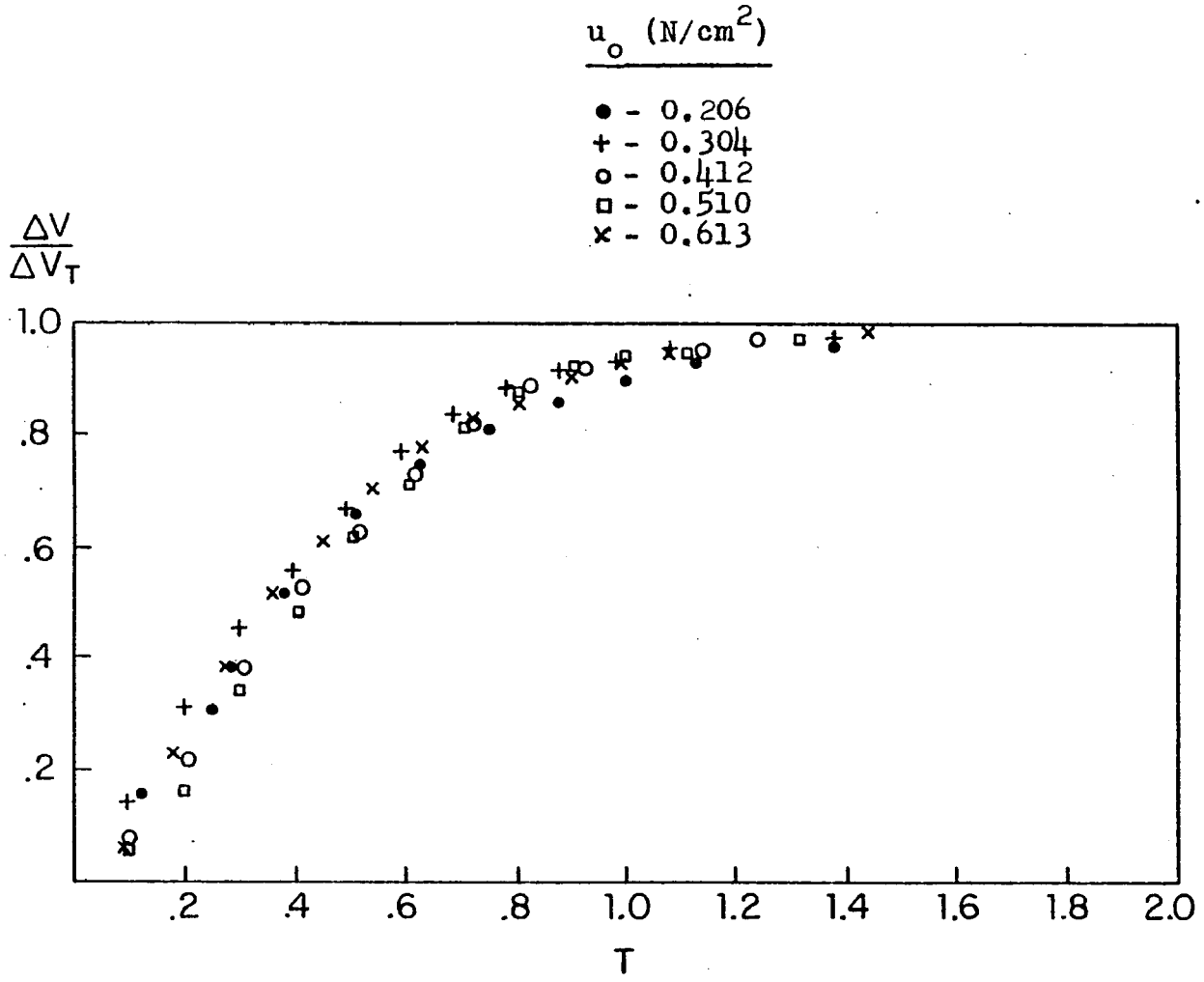

Figure II-9 Time dependent change in void volume, n = 0.15.

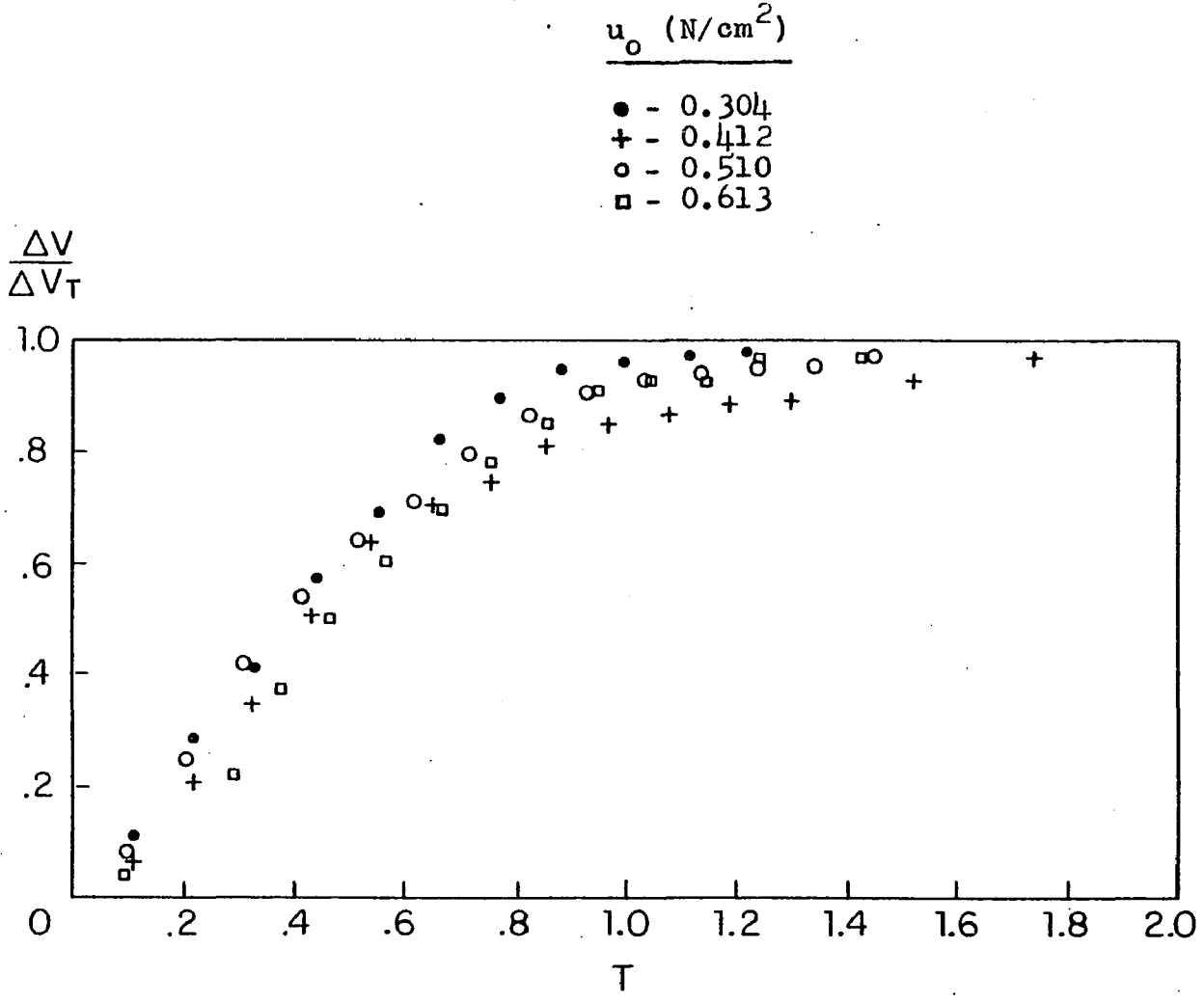

Figure II-10 Time dependent change in void volume, n = 0.125.

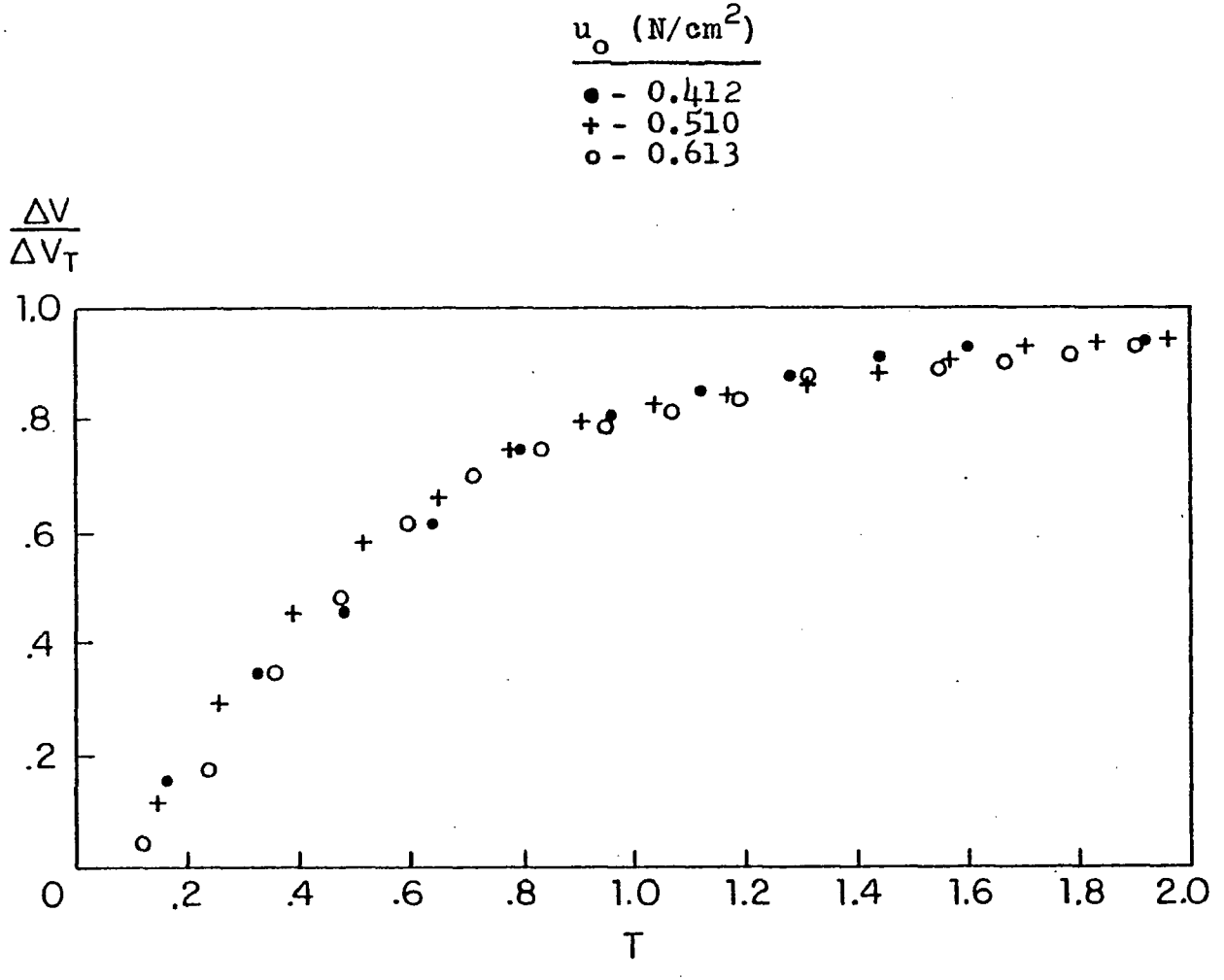

Figure II-11 Time dependent change in void volume, n = 0.10.

E - Discussion

Figure II-2 is a plot of non-dimensional excess pore pressure 1-U verses elevation for an initial porosity of 0.25 and an applied load of 4.5 kg, which results in an initial excess pore pressure of 0.206 N/cm^2. Figure II-2 shows that at this initial porosity agreement with Terzaghi's classical theory is excellent. The Reynold's number for this particular experimental run is 7.5, which is the largest value in the series of experimental cases. This fact and the excellent agreement with classical theory indicates that the Darcy law with constant permeability is valid for the conditions of this experimental case.

As the initial porosity is decreased the time parameter T for the experimental points begins to depart from those predicted by classical theory, at a given excess pore pressure. At an initial porosity of 0.20, with an initial excess pore pressure of 0.245 N/cm^2, figure II-3 shows that agreement with classical theory is still reasonable. However, when the initial porosity is equal to 0.15 the time parameter for the last set of data points, which is at the end of the consolidation process, in figure II-4 differsfrom the theoretical prediction by approximately 15 per cent. Although this difference is slight, it is the beginning of a transition from classical theory to a non-linear behavior. The non-linear behavior is more pronounced when the initial porosity is equal to 0.125,

as shown in figure II-5. In this graph the experimental time parameter for the final period of consolidation is less than the theoretical prediction by between 25 and 30 per cent of the theoretical value. This departure can be explained if one considers the method of determining the experimental value of the consolidation coefficient. Since this experimental value was based on average conditions during a consolidation test it is representative of the true value of C_v during the middle period of consolidation. If, for the theoretical curves in figure II-4 and II-5, the consolidation coefficient were allowed to decrease with increasing compaction of the assemblage, there would be closer correspondence between the theoretical and experimental values of T at a given location.

Another feature apparent upon closer examination of figure II-5 is that the spatial distribution of excess pore pressure is departing from the characteristic shape of the theoretical pressure curves. This implies that the consolidation parameters are becoming an increasingly non-linear function of time and location as the porosity is decreased from 0.20 to 0.125. The assumption of constant permeability no longer provides an accurate prediction for the rate of dissipation of excess pore pressure.

When the initial porosity is decreased to 0.10 similarities between theoretical prediction and experimental results are absent, as can be seen in figures II-6a, II-6b and II-6c. At this porosity the deformability of the

sacs influences the consolidation behavior to such an extent that the permeability must be a strong function of time and local excess pore pressure. The fact that the three figures II-6a through II-6c are not identical is due to the different initial excess pore pressures used for each case, which indicates a dependence on excess pore pressure.

For porosities of 0.10 the typical channel size is of order 10^{-2} of the particle size. In this range of channel to fluid cell dimensions an intriguing squeeze film behavior is present for the draining of a fluid film between two membrane bound fluid cells. This new phenomena is the subject of chapter III.

The change in volume of the consolidation specimen is a measure of the change in void ratio and piston displacement. At an initial porosity of 0.25, figure II-7 the settlement of the piston is nearly linear for the first 80 per cent of its total displacement at which point it asymptotes to its final value. This nearly linear displacement of the piston during the early period of consolidation diminishes in duration as initial porosity decreases until it is totally absent at an initial porosity of 0.125, as can be seen in figures II-7 through II-10.

In all the cases represented by figures II-7 through II-11 the non-dimensional volume change is independent of initial excess pore pressure. The relatively wide band of data points seen in figure II-10 can be attributed to

experimental scatter since there is no correspondence between applied load and location in the band of results. In comparing the volume change data it is clear that as packing increases the draining of the interstitial fluid is on a longer time scale. This can be explained with the membrane squeeze film theory developed in chapter III.

F - Conclusions

The results discussed in the previous section show that as packing of the assemblage increases the consolidation of the cellular-fluid matrix becomes increasingly non-linear. The transition between classical consolidation behavior at an initial porosity of 0.25 and the highly non-linear behavior at an initial porosity of 0.10 may be treated by a recent theory developed by Lai et al (1980). Lai and his co-workers have developed a theory for the compression of articular cartilage with a strain dependent permeability. Unfortunately, they have not applied their non-linear biphasic theory to the determination of local excess pore pressure in the interstitial space. However, I believe that their theory, when applied to the determination of excess pore pressure, will produce results that will compare favorably with the experimental results in figures II-3 through II-5.

To treat assemblages of membrane bound fluid filled cells undergoing consolidation at very small initial porosities (figures II-6a-c), a non-linear theory must be developed incorporating consolidation parameters that are a function of local conditions (ie; excess pore pressure and channel to particle size ratio). At a porosity of 0.10 the ratio of channel to particle size is of order 10^{-2} and the theory presented in chapter III shows that at this non-dimensional channel size the deformation of a membrane bound cell is not linearly related to the interstitial

pressure. The membrane squeeze film theory is the first step in developing a non-linear consolidation theory for a closely packed assemblage of membrane bound fluid filled cells.

CHAPTER III

TIME DEPENDENT DRAINING OF A FLUID FILM BETWEEN A HIGHLY DEFORMABLE CELL AND A PLANAR SURFACE

III- TIME DEPENDENT DRAINING OF A FLUID FILM BETWEEN A HIGHLY DEFORMABLE CELL AND A PLANAR SURFACE

A - Introduction

The time dependent draining of a fluid film between a rigid planar surface and a highly deformable membrane bound fluid cell or between two membrane bound fluid cells is a problem of fundamental interest both to the engineer and the physiologist. One frequently encounters situations where biological cells come in contact with relatively inelastic boundaries (micro-pipette experiments with red cells, entrance of red and white cells in capillaries and microscopic slide preparations of single cells) or with each other (smooth muscle cells in an artery wall, the centrifuging of cellular preparations and the formation of red cell rouleaux), where the fluid film adjacent to the membrane experiences a time dependent draining. On a larger scale this phenomena is seen when one inserts a soft contact lens on the relatively inelastic corneal surface. Three related engineering applications include a bubble approaching a solid surface, a thin walled balloon tire resting on an air or fluid film or a balloon settling on a solid surface.

While there has been no previous theory to explain the time dependent draining of a fluid film beneath a membrane bound fluid cell, there is an extensive literature on both the time dependent squeezing of a fluid film between linearly elastic surfaces and the steady state deformation

of these surfaces when in relative motion. The first paper to rigorously analyze the transient elastohydrodynamic interaction encountered in the normal approach of elastic solids separated by a lubricating film is attributed to Christensen (1962). In this work the elastic solids were circular cylinders and the approach was along a line joining their centers. Such motion is encountered in gears and rotating machine elements where vibrations are present. The displacement of the elastic surface is linearly related to local pressure between elastic elements. Lee and Cheng (1973) improved on Christensen's theory by removing the numerical convergence difficulties at small film thicknesses and incorporating the effect of deformation rate. Both papers deal with the hard elastohydrodynamic range (elastic modulus of materials are sufficiently high so that the lubricant pressures developed within the lubricating layer are large enough to substantially alter the lubricant viscosity). A more recent paper by Rohde et al (1976) treats the problem of elastohydrodynamic squeeze films in the soft range, where large deformations occur at low lubricant pressures. In the latter paper the deformation of the elastic element is also linearly related to the local pressure. Christensen's original work in the hard elastohydrodynamic range was extended in two other papers (Christensen, 1970; Herrebrugh, 1970), while the treatment of the soft range has received more recent attention (Gaman, Higginson & Norman, 1974; Roberts, 1974;

Browne, Whicker and Rohde, 1975; Whicker, Browne and Rohde, 1976).

The steady state hydrodynamic deformation of elastic or fluid filled bodies separated by a fluid film has been widely studied in connection with the theory of compliant surface bearings (Dowson and Higginson, 1960; Castelli, Rightmire and Fuller, 1967; Benjamin, 1969), the passage of bubbles and fluid droplets through tubes (Bretherton, 1961; Davis and Taylor, 1949; Goldsmith and Mason, 1962; Cox, 1962; Hyman and Skalak, 1970) and the motion of red cells through capillaries (Prothero and Burton, 1961; Barnard et al, 1968; Lee and Fung, 1969; Hochmuth et al, 1970; Sutera et al 1970, Seshadri et al, 1970; Lin et al, 1973). I shall describe further only the two latter applications, since the modeling of the fluid cell is directly related to the present study. Membrane bound fluid cells have been alternately modeled as elastic pellets, liquid droplets or fluid filled sacs whose membranes do not support bending moments. In the first treatment Lighthill (1968) and Fitz-Gerald (1969) examined the steady state parallel motion of an elastic compressible pellet through a closely fitting fluid filled tube. These papers were the first to attempt to predict the deformation of a red cell as it passes through a capillary whose dimensions were of the same order or smaller than the undeformed red cell. The deformation of the pellet is assumed to be a linear function of local film pressure, as hypothesized in the previously mentioned

transient squeeze film studies. More recently Tözeren and Skalak (1979) have examined the Lighthill and Fitz-Gerald analysis to correct for the pressure singularity that occurs in the vicinity of the point of minimum gap width and have applied this improved theory to model the motion of white cells translating along the axis of a tube (Tözeren and Skalak, 1978). The elastic deformations are of order 5 per cent to ensure the validity of the linear theory of elasticity. The validity of a linear deformation law for red cells has also been critically questioned (Lee and Fung, 1969; Skalak, 1972), since the thin walled red cell membrane does not support significant membrane bending stresses and is filled with an incompressible fluid.

A more appropriate model for the deformation of a highly deformable fluid filled membrane bound body is one where the instantaneous shape is related to the local variations in membrane tension and curvature, and membrane bending moments can be neglected. In this context, previous studies of the deformation of a bubble or liquid droplet interacting with a boundary in the creeping motion regime are of interest. Bretherton (1961) has modeled the pressure induced deformation of a bubble translating along the axis of a rigid tube. Hyman and Skalak (1972) have similarly developed a model for a periodic array of bubbles moving along the axis of a tube in the low Reynold's number limit. In both these studies the flow is steady, the surface tension is constant and one seeks a single steady state

equilibrium configuration for the shape of the deformed bubble. These surface tension problems in bubble dynamics differ from membrane bound bodies in that there is a continuity of tangential stress at the interface. The treatment of the membrane which most closely parallels the present analysis is the study by Barnard et al (1968). These authors modeled the approximation of a red cell in a capillary as a membrane bound fluid with negligible bending resistance. The steady state membrane shape was obtained by allowing the pressure difference across the membrane to be taken up by local variations in tension and curvature. Unlike the surface tension problem for bubbles, the membrane tension is not constant but allowed to vary as a function of the integrated fluid shearing stress on the cell surface.

There has been no previous study of the time dependent draining of the lubricating layer between a rigid surface and a membrane bound fluid cell with negligible bending and compressive stress. Although the deformation of the elastic solid in elastohydrodynamic squeeze film theory is somewhat similar to the deformation of the membrane in the membrane squeeze film theory developed in this work, there is an intriguingly different behavior for both the pressure and flow fields in the lubricating film. To assist the reader in following the theoretical development I shall briefly summarize the important differences. The fluid trapping phenomenon and the existance of an off axis pressure maximum are not intuitively predictable and were

discovered as a result of the investigation.

Figures III-1 and III-2 are schematic illustrations qualitatively comparing the film thickness h, pressure P and volume flow rate Q in elastohydrodynamic and membrane squeeze film theory. Sketches III-1a-c show typical profiles obtained in elastohydrodynamic squeeze film theory at small film thickness for the case where the indenter is a flat cylindrical body with its axis parallel to the direction of its motion. As seen from figures III-1a and III-1b the maximum pressure occurs at the point of maximum film thickness. Figure III-1c shows a positive outward flow rate increasing with distance from the origin. Figures III-2a-c are qualitative sketches for the same variables, as predicted by the membrane squeeze film theory presented herein, where the membrane bound body is initially an axisymmetric shape similar to an applanated fluid cell. The film thickness profiles of figures III-1a and III-2a are qualitatively similar, however, the pressure and flow fields are strikingly different. Two sets of curves are shown, $t_1 < t_{ct}$ and $t_2 >> t_{ct}$, where t_{ct} is the characteristic time to trap fluid in the near contact area. For the membrane squeeze film theory a pressure maximum quickly forms ($t << t_{ct}$) near the edge of the near contact area and there is flow inward and outward from this point. The curves for t_1 tct in figures III-2a, III-2b and III-2c are representive profiles for the time scale t_{ct} during which the edge region is established and the fluid trapping

occurs. As time increases the pressure peak near the edge region eventually disappears and the inflow of fluid will vanish. For large times $t_2 >> t_{ct}$ the pressure peak associated with the fluid trapping is replaced by a pressure plateau in the central region and a monotonically decreasing pressure in the edge region. This pressure profile produces an outward positive volume flow rate for all radii which slowly drains the trapped fluid in the interior on a much longer time scale. The two geometric parameters of importance are the radius of the near contact area and the radius of curvature of the static outer region. Numerical solutions are obtained for various aspect aspect ratios, radius of curvature of the static outer region to the radius of the near contact area.

The formulation of the theoretical problem is presented in section III-B. An order of magnitude analysis is preformed in section III-B-1, which isolates the characteristic lengths and the two characteristic times for the draining of a fluid between a planar surface and membrane bound fluid cell. The motivation for the two region approximation is an outcome of the order of magnitude analysis. The treatment of the edge region is discussed in section III-B-2. A description of the numerical procedure is in section III-B-3, while section III-C discusses the results.

In section III-D an experiment confirming the bidirectional flow behavior during the early period following the application of the load is discussed.

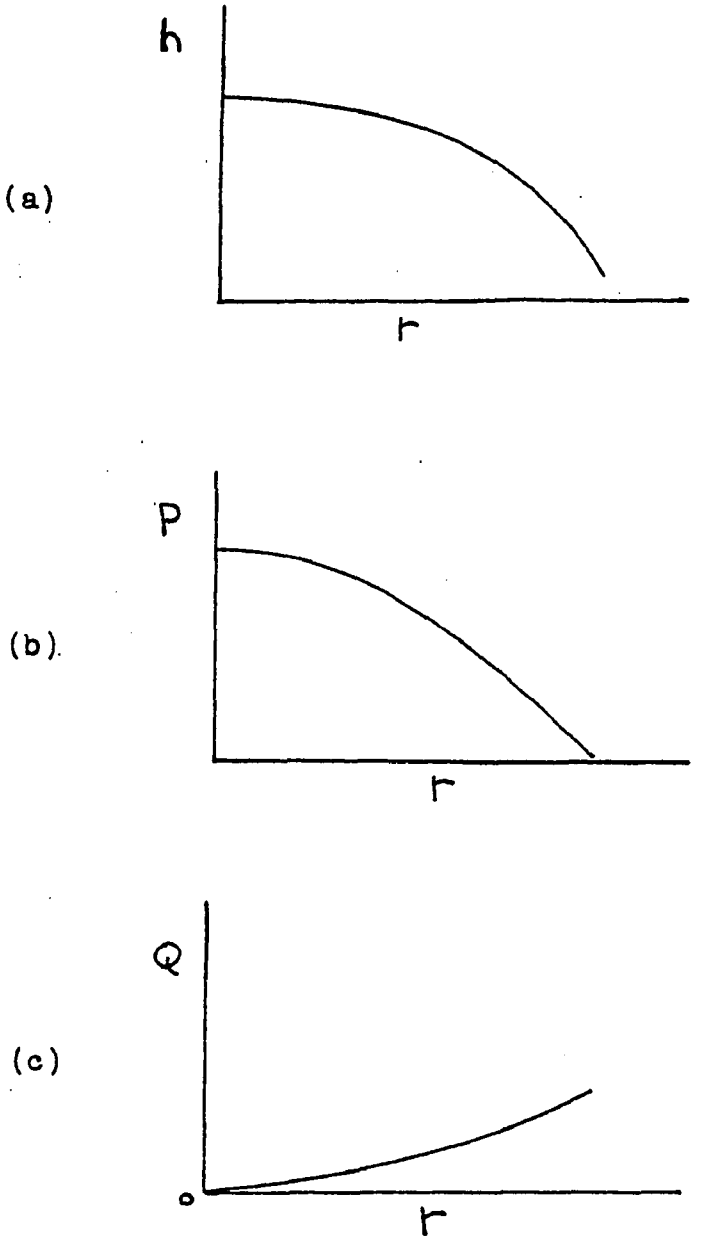

Figure III-1 Schematic representation of the spatial distribution of variables for elastohydrodynamic squeeze film theory. (a) h vs. r, (b) P vs. r, and (c) Q vs. r.

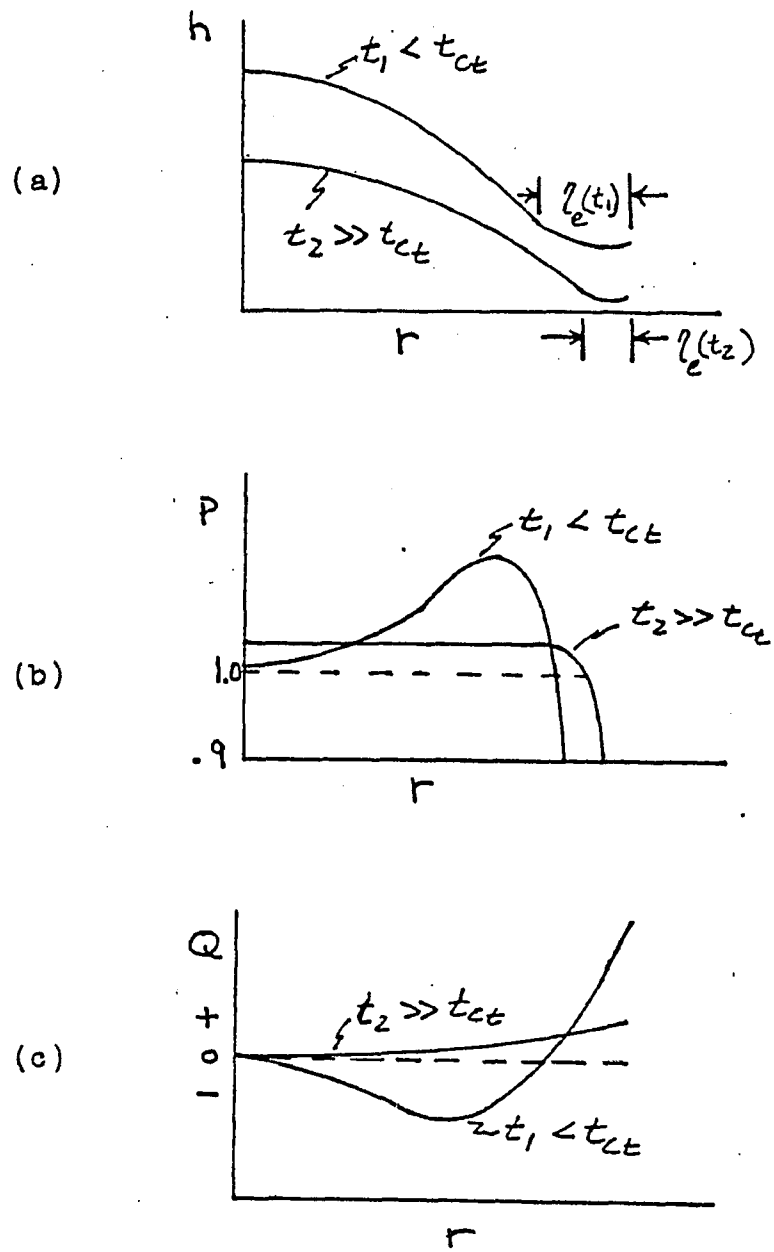

Figure III-2 Schematic representation of the spatial distribution of variables for membrane squeeze film theory. (a) h vs. r, (b) P vs. r and (c) Q vs. r.

B - Formulation

Consider the transverse motion of the membrane boundary of a fluid filled cell which squeezes out the fluid film adjacent to a rigid planar surface. The initial shape for the cell is an axisymmetric body with a plane boundary, parallel to the rigid surface, and a circular edge (much like a balloon squeezed between parallel plates). The initial film thickness ϵ is thus assumed constant and chosen to be two or more orders of magnitude smaller than the cell radius.

A constant load F is applied to the cell's upper surface, as shown in figure (III-3a), which induces a uniform internal cell pressure P_c. The difference in pressure across the membrane is related to the membrane tension and local membrane curvature.

For a film thickness h which is two or more orders of magnitude smaller than the near contact radius a and a vorticity diffusion time h^2/ν which is much less than the characteristic time for the draining of the film, the flow field may be assumed quasi-steady with a time and spatially varying film thickness. The fluid film is regarded as incompressible and radially symmetric so that the continuity and radial momentum equations are

$$\frac{1}{r}\frac{\partial ur}{\partial r} + \frac{\partial w}{\partial z} = 0 \qquad \text{(III-1)}$$

$$\frac{1}{\mu}\frac{\partial P}{\partial r} = \nabla^2 u - \frac{u}{r^2} \qquad \text{(III-2a)}$$

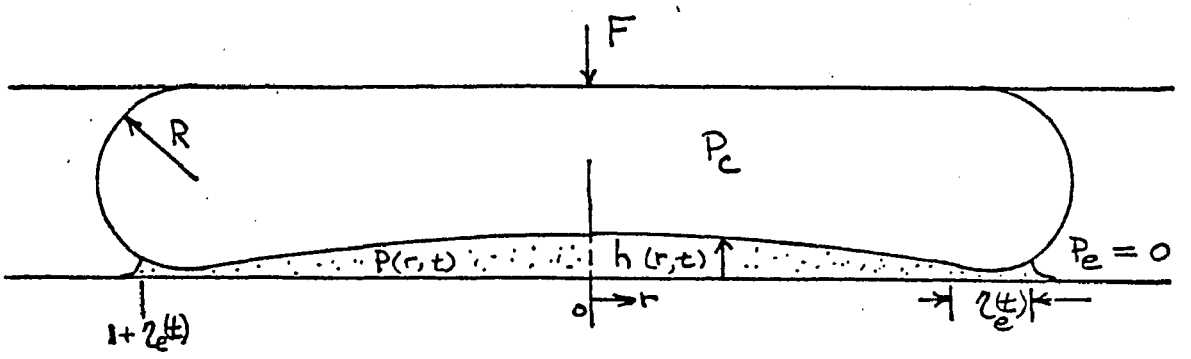

Figure III-3a Geometry for the membrane squeeze film theory.

where P is the fluid pressure u and w are the fluid velocity components in the radial and axial directions, respectively, and μ is the fluid viscosity.

If the term u/r^2 in equation (III-2a) is replaced by its expression from (III-1) and the approximations made that $w \ll u$ and $\frac{\partial}{\partial r} \ll \frac{\partial}{\partial z}$ in the resulting expression for the viscous stress, one obtains

$$\frac{1}{\mu} \frac{\partial P}{\partial r} = \frac{\partial^2 u}{\partial z^2} \qquad \text{(III-2b)}$$

Similarly, for the axial component of the momentum equation we assume that the fluid pressure is constant across the film thickness

$$\frac{\partial P}{\partial z} = 0 \qquad \text{(III-3)}$$

According to equation (III-3) pressure is not a function of z, so that the velocity u may be obtained by intrgrating equation (III-2b) twice. Applying the no-slip boundary condition at the planar surface z=0 and at the membrane boundary z=h(r,t) yields

$$u = \frac{1}{2\mu} \frac{\partial P}{\partial r} \left[z^2 - z\, h(r,t) \right], \qquad \text{(III-4a)}$$

where h(r,t) is the time dependent film thickness. For the problem of two cells squeezing out a fluid film between them, with the midplane between cells at z=0 and h/2 the

distance from midplane to either cell, the equivalent expression to equation (III-4a) which satisfies the symmetry condition at z=0 yields

$$u = \frac{1}{2\mu}\frac{\partial P}{\partial r}\left[z^2 - \frac{h^2(r;t)}{4}\right] \qquad \text{(III-4b)}$$

The flow rate Q is obtained by integrating equation (III-4a) or (III-4b) over the area normal to the flow direction. Equations (III-4a) and (III-4b) give the same results for the flow rate.

$$Q = -\frac{\pi}{6\mu} r \frac{\partial P}{\partial r} h^3(r;t) \qquad \text{(III-5a)}$$

If the membrane bound cell were replaced by an air bubble rising, due to buoyancy, against a planar surface perpendicular to the direction of gravity the no-slip boundary condition at the interface would be replaced by $\frac{\partial u}{\partial z}\Big|_{z=h(r,t)} = 0$, if the viscosity of the air was neglected. Equation (III-5a) would then be replaced by

$$Q = -\frac{2}{3}\frac{\pi}{\mu} r \frac{\partial P}{\partial r} h^3(r;t). \qquad \text{(III-5b)}$$

The continuity equation (III-1) when multiplied by $2\pi r$ and integrated across the film thickness gives

$$2\pi \int_0^{h(r;t)} \frac{\partial u r}{\partial r}\, dz = -2\pi r w(h) \qquad \text{(III-6a)}$$

Applying the Leibnitz rule for differentiating an integral with variable limits, introducing the definition of Q and replacing the fluid velocity w(h) by the local membrane velocity $\frac{\partial h}{\partial t}$, one has

$$\frac{\partial Q}{\partial r} = -2\pi r \frac{\partial h}{\partial t} . \qquad (III-6b)$$

The tangential force balance in the plane of the membrane in the near contact area requires an equilibrium between the fluid shearing stress τ in the radial direction and the membrane tensions σ_r and σ_θ in the radial and azimuthal directions

$$r\tau = \frac{\partial(\sigma_r r)}{\partial r} - \sigma_\theta \qquad (III-7a)$$

For a fluid cell whose unstressed state is that of a flacid membrane bound body and whose membrane area is preserved under loading, it is reasonable to assume that the membrane tension is everywhere isotropic, that is $\sigma_r = \sigma_\theta = \sigma$. Also the fluid shearing stress can be simply related to the fluid film pressure by taking a force balance on a cylindrical fluid shell of thickness dr whose height varies as the local film thickness. Equation (III-7a) becomes

$$\frac{\partial \sigma}{\partial r} = \frac{h}{2} \frac{\partial P}{\partial r} + \frac{hP}{2r} \qquad (III-7b)$$

The normal force balance for a membrane which offers

no bending resistance but is subjected to an isotropic but spatially varying tensile stress produced by a distributed pressure loading can be written in invariant vector form as

$$\sigma \nabla^2 h + \nabla\sigma \cdot \nabla h = P_c - P \qquad \text{(III-8a)}$$

where P_c is the uniform internal cell pressure and $P(r,t)$ is the instantaneous local film pressure. Equation (III-8a) is valid for arbitrary small amplitude membrane deflections in which inertia effects are neglible. For axisymmetric membrane deflections equation (III-8) reduces to

$$\sigma \frac{\partial}{\partial r}\left(r \frac{\partial h}{\partial r}\right) + r \frac{\partial \sigma}{\partial r} \frac{\partial h}{\partial r} = r(P_c - P). \qquad \text{(III-8b)}$$

Equations (III-5) through (III-8) differ from the formulation of elastohydrodynamic squeeze film theory (Christensen, 1962 and Rohde et al, 1976) in that equations (III-7) and (III-8) relating the pressure and membrane tension replace the pressure induced elastic deformation relation for a linearly elastic solid. Equations (III-5) through (III-8) provide four coupled non-linear equations for Q, P, σ and h.

The boundary conditions on equations (III-5) through (III-8) are

$$\frac{\partial h(0,t)}{\partial r} = 0 \qquad \text{(III-9a)}$$

$$Q(0,t) = 0 \qquad \text{(III-9b)}$$

$$P(a,t) = P_e \qquad \text{(III-9c)}$$

$$\frac{\partial^2 h(a,t)}{\partial r^2} = \frac{1}{R} \qquad \text{(III-9d)}$$

$$\sigma(a,t) = \sigma_e = (P_c - P_e)R \qquad \text{(III-9e)}$$

where a is the edge of the near eontact area, P_e is the constant exit pressure, R is the constant radius of curvature of the static outer region and σ_e is the membrane tension at the edge of the near contact area.

Boundary condition (III-9a) is the symmetry condition of the highly flexible membrane and equation (III-9b) represents the vanishing flow rate at the origin of the lubricating film. The pressure boundary condition at r=a (III-9c) requires the film pressure to reach the value of the constant exit pressure at the edge of the cell. Boundary conditions (III-9d) and (III-9e) represent the

requirements that the membrane returns to the curvature of the static outer edge and the membrane tension be continuous with the tension developed in the static outer edge. Equation (III-9e) is Laplace's law applied at the edge of the near contact area where the radius of curvature in the azimuthal plane normal to the membrane is assumed to be much larger than R. The initial condition is

$$h(r,0) = h_0. \qquad \text{(III-9f)}$$

To simplify the boundary value problem defined by equations (III-5) through (III-8) and boundary conditions (III-9) we shall first perform an order of magnitude analysis to identify the important time and length scales in the problem.

B1 - Order of magnitude analysis

For a cell that has an edge radius of curvature R, the tension force σ is of order $(P_c - P_e)$ R where P_e is the constant exit pressure, taken to be zero. Defining ϵ as the ratio of initial film thickness h(r,0) to near contact radius a, where $\epsilon << 1$, one can show after scaling all variables in equation (III-7b) by their characteristic values and rewriting in dimensionless form that $\frac{\partial \sigma}{\partial r} = 0$ to $O(\epsilon \frac{a}{R})$.

Equations (III-8a) and (III-8b) provide two order of magnitude relations for the pressure gradient in the inner region of the lubricating film.

$$\frac{\partial P}{\partial r} \sim O\left(\frac{Q_c}{\beta a h^3}\right) \qquad \text{(III-10a)}$$

and

$$\frac{\partial P}{\partial r} \sim O\left(\frac{P_c R h}{a^3}\right), \qquad \text{(III-10b)}$$

respectively. Here Q_c is the characteristic flow rate and $\beta = \frac{\pi}{6\mu}$. Equating (III-10a) and (III-10b) one finds

$$Q_c \sim O\left(\frac{P_c \beta R h^4}{a^2}\right). \qquad \text{(III-11)}$$

The characteristic time for draining the fluid film is obtained from equation (III-6) as

$$t_c \sim O\left(\frac{a^2 h}{Q_c}\right) \qquad \text{(III-12a)}$$

or from result (III-11)

$$t_c \sim O\left(\frac{a^4}{P_c \beta R h^3}\right) \qquad \text{(III-12b)}$$

Equation (III-12b) applies on the length scale a in the inner region of the film.

Since the film pressure must decrease to zero at the exit, the above analysis indicates a region of order a in which the pressure is slowly changing and a smaller region near the edge of the cell in which the pressure gradient is more rapidly varying. For this latter region h_{rr} is of order 1/R. Differentiating equation (III-8b), one obtains an order of magnitude estimate of the pressure gradient in the edge region

$$\frac{\partial P}{\partial r} \sim O\left(\frac{\sigma h_{rr}}{a}\right) \qquad \text{(III-13a)}$$

or since $\sigma = O(P_c R)$

$$\frac{\partial P}{\partial r} \sim O\left(\frac{P_c}{a}\right) \qquad \text{(III-13b)}$$

Using result (III-13b) in (III-5a) gives

$$Q \sim O(P_c \beta h^3). \qquad \text{(III-14)}$$

A second characteristic time t_{ct} is introduced when this new expression for Q is introduced into equation (III-12a).

$$t_{ct} \sim O\left(\frac{a^2}{P_c \beta h^2}\right). \qquad \text{(III-15)}$$

The characteristic time t_{ct} defined by (III-15) is of $O(\epsilon R/a)$ shorter than the characteristic time t_c defined by (III-12b).

To help the reader understand the difference between the two characteristic times, given by equations (III-12b) and (III-15), consider a rigid circular disk of radius a and a planar surface separated by a fluid film of thickness h. The fluid film is drained by pushing the disk with a constant force F directed along the axis of the disk toward the planar surface. A weighted average pressure P_c is defined as the force divided by the area in contact with the fluid film. One can easily show for this situation that the characteristic time for draining is identical to the expression given by equation (III-15). In the case of a fluid film being squeezed by a membrane bound cell the characteristic time given by equation (III-15) is the time it takes for the edge region to form, thus trapping fluid in the interior of the near contact area. The characteristic time given by equation (III-12b) is the time it takes

to drain this trapped fluid from the inner region.

The characteristic length η of this edge region is obtained from equation (III-8b). Since the pressure difference across the membrane in this region is of order P_c and the tension force is of order $P_c R$, one can show from equation (III-8b), if $\frac{\partial^2 h}{\partial r^2}$ is approximated by h/η^2, that

$$\eta \sim O\left[(Rh)^{1/2}\right]. \qquad \text{(III-16)}$$

This is a small part of the near contact radius a.

Due to the fact that the gradient of the membrane's tension force is zero to order $\epsilon a/R$ in the near contact area, and $\epsilon \ll 1$, equation (III-7b) will be approximated by

$$\frac{\partial \sigma}{\partial r} = 0 \;, \quad r<a. \qquad \text{(III-17)}$$

Thus for $r<a$ σ will be assumed uniform with its value determined by the edge condition (III-9e). To this same order equation (III-8b) will be approximated by

$$\sigma \frac{\partial}{\partial r}\left(r \frac{\partial h}{\partial r}\right) = r(P_c - P) \qquad \text{(III-18)}$$

Approximation (III-17) thus reduces the problem to the solution of equations (III-5a), (III-6) and (III-18) for the variables h, P and Q.

The existance of a small region in which the pressure is rapidly changing and a considerably larger region in

which the variables are slowly changing is conducive to a two region approximation of the near contact area. The full non-dimensionalized form of equations (III-5a), (III-6) and (III-18) will be solved for the inner region, whereas for the smaller edge region an approximate integral formulation will be developed.

Equations (III-5a), (III-6) and (III-18) are now non-dimensionalized using the following definitions;

$$r^* = \frac{r}{a} \qquad \text{(III-19a)}$$

$$h^* = \frac{h}{a} \qquad \text{(III-19b)}$$

$$p^* = \frac{p - p_e}{p_c - p_e} \qquad \text{(III-19c)}$$

$$\sigma^* = \frac{\sigma}{(p_c - p_e)R} \qquad \text{(III-19d)}$$

$$R_1^* = \frac{R}{a} \qquad \text{(III-19e)}$$

$$Q^* = \frac{Q}{\beta a^3 (P_c - P_e)} \qquad \text{(III-19f)}$$

$$T^* = \frac{t}{\left[\frac{1}{\beta (P_c - P_e)}\right]} \; . \qquad \text{(III-19g)}$$

Dropping the ()* notation, for convenience, the non-dimensional equations are

$$Q = - r \frac{\partial P}{\partial r} h^3 \qquad \text{(III-20a)}$$

$$\frac{\partial Q}{\partial r} = - 2\pi r \frac{\partial h}{\partial T} \qquad \text{(III-21a)}$$

$$r(1-P) = R1 \frac{\partial}{\partial r}\left(r \frac{\partial h}{\partial r}\right) \qquad \text{(III-22a)}$$

where R1 is the non-dimensional aspect ratio of the cell (radius of curvature of the outer region to radius of the near contact area).

The beginning of the edge region is arbitrarily chosen as the unknown location where P=1. This choice is convenient since the left hand side of equation (III-22a)

vanishes at this location and thus provides convenient matching conditions for the edge profile. The inner region is the bulk of the near contact region and terminates at r=1- η_e (T), where η_e (T) is the time dependent edge region size. This inner region-edge region interface is approximated to be at r=1 on the inner length scale because the computer program for the numerical solution of the inner region requires a fixed length. This approximation is consistent with the method of matched asymptotic expansions, where the larger scale is kept constant and the smaller scale is allowed to vary. The boundary and matching conditions for the inner region are;

$$\frac{\partial h(0,T)}{\partial r} \qquad \text{(III-23a)}$$

$$h(1,T) = H_o(T) \qquad \text{(III-23b)}$$

$$P(1,T) = 1 \qquad \text{(III-23c)}$$

$$Q(0,T) = 0 \; . \qquad \text{(III-23d)}$$

The initial conditions are:

$$h(r,0) = \epsilon \qquad \text{(III-24a)}$$

$$P(r,0) = 1 \qquad \text{(III-24b)}$$

$$Q(r,0) = 0 \qquad \text{(III-24c)}$$

$$H_o(0) = \epsilon \qquad \text{(III-24d)}$$

where $H_o(T)$ is the time dependent film thickness at the interface of the two regions. The value of $H_o(T)$ is obtained by matching the solutions from the inner and edge regions at each instant in time.

B-2 Treatment of the edge region

For the edge region, figure III-3b, a new coordinate η is defined as

$$\eta = r - 1 \; ; \quad [1 \leq r \leq 1 + \eta_e(T)]. \qquad \text{(III-25)}$$

Using the above definition, the governing equations (III-20a), (III-21a) and (III-22a) may be rewritten as

$$Q(\eta,T) = -(1+\eta)\frac{\partial P}{\partial \eta} h^3(\eta,T) \qquad \text{(III-20b)}$$

$$\frac{\partial Q}{\partial \eta} = -2\pi(1+\eta)\frac{\partial h}{\partial T} \qquad \text{(III-21b)}$$

$$(1+\eta)(1-P) = Rl \frac{\epsilon}{\partial \eta}\left[(1+\eta)\frac{\partial h}{\partial \eta}\right]. \qquad \text{(III-22b)}$$

The mathematical description of the edge region can be simplified by using an approximate integral formulation. A polynomial profile for pressure is assumed in the edge region

$$P(\eta,T) = C_1 + C_2\eta + C_3\eta^2 \qquad \text{(III-26)}$$

which satisfied the following matching and boundary conditions;

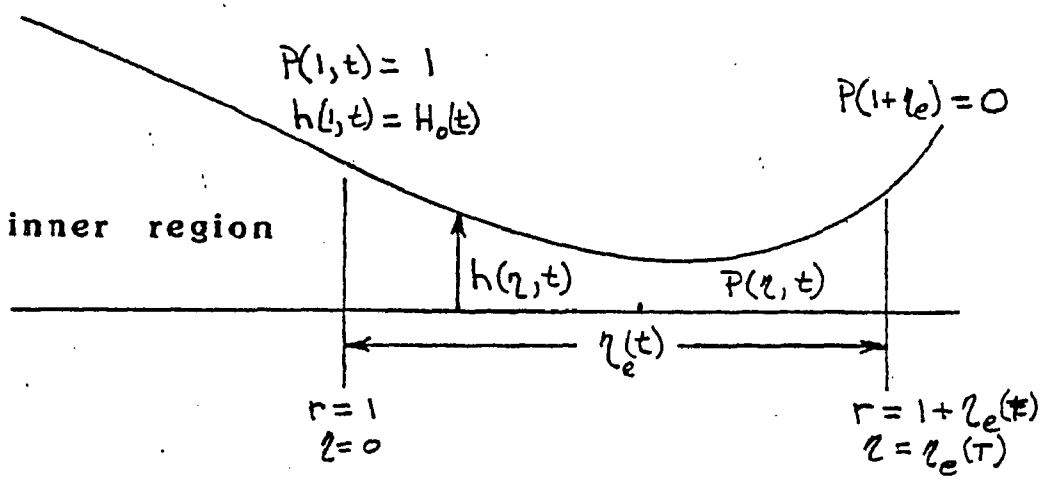

Figure III-3b Geometry for the edge region of the near contact area.

$$P(0,T) = 1 \qquad \text{(III-27a)}$$

$$\frac{\partial P(0,T)}{\partial \eta} = P_{o\eta}(T) \qquad \text{(III-27b)}$$

$$P(\eta_e(T),T) = 0\,, \qquad \text{(III-27c)}$$

where $P_{o\eta}(T)$ is the pressure gradient at the interface of the two regions, obtained from the inner region solution at r=1. The resulting expression for $P(\eta,T)$ is given by

$$P(\eta,T) = 1 + P_{o\eta}(T)\eta - \gamma(T)\eta^2, \qquad \text{(III-28)}$$

where

$$\gamma(T) = \frac{1 + P_{o\eta}(T)\,\eta_e(T)}{\eta_e^2(T)}\,. \qquad \text{(III-29)}$$

The membrane profile in the edge region is obtained by integrating the normal force balance equation (III-22b) twice using the pressure profile from equation (III-28). The resulting expression contains two coefficients which are found using the following interface matching conditions;

$$h(r=1,T) = H_o(T) = h(\eta=0,T) \qquad \text{(III-30a)}$$

$$\frac{\partial h(r=1,T)}{\partial r} = H_{o\eta}(T) = \frac{\partial h(\eta=0,T)}{\partial \eta}, \qquad \text{(III-30b)}$$

where $H_o(T)$ is the interface film thickness and $H_{o\eta}(T)$ is the membrane slope at the interface. The edge region membrane profile can then be written as

$$h(\eta,T) = H_o(T) + H_{o\eta}(T)\ln(1+\eta) + \frac{P_{o\eta}(T)}{R1}\left[\frac{\eta^3}{9} + \frac{\eta^2}{12} - \frac{\eta}{6} + \frac{1}{6}\ln(1+\eta)\right] - \frac{\gamma(T)}{R1}\left[\frac{\eta^4}{16} + \frac{\eta^3}{36} - \frac{\eta^2}{24} + \frac{\eta}{12} - \frac{1}{12}\ln(1+\eta)\right]. \qquad \text{(III-31a)}$$

Using a Taylor series expansion for $\ln(1+\eta)$, where $\eta << 1$, equation (III-31a) may be approximated by

$$h(\eta,T) = H_o(T) + H_{o\eta}(T)\left[\eta - \frac{\eta^2}{2}\right] - \frac{P_{o\eta}(T)}{R1}\left[\frac{\eta^3}{6} - \frac{\eta^4}{24}\right] + \frac{\gamma(T)}{R1}\left(\frac{\eta^4}{12} - \frac{\eta^5}{5}\right) \qquad \text{(III-31b)}$$

Since $\eta << 1$ the local membrane velocity in the edge region is approximated by (neglecting terms of order η^2 or higher)

$$\frac{\partial h}{\partial T} = \dot{H}_o(T) + \dot{H}_{o\eta}(T)\,\eta . \qquad \text{(III-32)}$$

The volume flow rate distribution in the edge region film may be obtained by integrating the continuity equation (III-21b) and using the result of equation (III-32).

$$Q(\eta,T) = Q_o(T) - 2\pi \dot{H}_o(T)\left[\eta + \frac{\eta^2}{2}\right] - 2\pi\, \dot{H}_{o\eta}(T)\left[\frac{\eta^2}{2} + \frac{\eta^3}{3}\right], \qquad \text{(III-33)}$$

where the value of the interface volume flow rate evaluated at r=1 $Q_o(T)$ is obtained from the solution of the inner region.

The momentum equation (III-20b) is now satisfied in integral form. Substituting (III-33) into (III-20b), integrating the latter across the edge region and applying the pressure boundary conditions (III-27a, c), one finds

$$1 = -2\pi \dot{H}_o I_1 + Q_o I_2 - 2\pi \dot{H}_{o\eta} I_3 , \qquad \text{(III-34)}$$

where

$$I_1 = \int_0^{\eta_e(T)} \frac{(\eta + \frac{\eta^2}{2})\, d\eta}{(1+\eta) h^3(\eta,T)} \qquad \text{(III-35a)}$$

$$I_2 = \int_0^{\eta_e(T)} \frac{d\eta}{(1+\eta)\, h^3(\eta,T)} \qquad \text{(III-35b)}$$

$$I_3 = \int_0^{\eta_e(T)} \frac{(\frac{\eta^2}{2} + \frac{\eta^3}{3})\, d\eta}{(1+\eta)\, h^3(\eta,T)} \qquad \text{(III-35c)}$$

Equation (III-34) is treated numerically as an ordinary differential equation to determine $H_o(T)$, with instantaneous values of $Q_o(T)$ and $\dot{H}_{o\eta}(T)$ considered known from the inner region solution at r=1 evaluated at the previous time step.

At this point the value of $\eta_e(T)$ is still unknown. An expression for determining $\eta_e(T)$ is obtained by requiring the momentum equation (III-20b) be satisfied exactly at $\eta = \eta_e(T)$. This has the effect of ensuring that the pressure gradient at the edge region exit provide a volume flux which is compatible with expression (III-33) evaluated at η_e. Substituting the relation for the unknown interface membrane velocity $\dot{H}_o(T)$ from equation (III-34) into (III-33) and inserting the latter into equation (III-20b) one obtains

$$Q_o(T) - 2\pi \dot{H}_{o\eta}(T)\left[\frac{\eta_e^2(T)}{2} + \frac{\eta_e^3(T)}{3}\right] -$$

$$\frac{\left[\eta_e(T) + \frac{\eta_e^2(T)}{2}\right]}{I_1}\left[Q_o(T) I_2 - 1 - 2\pi \dot{H}_{o\eta}(T) I_3\right] =$$

$$\left[1 + \eta_e(T)\right]\left[P_{o\eta}(T) + \frac{2}{\eta_e(T)}\right] h_e^3(T), \qquad \text{(III-36)}$$

where $h_e(T)$ is the film thickness at $\eta = \eta_e(T)$, from equation (III-31). Equation (III-36) is an integral equation for $\eta_e(T)$ since the limits on the integrals I_1, I_2 and I_3 defined by (III-35) are functions of $\eta_e(T)$. The solution of equation (III-36) at each time step is accomplished by a numerical trial and search procedure described in the next section.

B-3 Numerical solution procedure

The Rayleigh-Ritz-Galerkin method is used for spatial discretization of the inner region and the solution to the dependent variables are composed of a series of B-splines between spatial mesh points. This is accomplished with a partial differential equation code available from Bell Laboratories. The code package is called POST and with the addition of supporting subroutines the solution of the ordinary differential equation (III-34) may be used as a boundary condition at the inner-edge region interface.

A choice of B-spline order must be made and I chose a fourth order spline. This has the property of zero second derivatives at the ends of the inner region (at r=0 and r=1). Since the curvature of the membrane is equal to zero at these end points a fourth order spline is the logical choice. The inner region is then divided into unequally spaced nodal points, with the finer mesh near the interface of the two regions (largest gradients in this area).

To start the numerical procedure the initial conditions (III-24) are set for the variables h, P, Q and H_o. For the first few time steps the value of $\eta_e(T)$ is held constant due to the singularity of equation (III-36) for $\eta_e=0$. The value chosen for η_e during this early period is of order ϵ. The edge region size grows in time from its initial value to the characteristic size given by equation (III-16). Following this start up period equation (III-36) is interrogated for the determination of $\eta_e(T)$.

A typical iteration in time is advanced through equation (III-21a). Having established a new distribution for h(r,T) equations (III-20a) and (III-22a) are used to solve for the inner region distributions of P and Q, subject to the boundary and matching conditions of equations (III-23). In order to satisfy matching condition (III-23b) a subroutine containing the ordinary differential equation (III-34) is called. In this subroutine tentative values for $\frac{\partial h}{\partial r}$, Q, $\frac{\partial P}{\partial r}$ and $\dot{H}_{o\zeta}$ at r=1 are stored for use in determining $\zeta_e(T)$ for this iteration. Having computed a tentative value for $\zeta_e(T)$ the numerical program evaluates the definite integrals, given by equations (III-35a) through (III-35c), and equation (III-34) is solved for $H_o(T)$.

A comparison is made between the interface value of h obtained from the inner region solution and from the ordinary differential equation (III-34). If agreement does not meet the accuracy requirement imposed on the solution of all the variables the tentative time step is reduced and the iteration procedure is begun anew. When the accuracy requirement is met the time step is said to have been successful and the first iteration of the next time integration is begun.

There are typically twenty or more evaluations of equation (III-34) for convergence on a successful time step in the early period of the numerical solution and as few as three evaluations required at much later times. After the

tolerances on the dependent variables have been met the edge region distributions are solved for use in equations (III-28), (III-31) and (III-33).

A detailed discussion of the general solution procedure appears in a technical report by Schryer (1977).

C - Results and discussion

The assumption of negligable membrane bending stresses, although valid for the time scale of my solutions, is inaccurate at the edge region-outer region interface when the membrane makes contact with the rigid planar surface. Updike and Kalnins (1972) treated the problem of determining the contact pressure distribution between an elastic spherical shell and a rigid plate for a given degree of deformation. They found that as the deformation increases (corresponding to an increase in the shell coordinate α of the edge of the contact area and an increase in the discontinuous shell slope at that point) the contact pressure distribution approaches a line loading located at α. This type of pressure distribution is due to the influence of the increased slope at the edge of the contact area and of the shell bending moment at that point.

In the case of the membrane bound fluid filled cells bending stresses in the membrane become finite at the edge region-outer region interface when the interface slope becomes finite. This occurs on a time scale $t >> t_c$ and does not influence the results presented in this section. As in the problem solved by Updike and Kalnins for a shell, when the interface of the edge and outer regions of the membrane makes contact with the planar surface the interface slope becomes discontinuous with a finite value on the outer region side. On this time scale the membrane bending stress acts as a circular line load at the interface

of the edge and outer regions. This circular line load supports the portion of the applied load not supported by the contact pressure.

The solutions to the governing equations developed in section III-B are presented in non-dimensional form. The spatial variable r is renormalized with respect to the entire near contact radius $1+\eta_e(T)$. This renormalization allows the change in interface location to be viewed from the perspective of a constant near contact radius. Since time is normalized with respect to the fluid viscosity and the pressure difference across the outer region membrane, the solutions at a given time may be compared for each case to see the influence that the cell's aspect ratio R1 has on the draining behavior of the fluid film. The initial film thickness ϵ used for all of the numerical solutions is equal to 10^{-2} because this magnitude is representative of the film thickness seen in the applications mentioned earlier. Four values of the aspect ratio R1 are used, varying from 0.25 to 2.0, with the smaller aspect ratio representing a relatively flat cell.

The numerical solution of the fluid trapping phase requires approximately 30 minutes of computation time. The numerical solution to describe the long time draining of the trapped fluid to roughly 30 per cent of its initial thickness takes approximately 2 hrs. of IBM-370 computing time for a cell with an aspect ratio equal to 2.0. For decreasing values of the aspect ratio the computing time

required to obtain a given degree of membrane collapse increases. When the aspect ratio of the cell is equal to 0.25 the numerical solution uses approximately 3 hrs. of computation time to obtain a draining of the origin film to 80 per cent of its initial value. A more efficient computational scheme to describe the long time drainage needs to be developed for future calculations.

C-1 The film thickness

The graphs in figures III-4 through III-7 show the solutions for the time varying film thickness between a rigid planar surface and a membrane bound cell with the aspect ratio varying from 2.0 to 0.25, respectively. To obtain the membrane shape for the problem of a fluid film being squeezed between two membrane bound cells figures III-4 through III-7 would be replotted by halving the film thickness at any time T. The horizontal axis of the replotted graph would then be the plane of symmetry between the two cells. No replotting is necessary for the case of an air bubble rising against a planar surface. The difference between this problem and the membrane bound cell enters in the value of β. For the membrane problem $\beta = \frac{\pi}{6\mu}$, whereas for the bubble problem $\beta = \frac{2\pi}{3\mu}$. From the definition of the non-dimensional time

$$T = \frac{t}{\left[\frac{1}{\beta(P_c - P_e)}\right]} \qquad \text{(III-37)}$$

and the values of β for these two situations it is apparent that an air bubble will drain a fluid film four times faster than a membrane bound cell under identical conditions (ie; $P_c - P_e$, R1, ϵ and μ). Physically this difference in draining time is connected to the boundary conditions at the cell and bubble surface. The interface between an air bubble and the lubricating film cannot support a fluid shear stress when the viscosity of air is neglected. The shear

stress on the surface of a cell membrane tends to retard the fluid motion.

The time history of the fluid film with an aspect ratio for the cell equal to 2.0 appears in figure III-4. Each time curve is the location of the membrane with the horizontal axis representing the rigid planar surface. This figure shows the membrane in the vicinity of the edge of the near contact area collapsing much more rapidly than the membrane in the inner region, thus temporarily trapping a considerable volume of fluid in the inner region.

As the membrane near the edge descends on upward bulge in the membrane develops between the origin and the edge region. The film thickness in the area of the bulge is greater than the initial film thickness. The bulge migrates toward the origin and increases in height as time passes. After the bulge reaches the origin the entire membrane begins to descend toward the planar surface monotonically. The time that corresponds to this maximum film thickness at the origin is of the same order as the characteristic time for fluid trapping t_{ct}, from equation (III-37).

The dots on each curve in figures III-4 through III-7 indicate the location of the inner region-edge region interface. The edge region grows inward during the early period of the draining process. After the fluid trapping has occurred the size of the edge region begins to decrease. This suggests that as T approaches infinity the edge region

will vanish and the film thickness will approach zero for the entire near contact area.

The membrane velocity decays quite rapidly after the trapping period is over. Figure III-4 shows that it takes three or more orders of magnitude in time to drain the trapped fluid than it took to trap it. This is an expected result based on the order of magnitude analysis of section III-B-1.

Figures III-5, III-6, and III-7 (for aspect ratios equal to 0.75, 0.50 and 0.25, respectively) exhibit the same qualitative features as figure III-4. In comparing these figures it is apparent that for smaller values of the aspect ratio R1 it takes a longer time to trap and to drain the fluid film.

A comparison of the two extreme cases of aspect ratio is instructive. Figures III-4 (R1=2.0) and III-7 (R1=0.25) show that it takes nearly an order of magnitude longer time to complete the trapping period for the cell with the smaller value of R1. The maximum film thickness is larger for the cell with an aspect ratio of 0.25. This is due to the relatively shorter time it takes to form the edge region, for small R1, during the early phase of the membrane collapse. This relatively rapid collapse of the edge region traps a larger volume of fluid in the inner region. A longer transit time is required for this larger fluid bulge to migrate to the origin. This is the reason for the longer trapping time, although the edge region

forms more quickly. Figure III-7 also shows that for an aspect ratio of 0.25 the edge region film thickness reaches 10 per cent of its initial value at $T = 1.11 \times 10^4$, while the maximum film thickness is reached at $T = 3.41 \times 10^5$. For an aspect ratio of 2.0 figure III-4 indicates that the edge region film reaches a value equal to 10 per cent of its initial thickness after the maximum film thickness is reached at the origin, the respective times are $T = 1.74 \times 10^5$ and $T = 3.32 \times 10^4$.

Finally, in the time it takes for the origin film thickness to drain to 57 per cent of its initial value for a cell with an aspect ratio of 2.0 the smaller aspect ratio cell has drained to 149 per cent of its initial thickness from a maximum of 170 per cent. One can therefore conclude that under similar conditions a cell with a smaller aspect ratio, but same near contact radius a, will take longer time to drain a lubricating film adjacent to a planar surface.

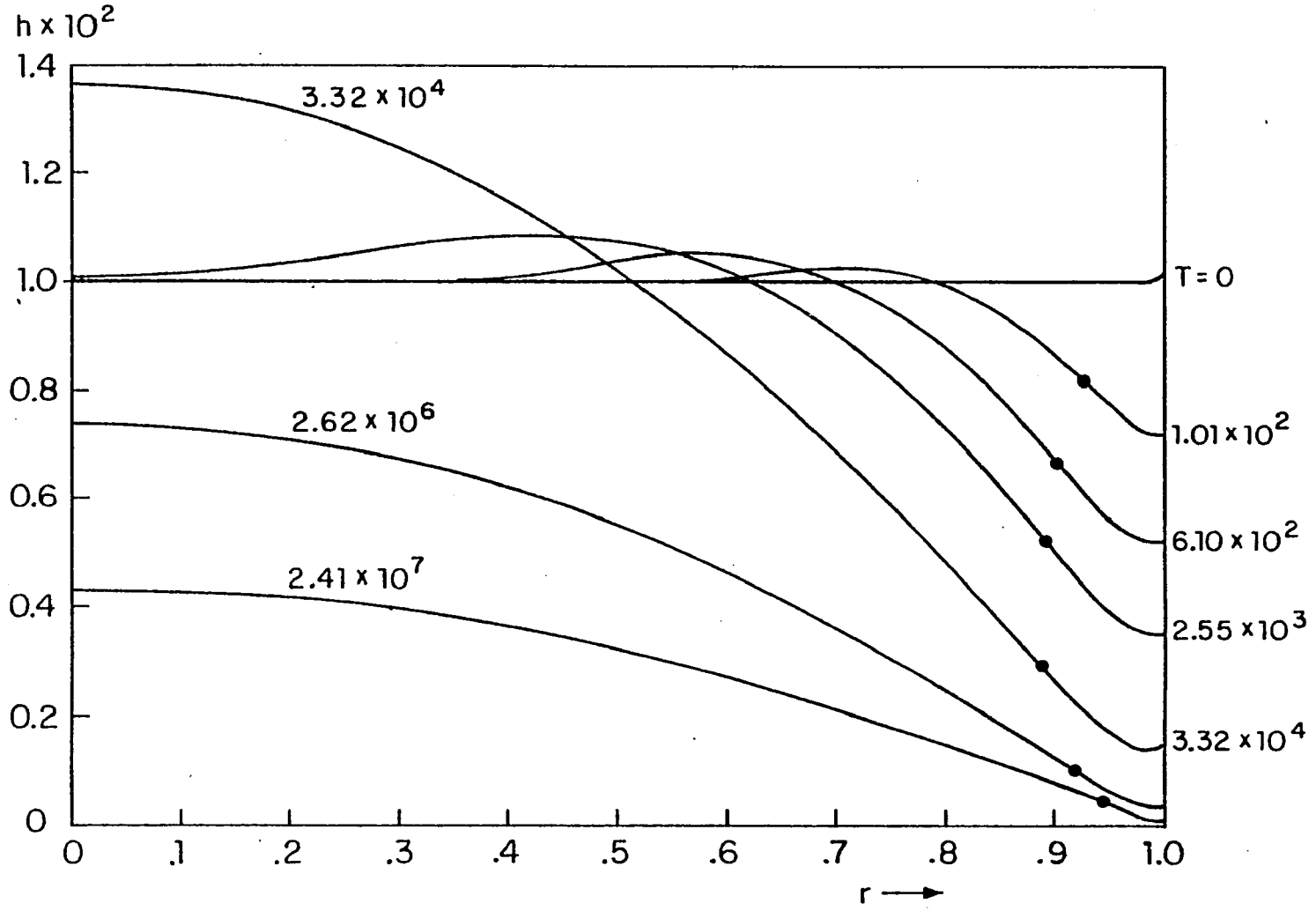

Figure III-4 Film thickness profiles, R1=2.0.

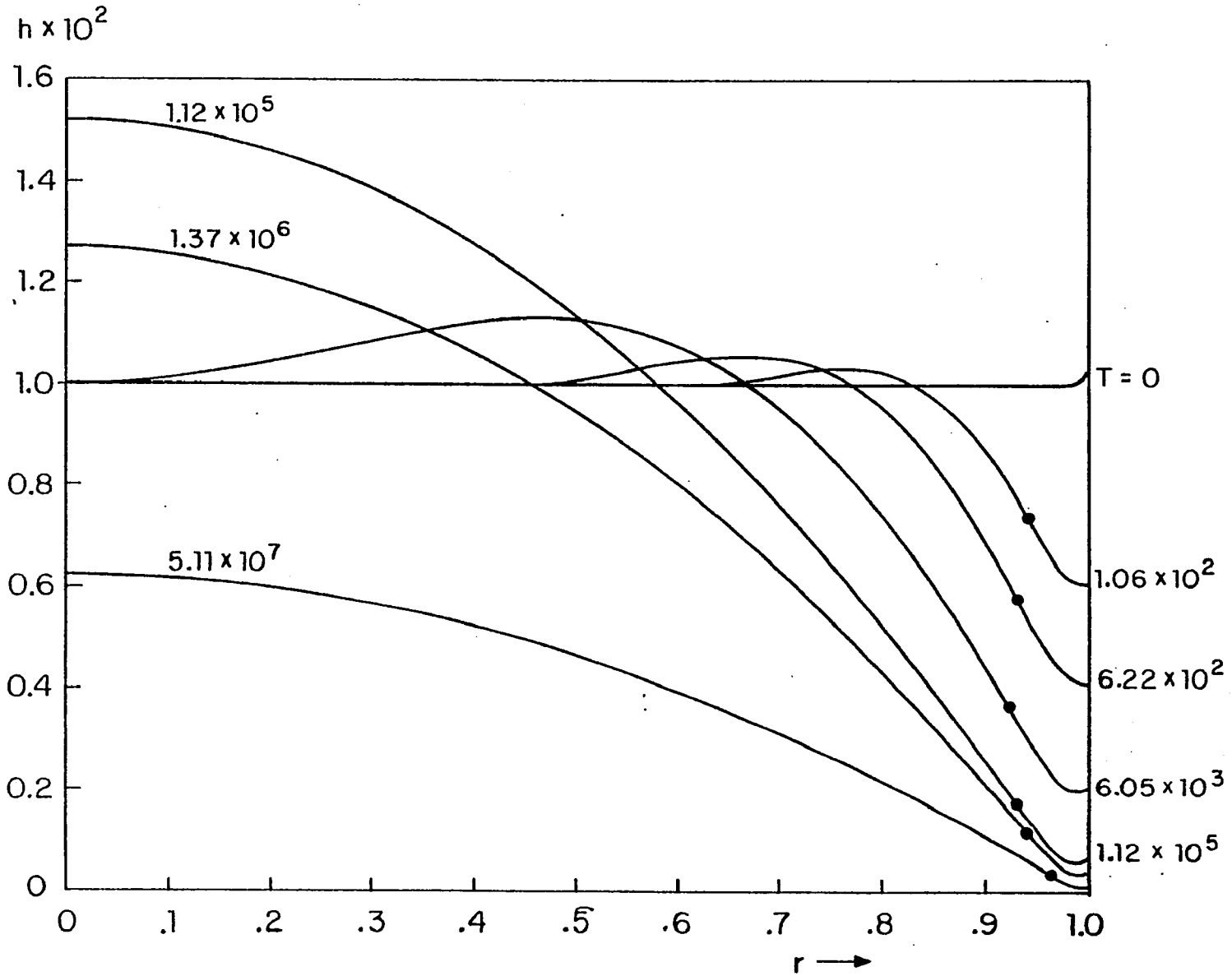

Figure III-5 Film thickness profiles, R1 = 0.75.

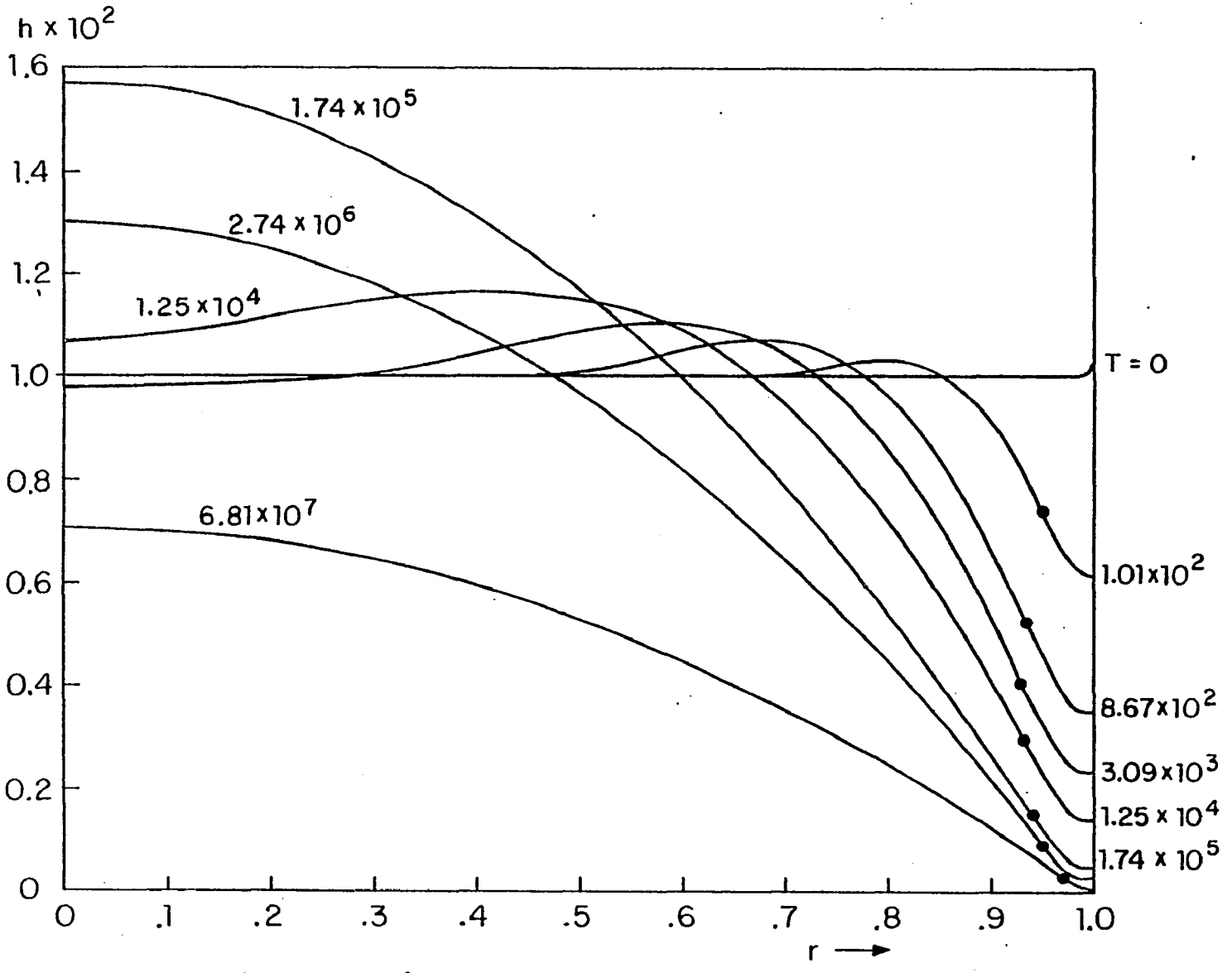

Figure III-6 Film thickness profiles, R1 = 0.50.

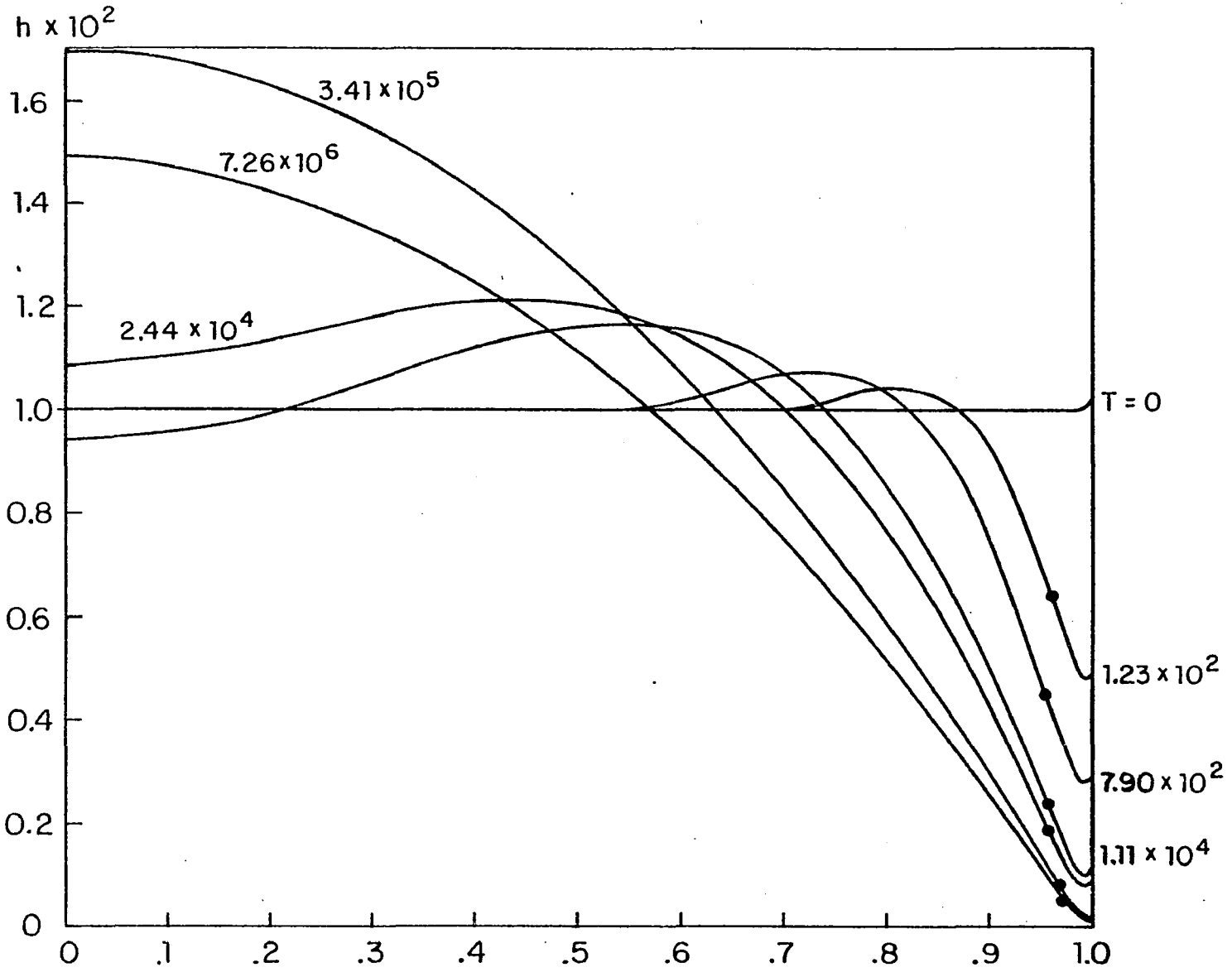

Figure III-7 Film thickness profiles, R1 = 0.25.

C-2 The pressure distribution in the film

When the load is applied to the cell's upper surface a uniform internal cell pressure P_c is produced which causes the edge of the cell to collapse toward the planar surface quite rapidly. The fluid film responds by generating a pressure larger than P_c just next to the edge region, as shown in figures III-8 through III-11. As the draining of the near contact area continues the magnitude of the pressure peak decreases and its location moves toward the origin. A pressure trough is also generated and it lies in the region between the origin and the pressure peak. This minimum pressure point moves toward the origin much more quickly than the pressure peak. Once the pressure trough reaches the origin the pressure in the film begins to increase near the origin and decrease in the vicinity of the pressure peak.

At the time when the film thickness attains its maximum value at the origin the pressure distribution takes on a characteristic plateau shape that will be maintained for the duration of the draining process. As the draining process continues the length of the plateau pressure region increases, while its magnitude slowly decreases.

Figure III-8 shows the time history of the pressure distribution for an aspect ratio equal to 2.0, with P normalized using equation (III-19). The peak pressure for each time curve corresponds with the location of the reverse flow point, which will be fully described in the

next subsection. The pressure plateau is attained at a time $T = 3.32 \times 10^4$, which corresponds with the characteristic time for fluid trapping. The magnitude of the pressure plateau at this time is 1.09. As discussed earlier the decay of the pressure plateau occurs on a time which is several orders of magnitude longer that the fluid trapping time. One observes in figure III-8 that after three orders of magnitude later in time the pressure plateau has an appreciable value of 1.03.

The point at which the pressure curves intersect the $P = 1$ line is the location of the interface between the inner region and edge region. Figure III-8 clearly shows that after the pressure plateau is formed the interface migrates outward and the plateau occupies an ever increasing area.

In figure III- 9 is plotted the time varying pressure distribution for an aspect ratio of the cell equal to 0.75. In comparing the results for pressure in figures III-8 and III- 9 one notices that the qualitative features in figure III-8 are present in figure III- 9. The smaller aspect ratio cell produces a smaller pressure peak and the magnitude of this pressure peak controls the rate of membrane collapse in the edge region.

As was mentioned in the previous subsection the cell with an aspect ratio of 0.25 formed its edge region more quickly than the other cases. Figure III-11 shows that at this aspect ratio the magnitude of the pressure peak is

the smallest of all the cases studied. Therefore, the resisting force on the membrane is smaller allowing the edge region membrane to collapse at a faster rate. The smaller pressure peak also produces a correspondingly smaller magnitude for the pressure plateau, after the fluid trapping phase has been completed. This lower level pressure plateau is responsible for the longer draining times for a fluid film being squeezed by a flatter cell. With a larger volume of fluid trapped and a longer draining time for this fluid, the membrane velocity must be smaller in the case of a flatter cell. The discussion on the film thickness bears this out, that is, the rate of descent of the membrane is slower for a cell with a smaller value of edge region radius of curvature.

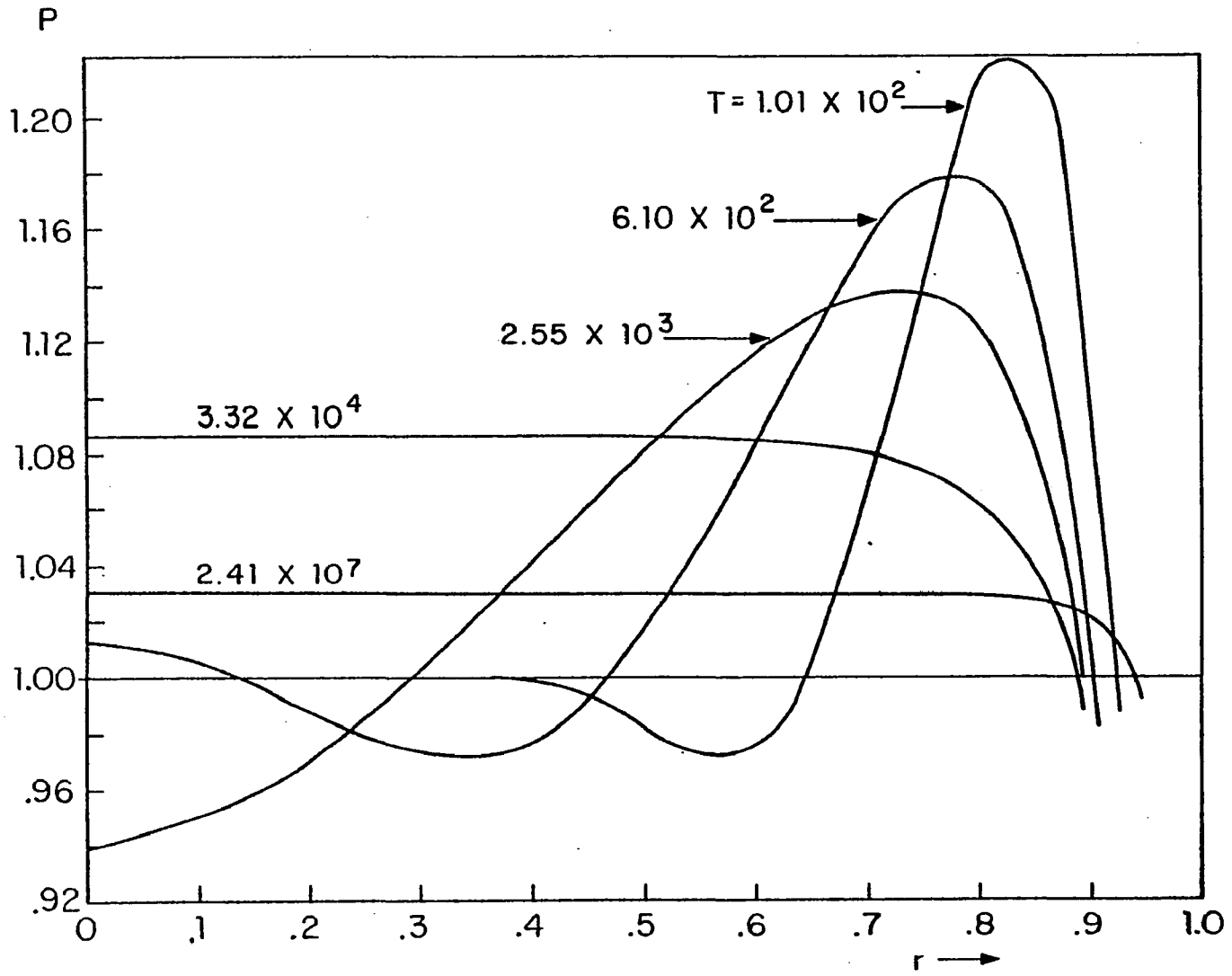

Figure III-8 Pressure distributions in the fluid film, R1 = 2.0.

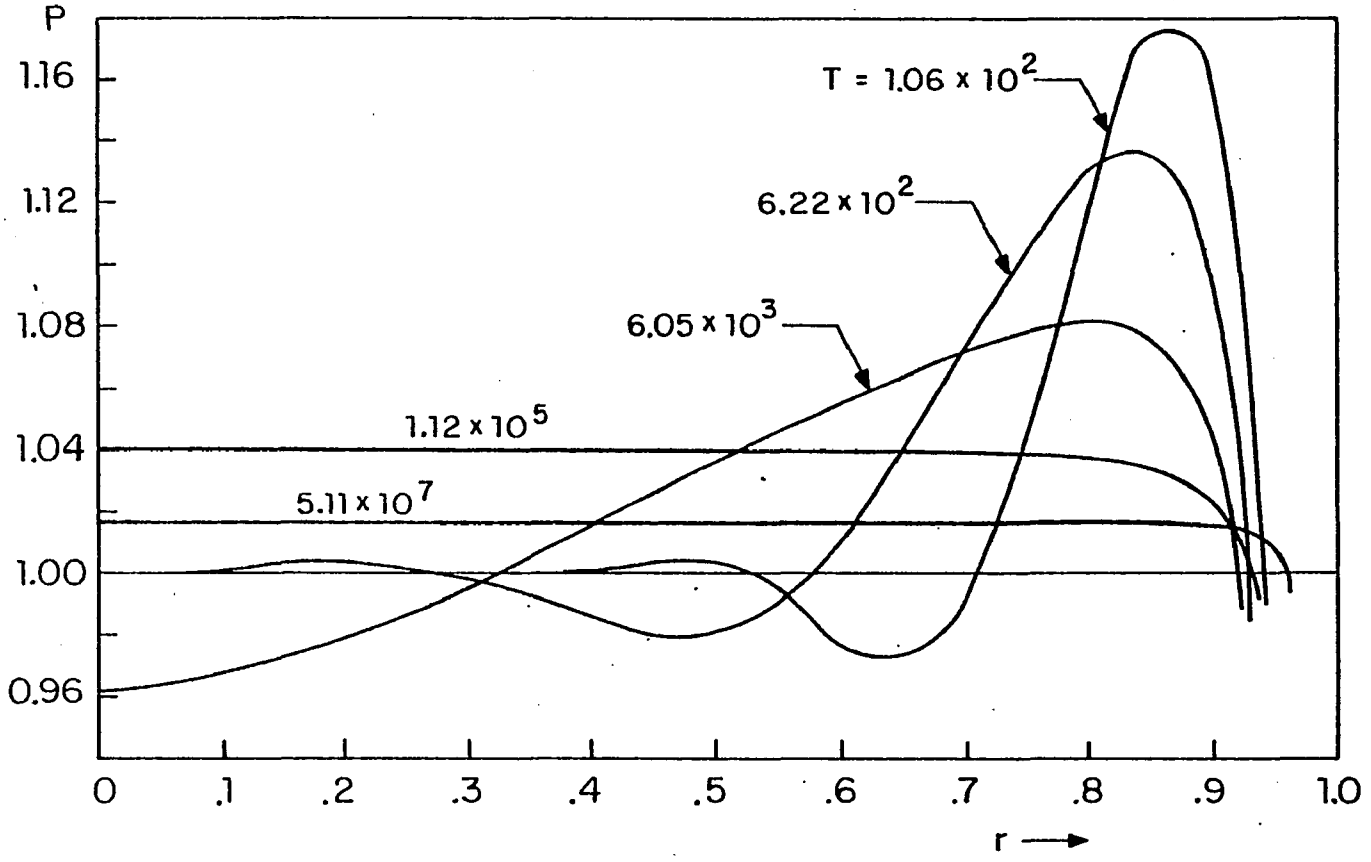

Figure III-9 Pressure distributions in the fluid film, R1 = 0.75.

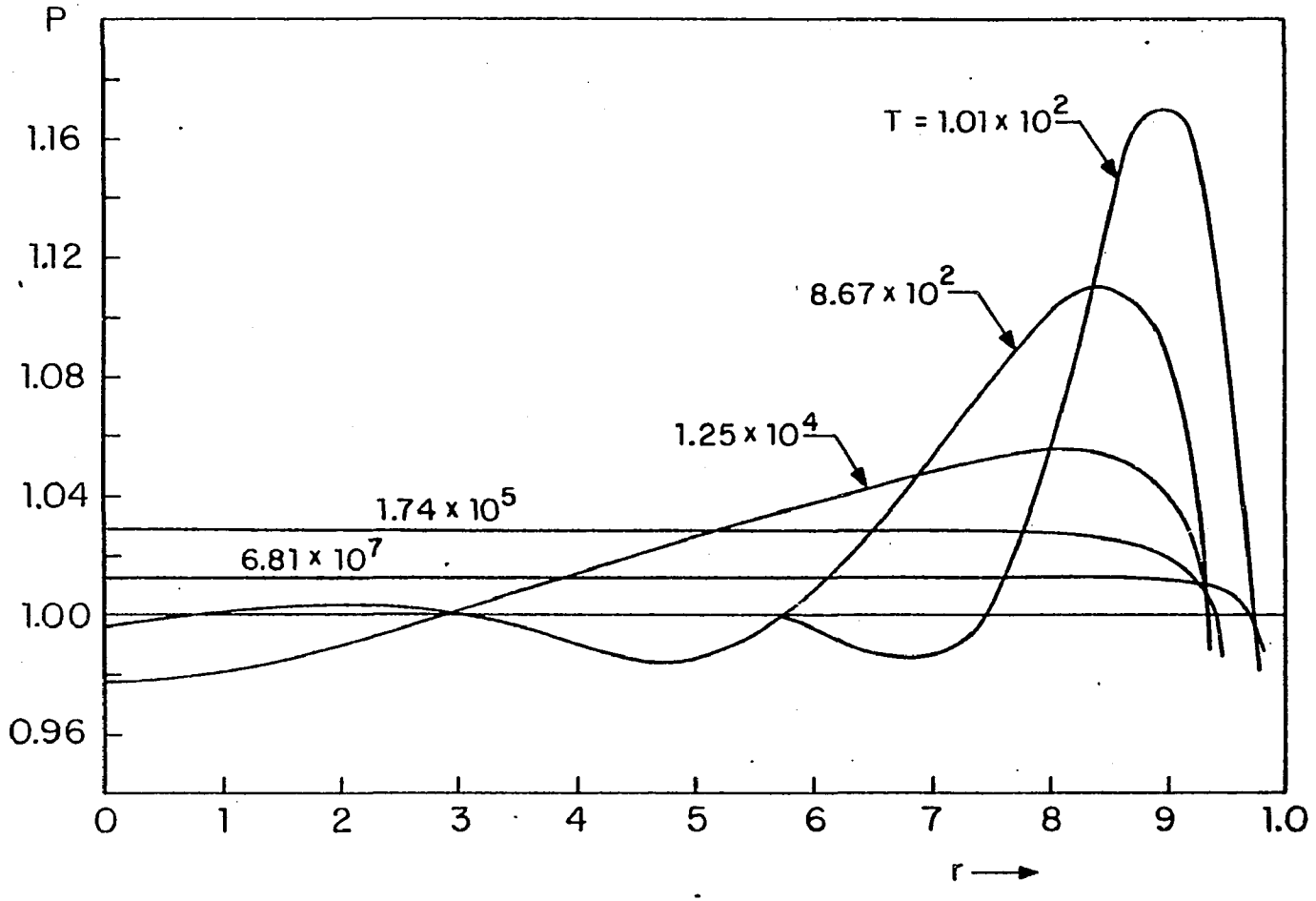

Figure III-10 Pressure distributions in the fluid film, R1 = 0.50.

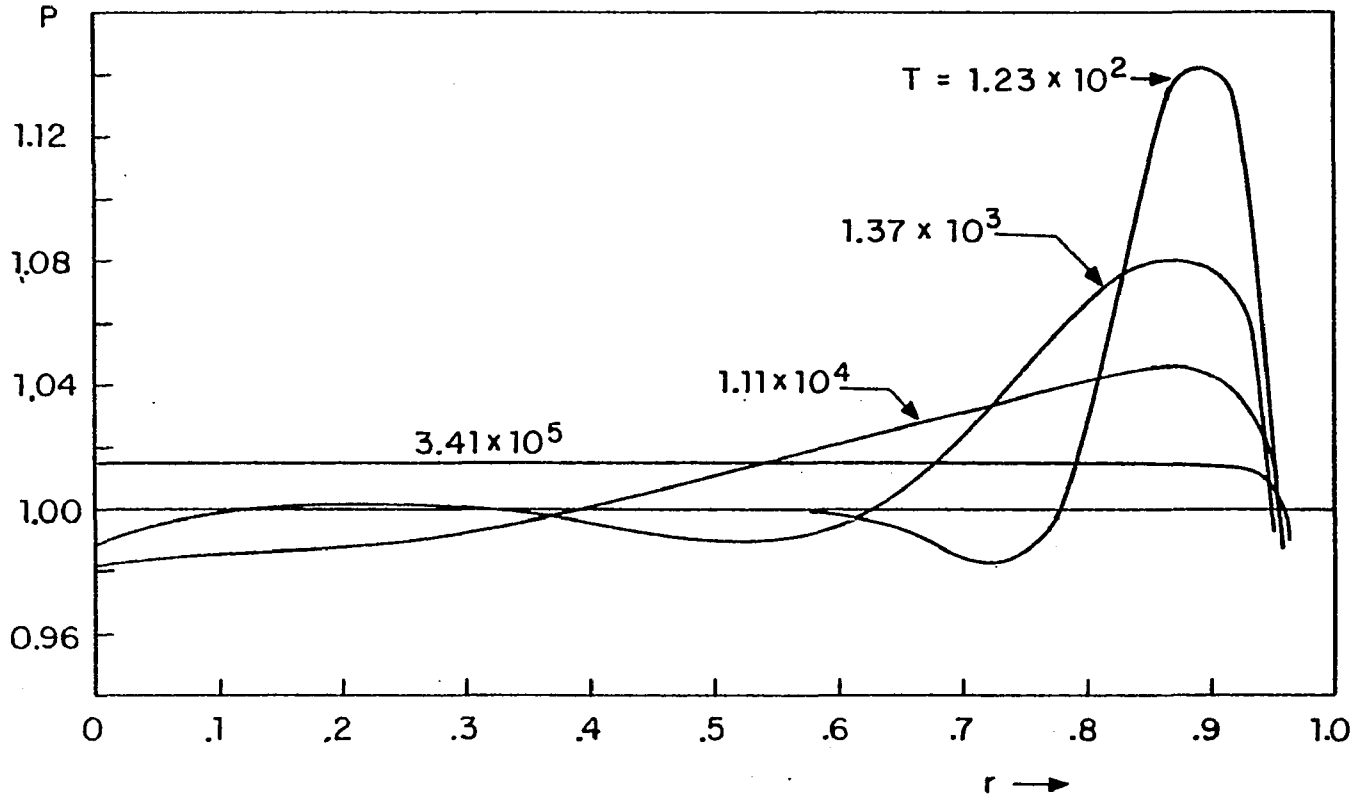

Figure III-11 Pressure distributions in the fluid film, R1 = 0.25.

C-3 The volume flow rate

For each value of the aspect ratio there are two graphs for the volume flow rate Q. The first for each case is the volume flow rate for the time period before trapping of the fluid is complete, as can be seen in figures III-12, III-14, III-16 and III-18a. All of these figures show a bidirectional flow pattern for times less than the characteristic time for fluid trapping. This phenomena is not seen in elastohydrodynamic squeeze film theory, where the flow rate is always positive in the radial direction.

In figure III-12 are the results for $Q \times 10^6$ with a cell aspect ratio equal to 2.0. The first value of T plotted in this figure is 6.10×10^2. At this early time the minimum fluid gap in the edge region has drained to 53 per cent of the initial film thickness. The negative volume flow rate during this early period causes the gradual thicknening of the fluid film near the origin that is seen in the film thickness profiles. As time passes the decrease in the local pressure gradient causes a corresponding decrease in the local volume flow rate.

A comparison of the exit volume flow rate (at r = 1) for the various cases shows that at a given time following the application of the load a flatter cell will have a smaller exit flow rate. This is consistent with the larger draining time required for the flatter cell. Another feature that is apparent in comparing the results for the

different values of R1 is that for a larger value of R1 the location of the flow bifurcation point is closer to the origin. At T equal to 6×10^2 figure III-12 (R1 = 2.0) shows this point to be at r = 0.77 and figure III-18a (R1 = 0.25) shows this point to be at r = 0.88. This is due to the smaller edge region size produced by the cell with a smaller aspect ratio. The smaller edge region produces a maximum pressure closer to the outer edge of the cell and this point coincides with the location of the flow bifurcation point.

After the membrane has completed its fluid trapping phase the volume flow rate becomes positive at every location, this is seen in figures III-13, III-15, III-17 and III-18b. In figure III-13 are the results for $Q \times 10^7$, when the cell's aspect ratio is equal to 2.0. At $T = 3.3 \times 10^4$ the membrane has reached the point where it begins to descend everywhere. This is the reason for the larger flow rate at $T = 6.5 \times 10^4$ for r less than 0.68. Between these two times the membrane near the origin is accelerating to a maximum downward velocity. After this short period of adjustment the volume flow rate decreases monotonically with time. The exit flow rate for this case has decreased by one order of magnitude between the first and last time curves in this figure.

Due to the smaller magnitudes for flow rate in the cases of smaller aspect ratio the coordinate Q is expanded for each decreasing value of R1, as can be seen in figures

III-15, III-17 and III-18b. These figures show the same qualitative features seen in figure III-13. Since the driving force for draining is smaller in the film adjacent to flatter cells, the draining rate is correspondingly smaller. Figure III-13 shows that $T = 6 \times 10^{5}$ a cell with R1 = 2.0 has an exit volume flow rate of approximately 0.50×10^{-8}, whereas for a cell with an aspect ratio of 0.25 the exit flow rate at the same time is an order of magnitude less than the value of the larger cell. Thus, the rate of draining is influenced to a large extent by the aspect ratio of the membrane bound cell.

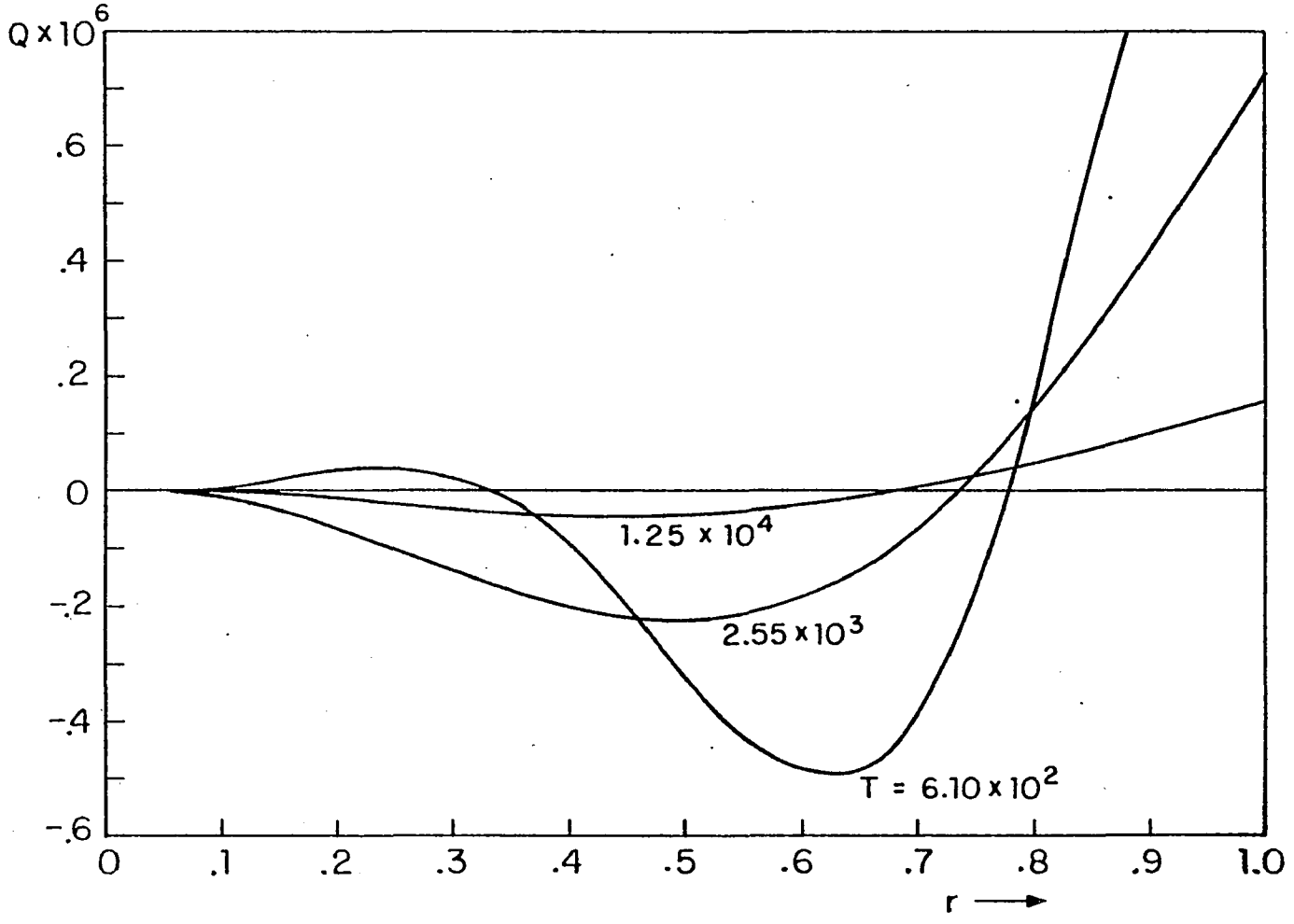

Figure III-12 Volume flow rate, R1 = 2.0, $t < t_{ct}$.

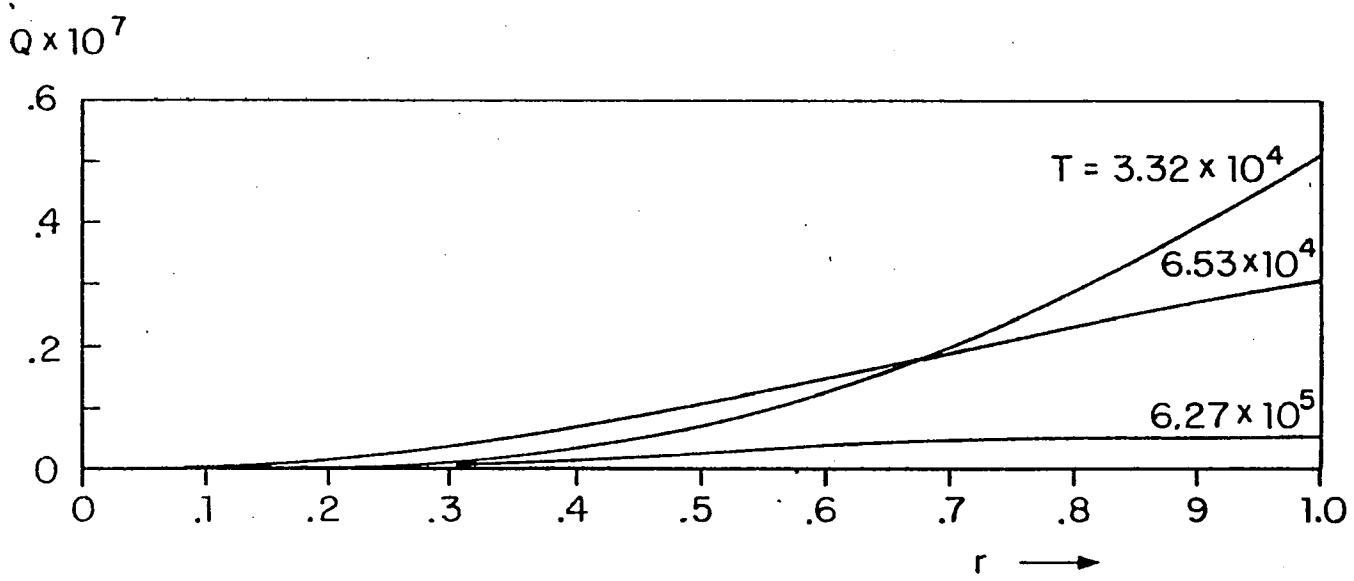

Figure III-13 Volume flow rate, R1 = 2.0, $t > t_{ct}$.

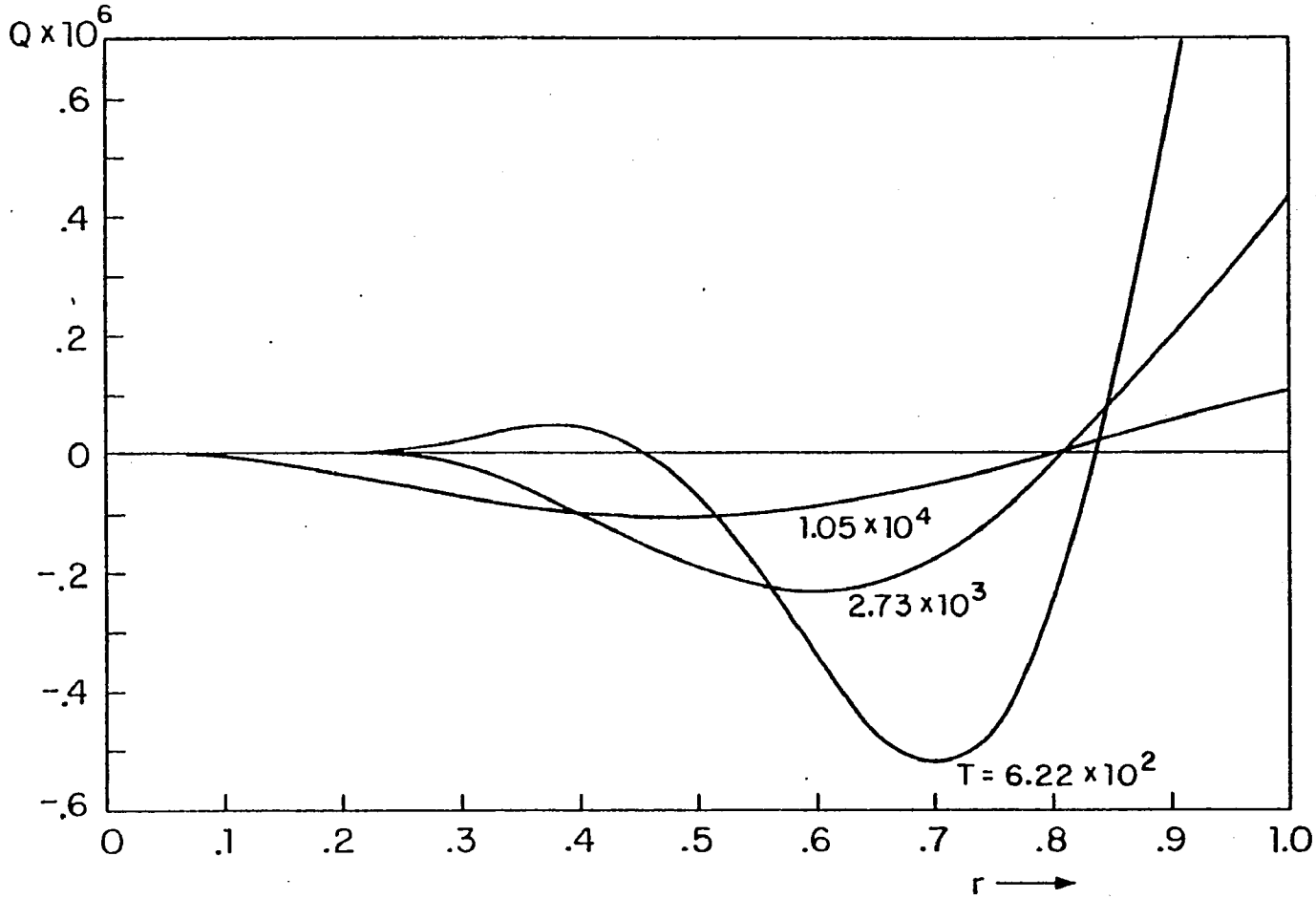

Figure III-14 Volume flow rate, R1 = 0.75, $t < t_{ct}$.

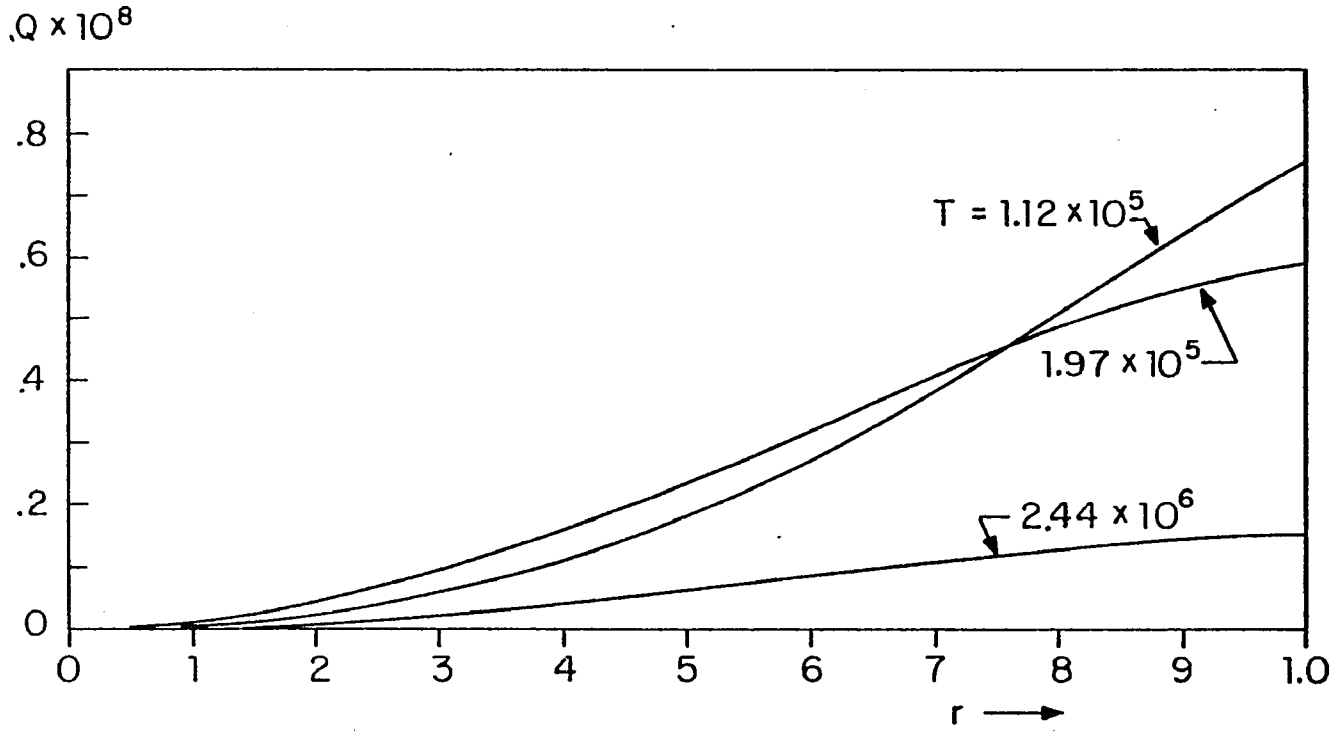

Figure III-15 Volume flow rate, R1 = 0.75, $t > t_{ct}$.

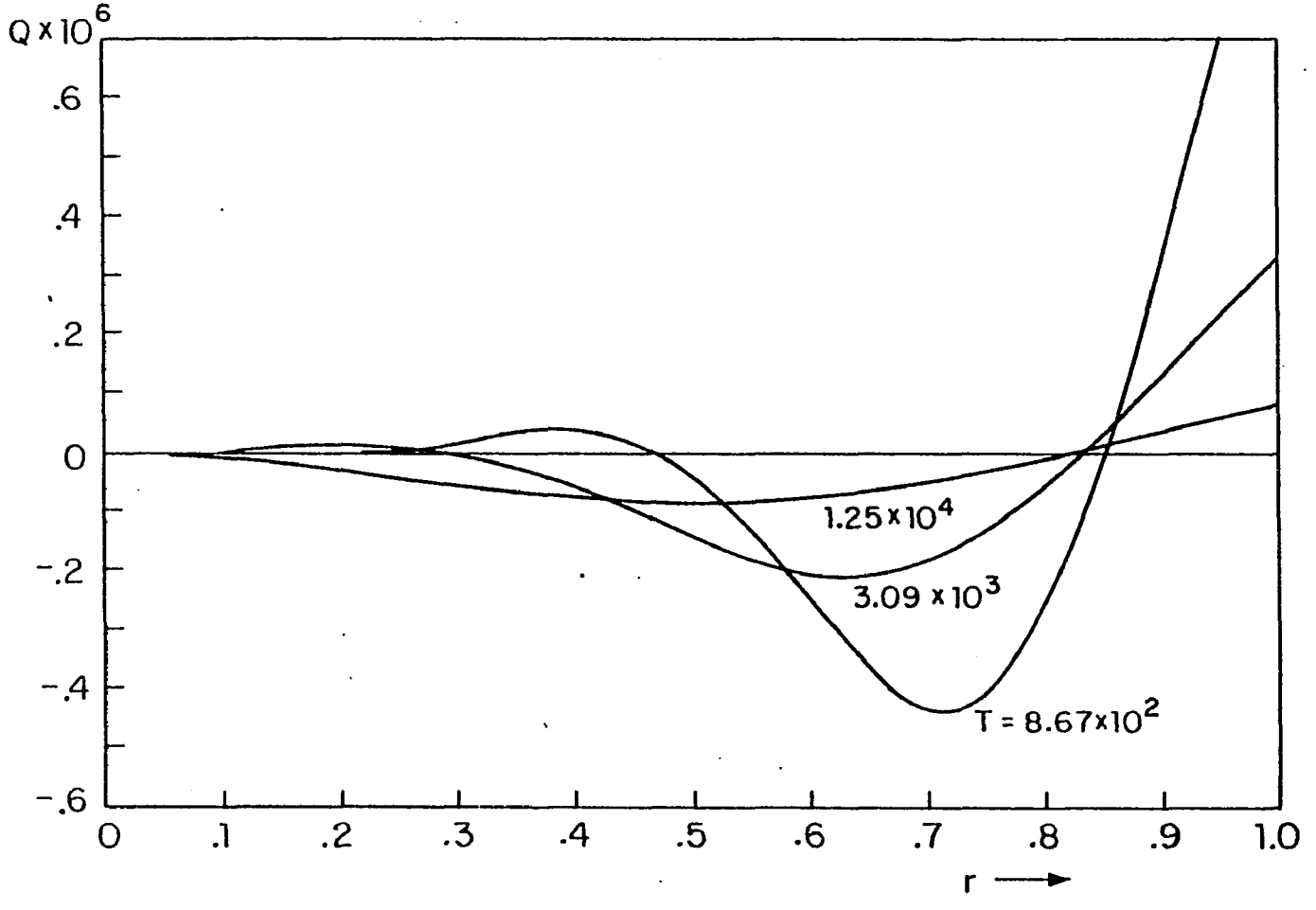

Figure III-16 Volume flow rate; R1 = 0.50, $t < t_{ct}$.

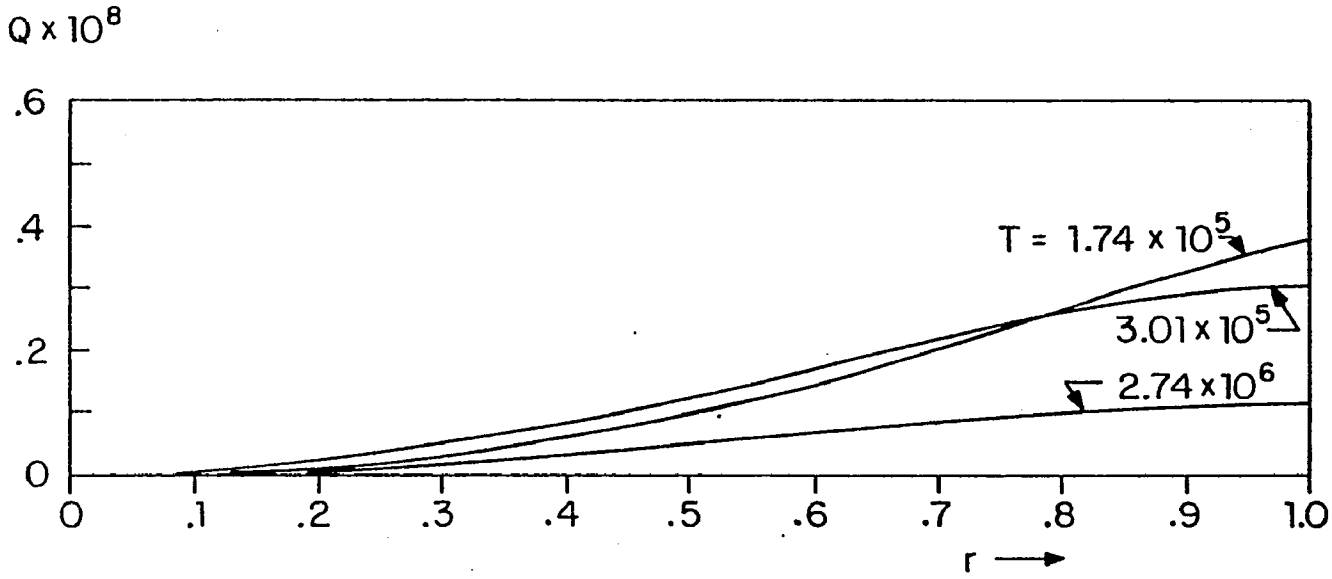

Figure III-17 Volume flow rate, R1 = 0.50, $t > t_{ct}$.

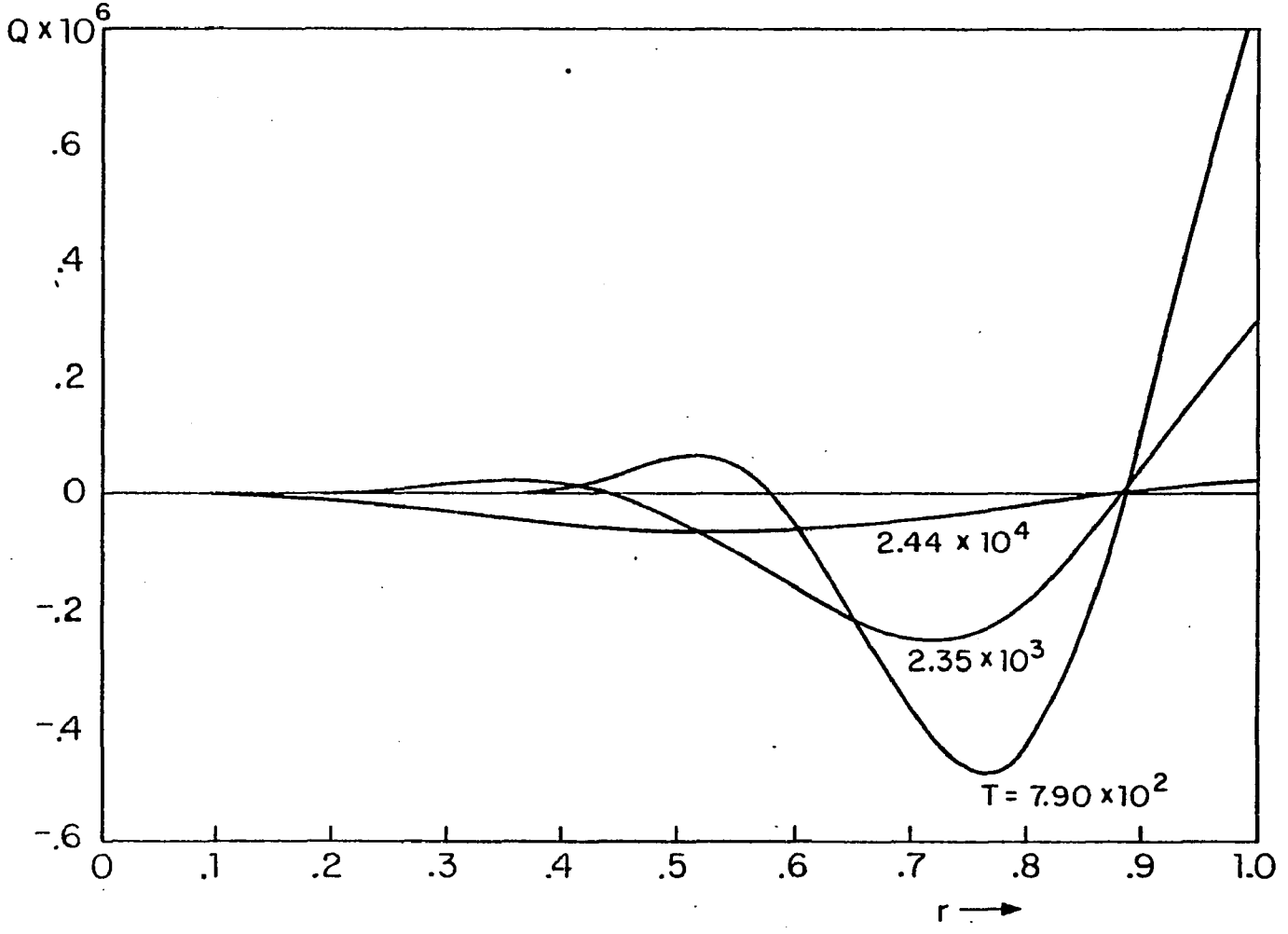

Figure III-18a Volume flow rate, R1 = 0.25, $t < t_{ct}$.

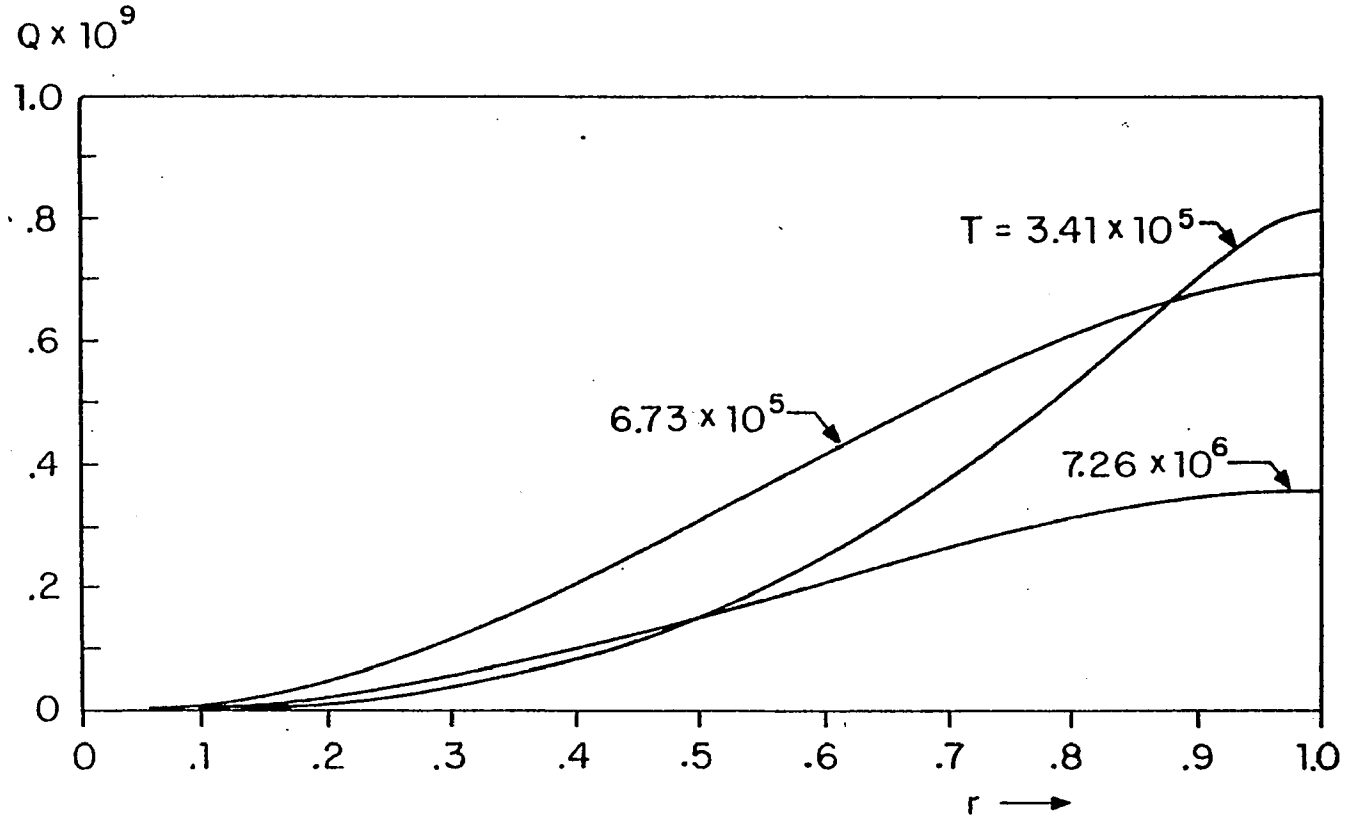

Figure III-18b Volume flow rate, R1 = 0.25, $t > t_{ct}$.

D - Experiments confirming the early time behavior

The bifurcating flow behavior of the fluid film during the early period following the initial application of the load has not been previously reported. A simple validating experiment was therefore conducted to demonstrate the existence of this unusual fluid film behavior.

A schematic representation of the apparatus used to confirm the existence of the bifurcating flow condition is depicted in figure III-19. An air filled balloon is used as the model for a membrane bound fluid and a glass plate serves as the rigid planar surface. The fluid film between the plate and balloon is a common vegetable dye. A motor driven camera is mounted above the glass plate to capture the change in film thickness with time. The camera's motor drive shoots four frames per second, which is sufficiently fast to capture the changes in film thickness because the characteristic time for fluid trapping is of order 5-10 seconds for this experiment. The radius of the balloon is 7.6 cm and the position of the support blocks produces a near contact area of 4.1 cm. The non-dimensional aspect ratio is, thus, equal to 1.84.

The balloon is coated with the vegetable dye and then the glass plate is released. The balloon carries 0.9 kg of the plate's mass and the support blocks the remainder of the load. At the instant that the plate makes contact with the support blocks the fluid film is nearly uniform

in thickness.

Figure III-20 shows the changes in the fluid film during the early period following the application of the glass plate. Photograph a in figure III-20 is taken at the instant the plate touches the support blocks. Here the contrast of the fluid film is uniform indicating that there is a nearly constant film thickness. In photograph b, after 0.25 s has elapsed, there is a light colored ring forming at the perimeter of the fluid film. This ring is the edge region and the light color is indicative of a very narrow gap between the plate and the balloon. The dark ring just outside of the edge region is a reservoir of dye at the point where the balloon surface falls away from the glass plate. Photographs c and d show the growth of the edge region with time.

For this experimental run a small air bubble happened to lie in the edge region. As time passed the air bubble was forced toward the fluid meniscus at the border of the near contact area indicating a net decrease in film volume in the near contact area and a radial outflow from the edge region. Another feature that can be seen in figure III-20 is the gradual darkening of the central portion of the near contact area. This darkening is produced by the gradual thickening of the fluid film near the origin, which is produced by the inward flow of dye predicted by the theory of section III-B.

The gradual darkening in the central region of the

fluid film can be more clearly demonstrated by performing an experiment in which the fluid film near the origin is initially depleted. This is accomplished by lightly pressing the plate against the balloon producing a small near contact area. One then allows the fluid to drain in this small area by holding the plate for several seconds. The plate is then released to form the larger near contact area.

Photograph a in figure III-21 shows the light spot surrounding the origin following the release of the plate. Photographs b, c and d of figure III-21 show the gradual darkening of this area. These photographs clearly show an influx of fluid toward the center of the lubricating layer.

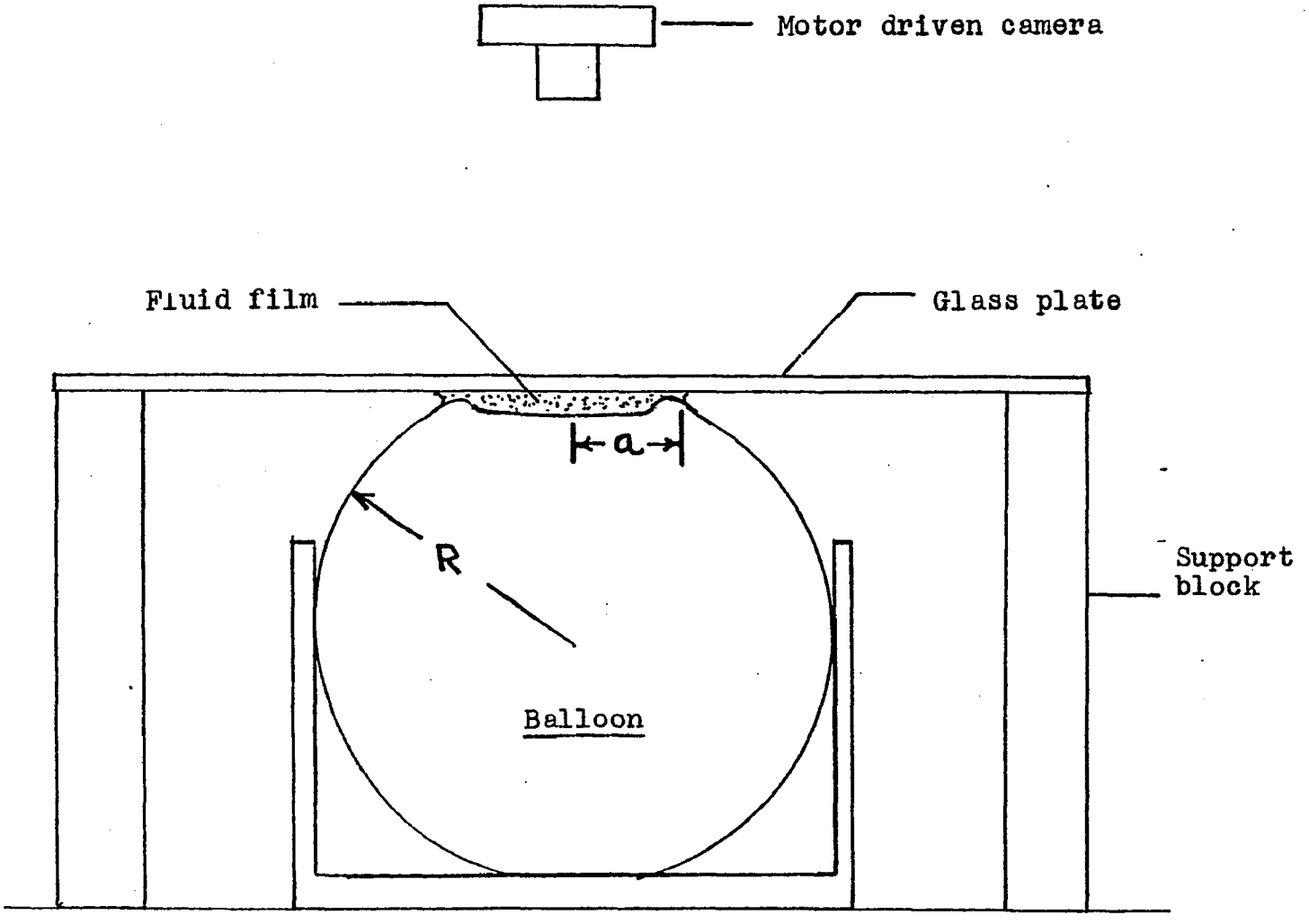

Figure III-19 Schematic representation of the membrane squeeze film experiment.

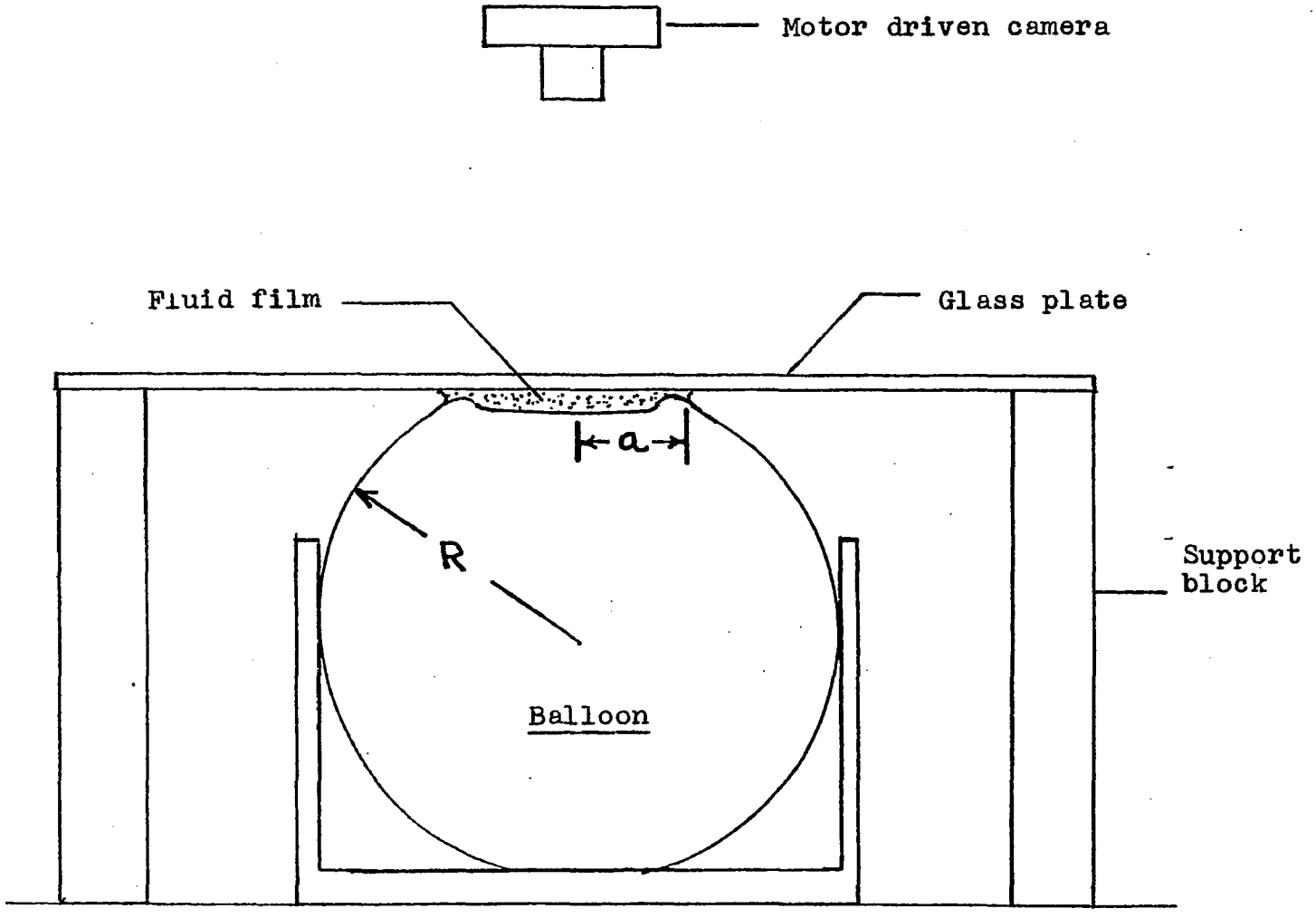

Figure III-19 Schematic representation of the membrane squeeze film experiment.

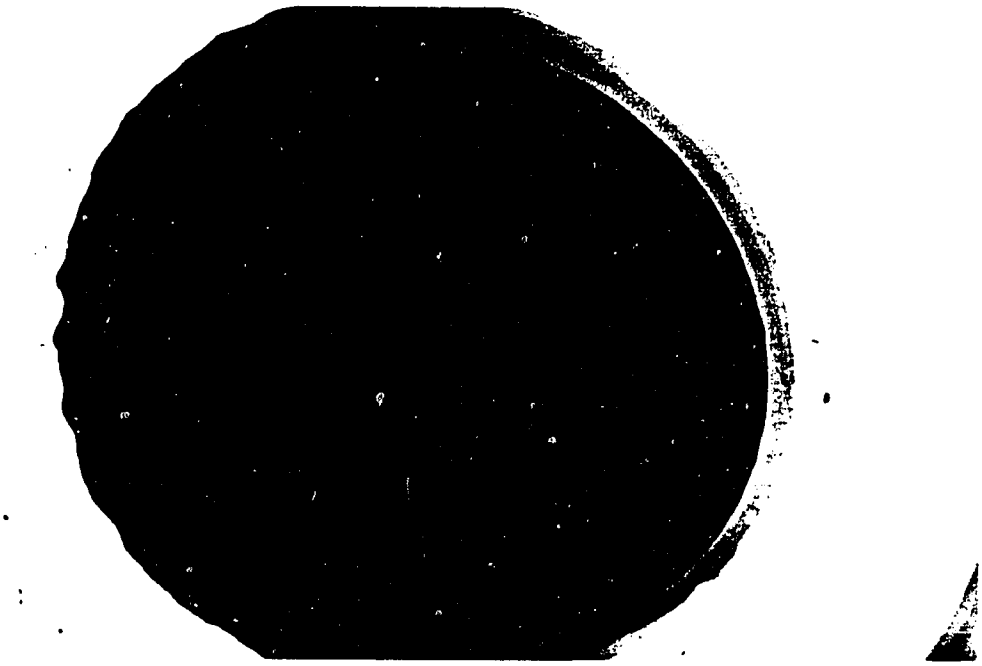

(a)

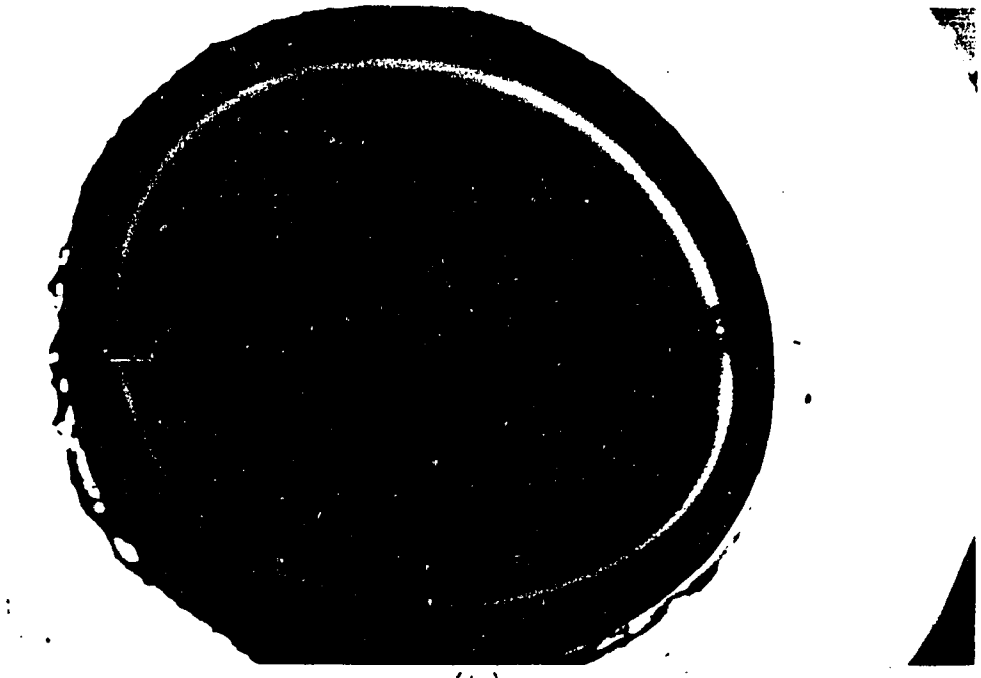

(b)

Figure III-20 Time history of a fluid film being squeezed between a glass plate and an air filled balloon, showing the formation of the edge region and the dual flow condition (outward motion of the air bubble and the thickening of the origin fluid film). Applied load = 0.9kg, a = 4.1cm, R1 = 1.84, time = (a) 0.0 s, (b) 0.25 s, (c) 1.25 s, (d) 5.50 s.

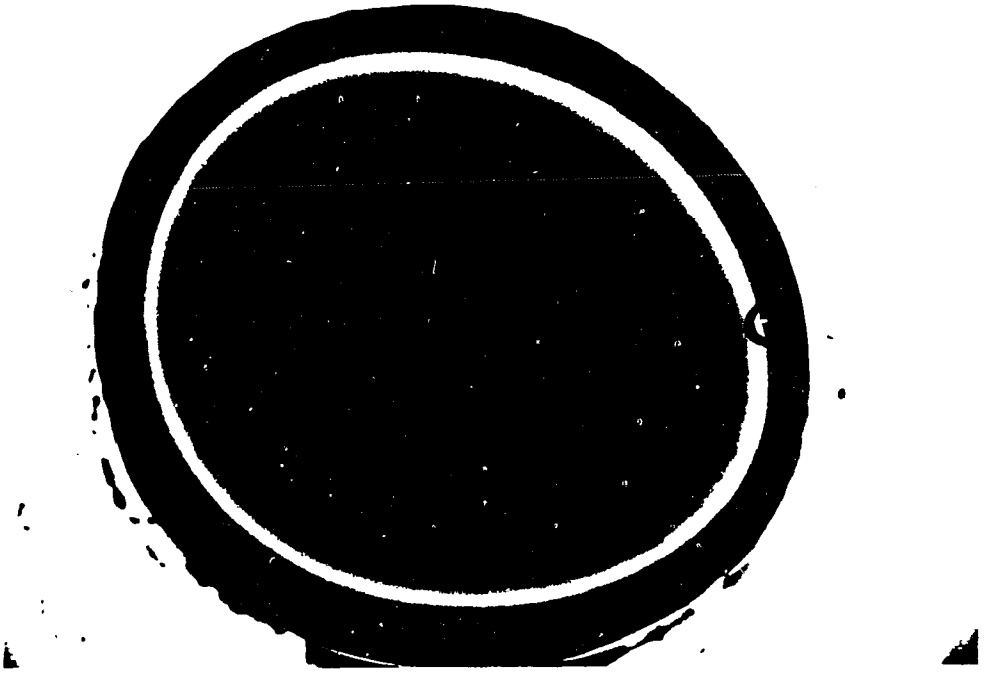

(c)

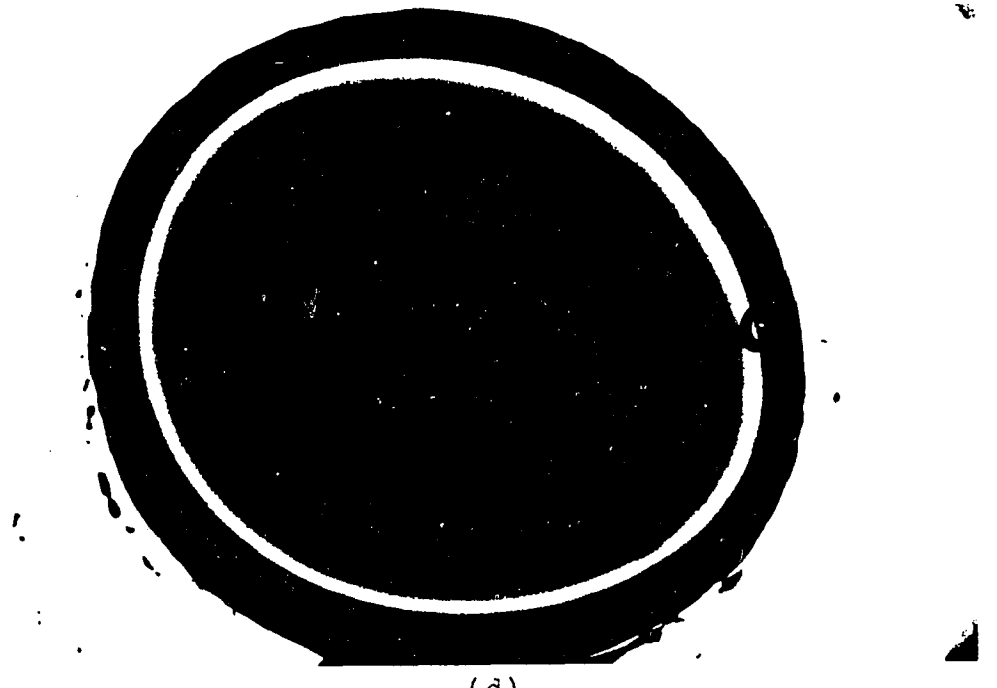

(d)

Figure III-20 Time history of a fluid film being squeezed between a glass plate and an air filled balloon, showing the formation of the edge region and the dual flow condition (outward motion of the air bubble and the thickening of the origin fluid film). Applied load = 0.9 kg, a = 4.1 cm, R1 = 1.84, time = (a) 0.0 s, (b) 0.25 s, (c) 1.25 s, (d) 5.50 s.

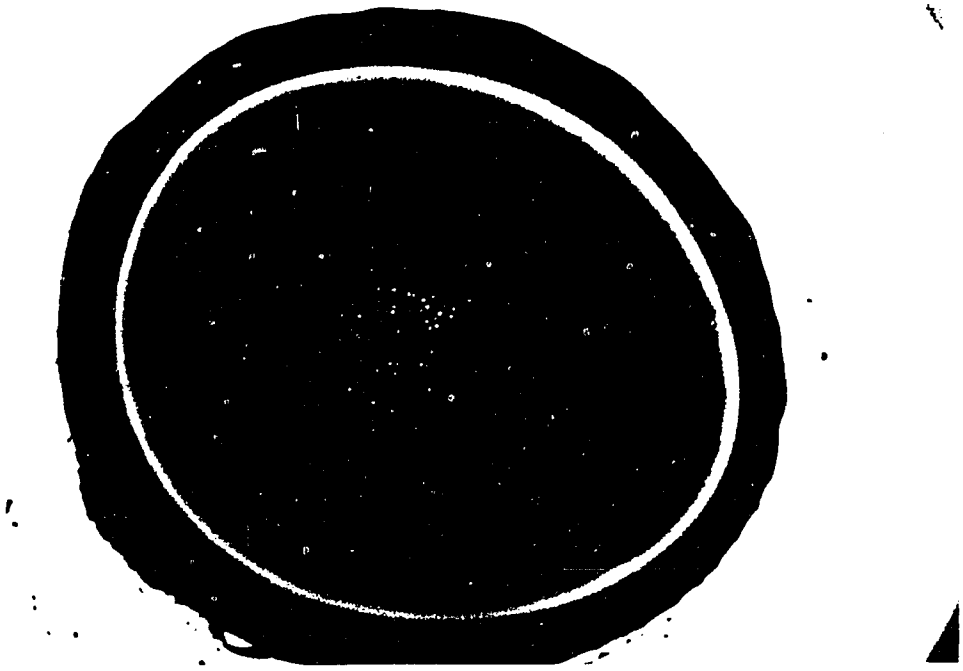

(a)

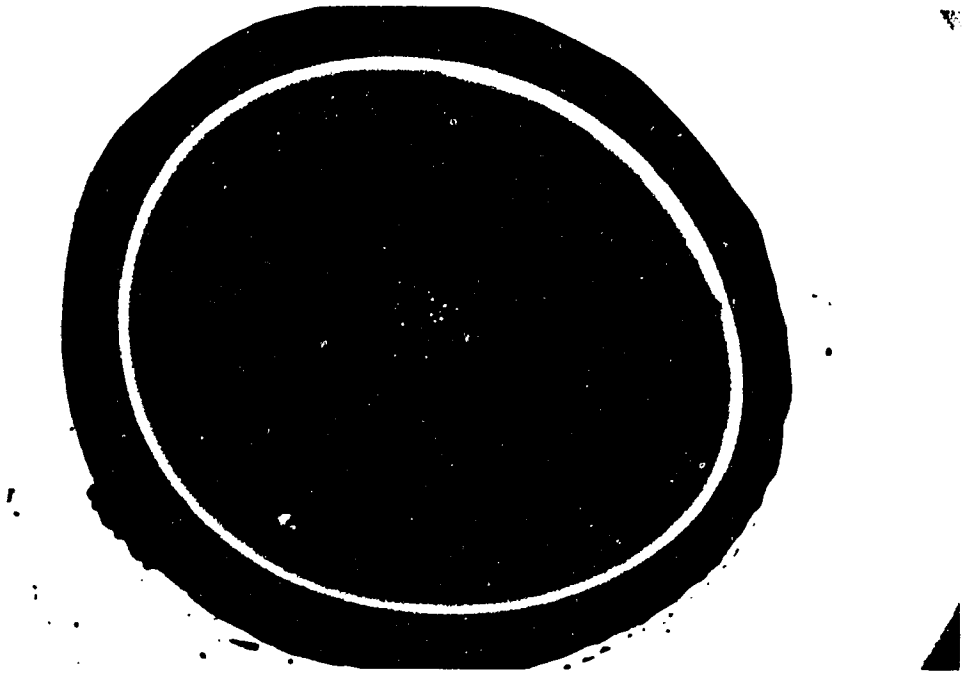

(b)

Figure III-21 Time history of a fluid film, with an initially depleted origin, being squeezed between a glass plate and an air filled balloon. Applied load = 0.9 kg, a = 4.1 cm, R1 = 1.84, time = (a) 0.0 s, (b) 1.0 s, (c) 2.0 s, (d) 9.0 s.

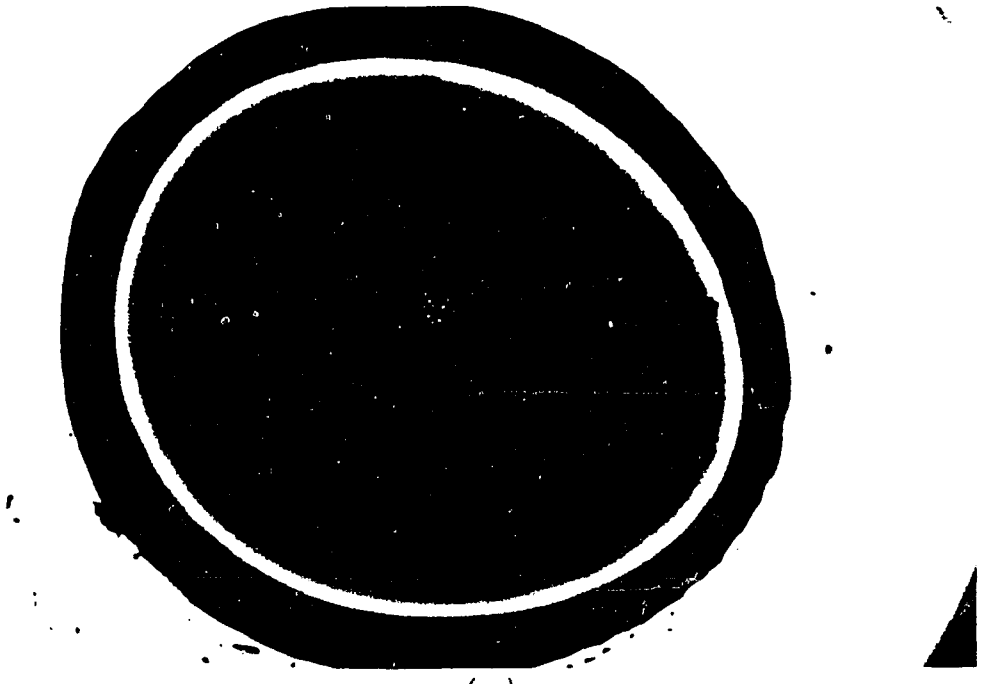

(c)

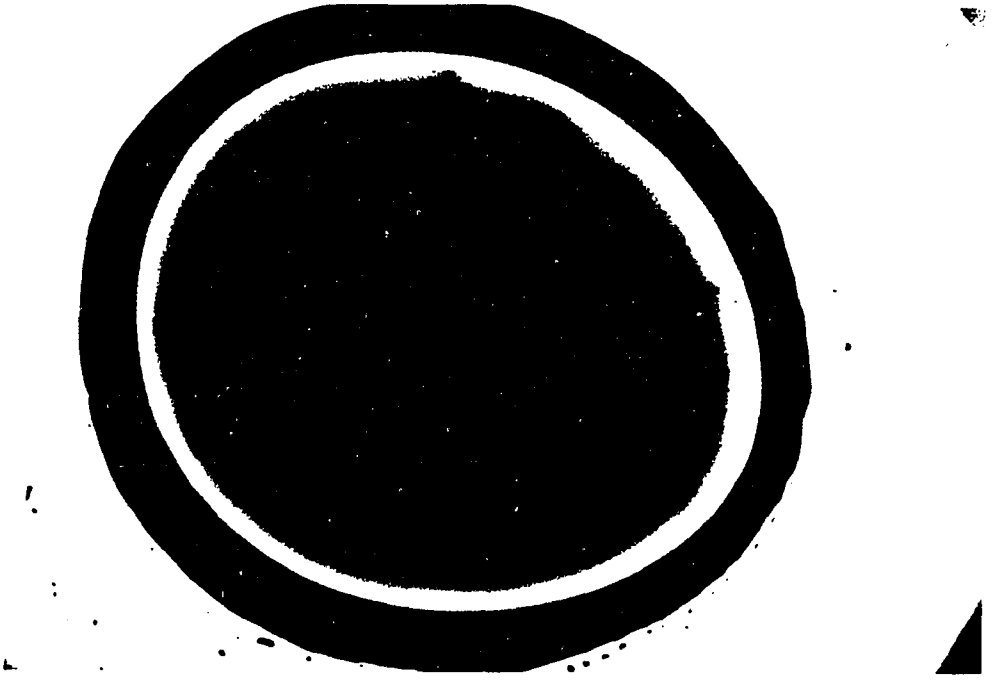

(d)

Figure III-21 Time history of a fluid film, with an initially depleted origin, being squeezed between a glass plate and an air filled balloon. Applied load = 0.9 kg, a = 4.1 cm, R1 = 1.84, time = (a) 0.0 s, (b) 1.0 s, (c) 2.0 s, (d) 9.0 s.

E - Conclusions

The membrane squeeze film theory presented in section III-B predicts a unique bidirectional flow behavior in the fluid film for times less than the characteristic time for fluid trapping. This early time behavior is easily observed in a simple experiment with a balloon, glass plate and vegetable dye. The experimental photographs clearly illustrate the presence of the bidirectional flow in the dye following the application of the plate.

This phenomenon is unique to membrane squeeze film problems. The linear deformation law for elastohydrodynamic squeeze film problems and the membrane force balance relations for this problem are the contributing factors in producing the different flow behavior in these two situations. This difference in flow characteristics points out the need for a realistic assesment of the deformable body before a particular theory is applied. The membrane squeeze film theory presented in this work is the one most applicable to biological cells with easily deformable phospholipid bilayer membranes.

A logical extension of this work would be to include relative translational motion between the planar surface and membrane bound fluid filled cell. This extension of the membrane squeeze film theory may be applied to the problem of a red blood cell translating through a capillary. The problem of an air bubble squeezing a fluid film adjacent to a planar surface inclined at an arbitrary angle, as

the bubble slides up along the planar surface due to buoyancy, could also be treated by including translational motion.

The membrane squeeze film theory has shown the influence that the membrane boundary has on the pressure field developed in the fluid film (off axis pressure maximum and the pressure plateau). The theoretical treatment of an assemblage of membrane bound fluid filled cells at very small porosities undergoing consolidation would have to consider this unusual flow characteristic in the determination of the local excess pore pressure.

REFERENCES

Barnard, A., Lopez, L. and Hellums, J.D. 1968 Microvas. Res. 1, 23.

Benjamin, M.K. 1969 Compliant Surface Bearings: An Analytic Investigation, Doctoral Thesis, Columbia University, New York.

Biot, M.A. 1941a J. Appl. Phys. 12, 155.

Biot, M.A. 1941b J. Appl. Phys. 12, 426.

Biot, M.A. and Clingan, F.M. 1941 J. Appl. Phys. 12, 578.

Biot, M.A. and Clingan, F.M. 1942 J. Appl. Phys. 13, 35.

Biot, M.A. 1955 J. Appl. Phys. 26, 182.

Biot, M.A. 1956 J. Appl. Phys. 27, 459.

Bretherton, F.P. 1961 J. Fluid Mech. 10, 166.

Browne, A.L., Whicker, D. and Rohde, S.M. 1975 Tire Sci. and Tech. 3, 16.

Carew, T.E., Varshnav, R.N. and Patel, D.J. 1968 Circ. Res. 23, 61.

Carrillo, N. 1943 J. Math. and Phys. 21, 1.

Castelli, V., Rightmire, G.K. and Fuller, D.D. 1967 Trans. ASME Series F 89, 510.

Christensen, H. 1962 Proc. Roy. Soc. Series A 266, 312.

Christensen, H. 1970 Trans. ASME Series F 92, 145.

Cox, B.G. 1962 J. Fluid Mech. 14, 81.

Davis, E.H. and Raymond, G.P. 1965 Geotech. 15, 161.

Davis, R.M. and Taylor, G.I. 1949 Proc. Roy. Soc. Series A 200, 375.

Dowson, D. and Higginson, G.R. 1960 J. Mech. Eng. Sci. 2, 188.

Edwards, J. 1967 Proc. Inst. Mech. Eng. 181, 16.

Fitz-Gerald, J.M. 1969 Proc. Roy. Soc. Series B 174, 193.

Fry, D.L. 1972 "Localizing factors in atherosclerosis" in Atherosclerosis and Coronary Heart Disease (eds.) W. Likoff et al, Grune and Stratton, N.Y.

Gaman, I.D.C., Higginson, G.R. and Norman, R. 1974 Wear 28, 345.

Gibson, R.E., England, G.L. and Hussey, M.J.L. 1967 Geotech. 17, 261.

Goldsmith, H.L. and Mason, S.G. 1962 J. Fluid Mech. 14, 42.

Guyton, A.C., Scheel, K. and Murphee, D. 1966 Circ. Res. 19, 412.

Harrison, R.G. and Massaro, T.A. 1976 Athero. 24, 363.

Herrebrugh, K. 1970 Trans. ASME Series F 92, 292.

Hochmuth, R.M., Marple, R.N. and Sutera, S.P. 1970 Microvas. Res. 2, 409

Horn, M.R. 1964 Inter. J. Mech. Sci. 6, 187.

Hyman, W.A. and Skalak, R. 1970 "Viscous Flow of a Suspension of Deformable Liquid Drops in a Cylindrical Tube." Tech. Rep. No. 5, Proj.: NR 062-393, Dept. of Civil Eng. and Eng. Mech., Columbia University.

Kenyon, D.E. 1976 ASME J. Appl. Mech. 98, 594.

Kenyon, D.E. 1978 ASME J. Appl. Mech. 45, 727.

Lai, W.M. Mow, V.C. and Roth V. 1980 "Effects of Strain-Dependent Permeability and Rate of Compression on the Stress Behavior of Articular Cartilage." in 1980 Advances in Bioengineering, ed. V.C. Mow, presented at the ASME Winter Annual Meeting, Chicago, Ill. Nov. 16-21, 1980.

Lee, J.S. and Fung, Y.C. 1969 Microvas. Res. 1, 221.

Lee, K.M. and Cheng, H.S. 1973 Trans. ASME Series F 95, 308.

Lighthill, M.J. 1968 J. Fluid Mec. 34, 113.

Lin, K.L., Lopez, L. and Hellums, J.D. 1973 Microvas. Res. 5, 7.

Lo, K.Y. 1960 Geotech. 10, 36.

Mankin, H.A. and Thrasher, A.Z. 1975 J. Bone and Joint Surg. 57-A, 76.

Mansour, J.M. and Mow, V.C. 1976 J. Bone and Joint Surg. 58-A, 76

Mow, V.C. and Mansour, J.M. 1977 J. Biomech. 10, 31.

Prothero, J.W. and Burton, A.C. 1961 Biophys. J. 1, 565.

Prothero, J.W. and Burton, A.C. 1962 Biophys. J. 2, 199.

Richart, F.E. 1957 Proc. Am. Soc. Civil Eng. SM3, No. 1301

Roberts, A.D. 1974 "Lubrication Studies of Smooth Rubber Contacts" in The Physics of Tire Traction, Theory and Experiment. D.F. Hays and A.L. Browne, eds, Plenum Press.

Rohde, S.M., Whicker, D. and Browne, A.L. 1976 Trans. ASME Series F 98, 401.

Rowe, P.W. 1959 Geotech. 9, 107.

Schryer, N.L. 1977 "Numerical Solution of Time-Varying Partial Differential Equations in One Space Variable", Bell Laboratories Computing Science Technical Report No. 53.

Seshardi, V., Hochmuth, R,M,. Croce, P.A. and Sutera, S.P. 1970 Microvas. Res. 2, 434

Siflinger, A., Parker, K. and Caro, C.G. 1975 Cardio. Res. 9, 478

Skalak, R. 1972 from Biomechanics: Its Foundations and Objectives, Y.C. Fung, ed., pp 457-499, Prentice-Hall, N.J.

Sutera, S.P., Seshardi, V., Croce, P.A. and Hochmuth, R.M. 1970 Microvas. Res. 2, 420.

Terzaghi, K. 1925 Erdbaumechanik auf Bodenphysikalischer Grundlage, Vienna.

Torzilli, P.A. and Mow, V.C. 1976a J. Biomech. 9, 541.

Torzilli, P.A. and Mow, V.C. 1976b J. Biomech. 9, 587.

Tözeren, H. and Skalak, R. 1978 J. Fluid Mech. 87, 1.

Tözeren, H. and Skalak, R. 1979 J. Fluid Mech. 95, 743.

Updike, D.P., and Kalnins A. 1972 A.S.M.E. Journal of Applied Mechanics paper no. 72-APM-31.

Vargas, C.B., Vargas, F.F., Pribyl, J.G. and Blackshear, P.L. 1979 Am. J. Physiol. 236 (1), H53.

Whicker, D., Browne, A.L. and Rohde, S.M. 1976 J. Fluid Mech. 78, 247.

Wilens, S.L. and McCluskey, R.T. 1952 Am. J. Med. Sci. 22, 540.

Wilens, S.L. and McCluskey, R.T. 1954 Circ. Res. 2, 175.

Yamartino, E., Bratzler, R., Colton, C. and Smith, K. 1974, Circulation 49 and 50 (SIII), 273.